Mechanical Properties and Microstructural Characterization of Aged Nickel-based Alloy 625 Weld Metal

Cleiton Carvalho Silva[1*], Emerson Mendonça Miná[1], Elineudo P. Moura[1], Victor Hugo C. de Albuquerque[2],
João Manuel R. S. Tavares[3]

[1*]Universidade Federal do Ceará, Departamento de Engenharia Metalúrgica e de Materiais, Fortaleza, Ceará, Brasil.

Email: cleiton@metalmat.ufc.br

[2]Programa de Pós-Graduação em Informática Aplicada, Universidade de Fortaleza, Fortaleza, Ceará, Brasil.

[3]Instituto de Ciência e Inovação em Engenharia Mecânica e Engenharia Industrial, Departamento de Engenharia Mecânica, Faculdade de Engenharia, Universidade do Porto, Porto, Portugal

***Corresponding author:**

Prof. Dr. Cleiton Carvalho Silva

Universidade Federal do Ceará

Campus do Pici, s/n

60455-760, Fortaleza, CE, Brazil

email: cleiton@metalmat.ufc.br

Phone: +55 85 33669078, Fax: +55 85 33669358

Abstract

The aim of this work was to evaluate the different phases formed during solidification and after thermal aging of the as-welded 625 nickel-based alloy, as well as the influence of microstructural changes on the mechanical properties. The experiments addressed aging temperatures of 650 and 950 ^{o}C for 10, 100 and 200 h. The samples were analyzed by electron microscopy, microanalysis and X-ray diffraction in order to identify the secondary phases. Mechanical tests such as hardness, microhardness and Charpy-V impact test were performed. Nondestructive ultrasonic inspection was also conducted to correlate the signals with mechanical and microstructural properties. The results show that the alloy 625 when aged at 650 °C experienced microstructural changes that were responsible by the dissolution of Laves phase formed during the solidification and the appearance of fine carbides along the solidification grain boundaries. When aged at 950°C, the Laves phase was continuously dissolved and the excess Nb caused the precipitation of δ-phase (Ni_3Nb), which was intensified at 10 hours of aging, with subsequent dissolution for longer periods such as 200 h. Even when subjected to significant microstructural changes, the mechanical properties, especially toughness, were not sensitive to the dissolution and/or precipitation of the secondary phases.

Keywords: Electron microscopy; microanalysis; nickel based superalloys; welding; aging; phase transformation.

1 Introduction

One of the most interesting characteristics of the nickel-based superalloys is its high corrosion resistance to an aqueous chloride medium.[1] Furthermore, these alloys exhibit extraordinary resistance to a wide range of organic and mineral acids due to their excellent corrosion resistance properties, mainly, at high temperatures, and, therefore, are commonly found in the marine, aerospace, chemical and oil and gas industries.[2-5]

The alloy Inconel® 625 stands out as one of the leading commercial Ni–Cr–Mo–Nb alloy grades.[2] The development of this alloy in 1964 was designed to meet the market of alloys for high temperature service. However, with the discovery of its exceptional corrosion resistance, it also came to assume a prominent position in other applications, where corrosion resistance is essential.[1]

In addition, the 625 nickel-based superalloy exhibits an outstanding combination of mechanical properties and resistance to pitting, crevice and intergranular corrosion due to the solid-solution strengthening effect of chromium, molybdenum and niobium in its nickel matrix, making precipitation-hardening treatments unnecessary.[1] However, elements such as Cr, Ti, Nb and Mo are also strong precipitate formers. According to many studies, the presence of these elements influences the formation of the metastable γ'' phase (Ni_3Nb), primary MC carbides where M denotes Nb and Ti. There are other types of carbides such as M_6C, where M denotes Si, Ni and Cr, and also $M_{23}C_6$ where M denotes mainly Cr and/or Mo.[6–9]

Nevertheless, the high cost of nickel based superalloys makes them unviable for massive applications in some situations. In order to overcome this obstacle and make the use of Ni-based alloys attractive to equipment manufacturers, providing high service performance

using this particular class of material, overlays with Ni-based alloys on C-Mn low alloy and stainless steels have become an option in recent years.[10-12]

During welding with the Inconel 625 alloy as filler metal, there is an intense microsegregation of elements, such as niobium and molybdenum, within the interdendritic regions causing the supersaturation of the liquid metal in its final stage of solidification.[10] This important phenomenon results in the precipitation of Nb-rich Laves phase and MC primary carbides of type NbC.[13, 14] The segregation and precipitation of secondary phases like Nb-rich Laves phase, which has a low melting point, can cause an increase in the temperature solidification range, making the alloy susceptible to solidification cracking.[15] However, an adequate selection of the welding conditions can minimize the formation of the Nb-rich Laves phases, thus reducing susceptible to solidification cracking.

Although several studies have reported the presence of Laves phase in alloys containing Nb and Mo, such as 625 and 718, there are few studies that address the effect of the presence of this phase on the mechanical properties, especially impact resistance.[16,17] However, there are several studies on the effect of high temperature exposure on secondary phase precipitation and the effect of such precipitations on the mechanical properties has been investigated.[18-21] Nonetheless, on many occasions, these alloys are evaluated from wrought or annealing bars, which are very different when compared with the as-welded condition.

As a general rule, the microstructural changes in these alloys, and consequently any changes to their mechanical properties are extensively investigated using metallographic evaluations supported by microscopic techniques. These investigations can be difficult, especially in field applications where access to the affected areas may be restricted.[22] Recently, the potential of nondestructive testing methods, based on ultrasonic signals, to evaluate microstructural characterization and mechanical properties in ferrous alloys has been systematically evaluated. These authors analyzed ultrasonic results of velocity and attenuation

and compared them against the ones obtained by destructive testing such as the Charpy impact, X-ray diffraction and hardness tests.[23-25] The findings showed that ultrasonic testing is a promising technique to follow-up material phase transformations. This approach was used with the 625 alloy to detect microstructural changes based on ultrasonic attenuation and velocity measurements by Albuquerque et al.,[26] confirming again its main advantages.

Besides such approaches, further research work has been developed to obtain faster and more accurate methods for microstructural characterization. One such example is the ultrasonic signal classification method using the recent and powerful Optimum Path Forest classifier[27] and the traditional Support Vector Machines, with Bayesian and Artificial Neural Network algorithms[28]. Results with more than 90% of accuracy were achieved in 1.40 ± 0.57 milliseconds with material samples aged at 650º C and aging times of 0, 10, 100, 200 hours. However, the performance of these techniques is lower for the samples aged at temperatures of 950º C for the same period of times, with an accuracy of approximately 73% in 0.77 ± 0.02 milliseconds.

Recently Silva et al.[29] evaluated the performance of magnetic permeability as a nondestructive low-cost and alternative tool for the microstructural characterization of a duplex stainless steel, and was able to confirm that the magnetic permeability can be used to successfully track the formation of the alpha line phase from the alpha phase on a duplex stainless steel.

Thus, the aim of this study was to evaluate the microstructural evolution during aging heat treatments performed on welds of 625 nickel-based alloys. Extensive microstructural characterization was carried out by scanning electron microscopy and energy dispersive spectroscopy, as well as by non-destructive testing. In addition, the influence of the

microstructural changes on the mechanical properties such as impact strength and hardness were also evaluated.

2 Experimental procedures

Inconel 625 alloy coatings deposited on an ASTM A36 steel base were used in the experiments. The chemical compositions of these materials are shown in Table 1. A 4.0 mm diameter tungsten electrode doped with thorium was used, and pure argon (99.99%) was chosen as the shielding gas.

An electronic multi-process power source connected to the data acquisition system was used during the welding to monitor the current and tension applied. The manipulation of the torch was carried out using an industrial robot system, Figure 1a. An automatic cold wire feed system for the gas tungsten arc welding (GTAW) was used to supply the filler metal. A positioning unit was used to guide the wire into the arc so that adjustments to the configuration parameters and geometry of the wire feed could be made, Figure 1b.

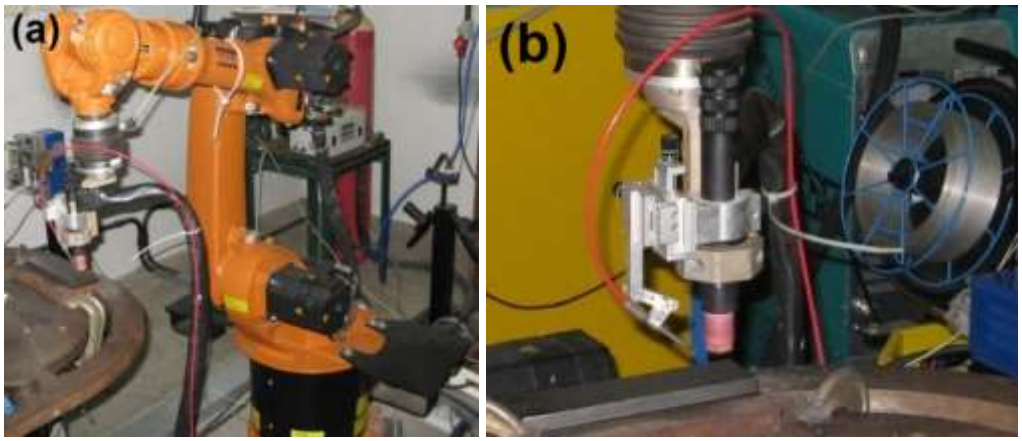

Figure 1. Experimental setup used in the welding process: (a) robotic system, (b) GTAW guide wire feed and torch.

147 The coating was welded onto an ASTM A36 steel base plate, resulting in a coating of
148 350x60x14 mm^3. The other welding parameters were: 285 A of welding current (DCEN), arc
149 voltage of 20 V, travel speed equal to 21 cm/min, welding heat input of 16 kJ/cm, wire feed
150 speed equal to 6.0 m/min, arc length of 10 mm, 15 l/min of gas flow and arc oscillation
151 describing a double-8 trajectory. Other minor settings included the wire feed direction ahead
152 of the arc weld, wire tip to pool surface kept at a distance of 3 mm, wire feeding angle
153 maintained constant and equal to 50º, and electrode tip angle fixed at 50º.

154 To guarantee a good overlaying due to multiple pass deposited side by side, a distance
155 equal to 2/3 of the initial weld bead width was established as an ideal step. Other arc
156 oscillating parameters adopted were: oscillation amplitude of 8 mm and wave length equal to
157 1.2 mm. To produce a 10 mm thick coating on the substrate, seven layers with eight passes
158 were deposited under identical welding conditions.

159 After the welding, the coating was detached from the substrate by conventional
160 machining, as the material of interest was only the Inconel 625 alloy. Then, the coating was
161 divided into seven plates, three plates were submitted to aging heat treatments at 650 ºC for
162 times of 10, 100 and 200 h, another three plates were submitted to aging heat treatments at
163 950 ºC for times of 10, 100 and 200 h, and the remaining plate was kept in the as-welded state
164 (0 h). The aged plates were water cooled with moderate agitation at room temperature.

165 Afterwards, the seven samples were cut and subjected to metallographic preparation
166 that included grinding using silicon paper with several granulometries, followed by
167 mechanical polishing using diamond paste with 3 μm and 1 μm. Electrolytic etching using
168 aqueous solution with 10% chromic acid and a tension of 2 V for 15 seconds was used to
169 reveal the nickel-alloy microstructure. Microstructural analysis of all samples was performed
170 by a scanning electron microscope (SEM) Philips XL30 (Oxford Instruments, England), and a

study of the chemical composition of the secondary phases was carried out through energy dispersive spectroscopy of X-rays (EDS).

X-ray diffraction analysis (XRD) was also used to characterize the secondary phases precipitated during solidification and due to solid state transformation during aging treatment. Since the quantities and dimension of the particles are quite small, an alternative evaluation was carried out according the ASTM 936 standard, which covers the procedures for the isolation of TCP (topologically close-packed) in nickel-based alloys. The Panalytical XPert Pro MPD X-ray spectrometer was used in the present investigation. For post-processing and peak matching the X´Pert HighScore software and its database were used. The scan details applied in these analyses were: 2 Theta range from 10 to 120º with a step size of approximately 0.02º and counting at each step for 4 seconds; Cu Ka radiation was used and the X-ray generator power was set at 40 kV and 40 mA.

To evaluate the influence of TCP precipitation on mechanical performance of weld metals, the impact Charpy test was performed according to ASTM E23 using specimens with dimensions of 55x10x10 mm3 with a 45º V-notch, a notch radius of 0.25 mm and a notch depth of 2 mm, Figure 2. The impact tests for all conditions were performed at room temperature. The micro-hardness test was performed on as-welded and aged samples using a Vickers hardness tester Shimadzu (HVMG) using a 200 g load and a dwell time of 15 second.

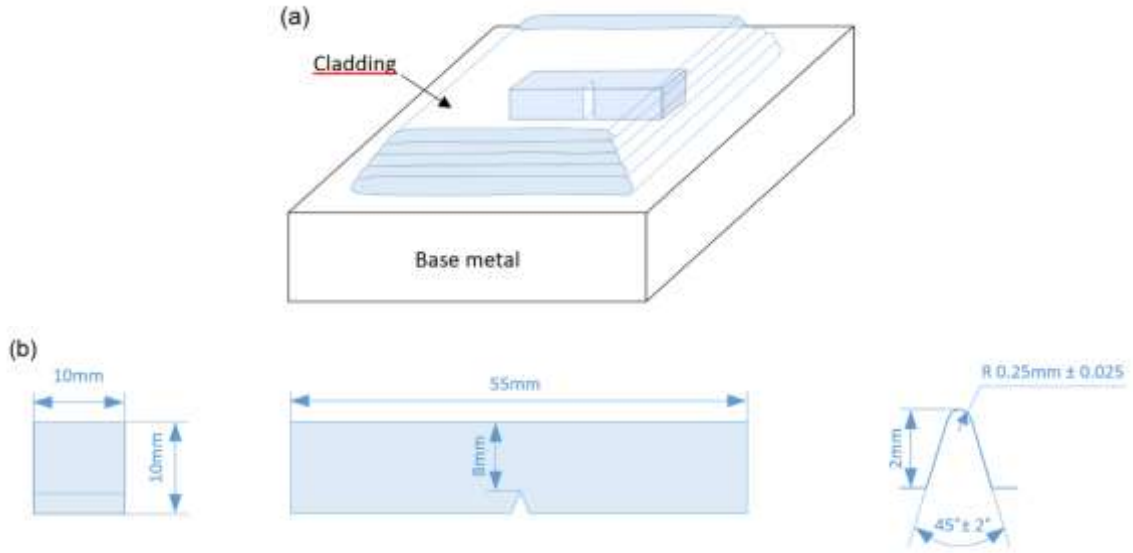

Figure 2. Schematic diagram showing: (a) the location and orientation of the Charpy-V specimens taken from the weld cladding; (b) dimensions of the Charpy impact specimens.

For the physical property assessment via ultrasonic nondestructive testing (aka ultrasonic NDT), the pulse echo technique was used to obtain average ultrasonic velocity and attenuation measurements considering twenty signals acquired with 10,000 points, sampling rate of 1 Gs/s, and ultrasonic transducers of 4 and 5 MHz.

For each sample, twenty signals with two adjacent echoes per signal were acquired for the velocity measurements. Next, the time between the first two echoes was measured through an echo overlapping algorithm.[30] With the wave propagation time and the thicknesses of the samples, obtained by using a micrometer at the same signal acquisition points, it was possible to determine the average velocity of wave propagation through the equation:[31]

$$v = \frac{2X}{\tau_0}, \tag{1}$$

in which X is the thickness of the sample [m] and τ_0 is the time of the wave course [s] until the two adjacent echoes (B_1 and B_2) overlap each other, and its value is determined using:[31]

$$\left| \int_{-\infty}^{\infty} B_1(t).B_2(t-\tau)dt \right|. \tag{2}$$

Although, the time measurement can be obtained directly from the oscilloscope, as previously mentioned, the echo overlapping method was used for it provides greater sensitivity and maximum accuracy.[30]

The ultrasonic attenuation coefficient, α, [dB/mm], was calculated using:[31]

$$\alpha = \frac{20}{2x}\log\frac{A_0}{A_1}, \quad (3)$$

in which x is the thickness of the sample [mm], A_0 is the amplitude of the first echo [dB], and A_1 is the amplitude of the second echo [dB]; more details can be found in Normando et al.[30]

3 Results

3.1 Microstructural characterization

The microstructures of the coatings deposited with Inconel 625 alloy by the GTAW cold wire feed process were analyzed by SEM, and the results revealed a Ni-fcc matrix that solidified in a cellular/dendritic mode. During the solidification process, an intense Mo and Nb microsegregation occurred. Due to this particular phenomenon, extensive amounts of secondary phases were formed at the intercellular or interdendritic regions. An example of the representative microstructure of the as-welded alloy condition (0 h) can be seen in Figure 3a, which also shows in detail the secondary phase formed in the interdendritic region, confirming the large amount of these secondary phases. Figure 3b shows that there are two different types of particles. The first is a bright phase with a shapeless or eutectic morphology, which is due to this phase taking on the shape of the remaining liquid volume during solidification. The second is a faceted or cubic morphology, which is indicated in the Figure.

The chemical composition obtained by EDS in some of these phases, indicated an enrichment of Mo and Nb, as well as the presence of Si at higher concentrations (Figure 3c). With reference to the other elements, such as Ni, Fe and Cr, a lower concentration in the secondary phase was found relatively to the nominal composition of the weld metal, Table 2.

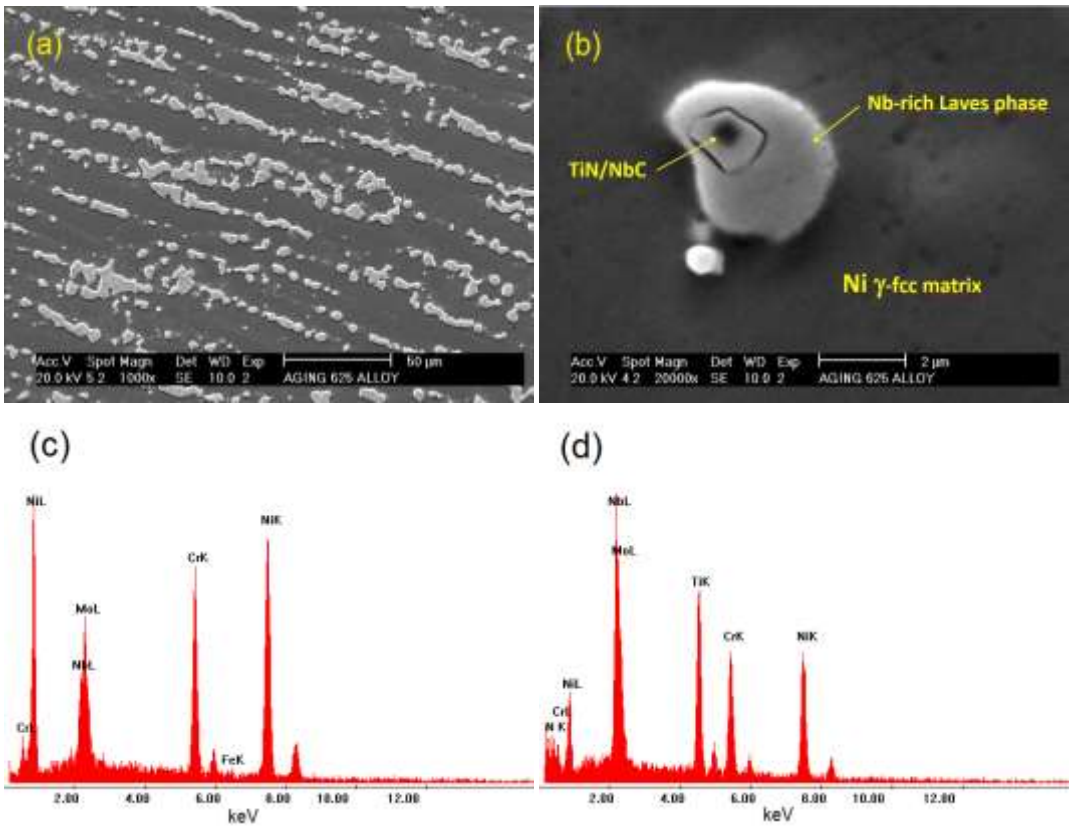

Figure 3. (a) SEM micrographs using secondary electrons showing the Ni-fcc matrix and the secondary phases of the sample as-welded, (b) In detail, an agglomerate formed by a cuboidal precipitate of NbC/TiN wrapped by Nb-rich Laves phase, (c) EDS spectrum of Laves phase, (d) EDS spectrum of NbC/TiN cuboidal precipitate.

SEM/EDS analysis performed on the cubic precipitate showed higher concentrations of Nb and Ti and lower concentrations of Cr, Ni and Mo (Figure 3d). It is important to point that the MoLα peak overlaps with Nb Lα. In addition, a NKα peak was found. The concentration of the main elements is shown in Table 2.

Figures 4, 5 and 6 show the micrographs of the aged samples at 650 ºC for 10, 100 and 200 h, respectively, and the microstructural modifications can be seen. These micrographs show that the microstructural evolution is mainly due to dissolution of the Nb-rich Laves phase, and the cubic particles of Nb and Ti complex carbides/nitrides remain in the microstructure.

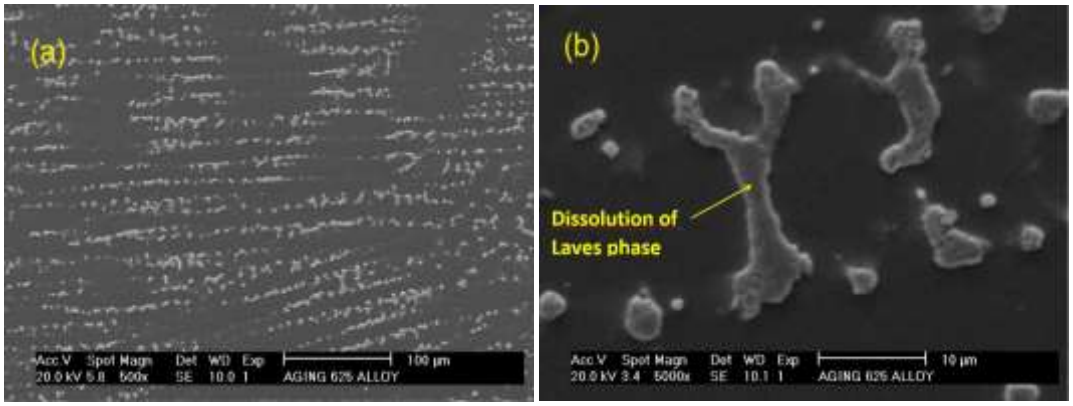

Figure 4. (a) Representative microstructure of the sample aged at 650^{o}C for 10 hours; (b) Detail of the Eutectic-like Laves phase and some cuboidal precipitates of NbTi carbides/nitrides

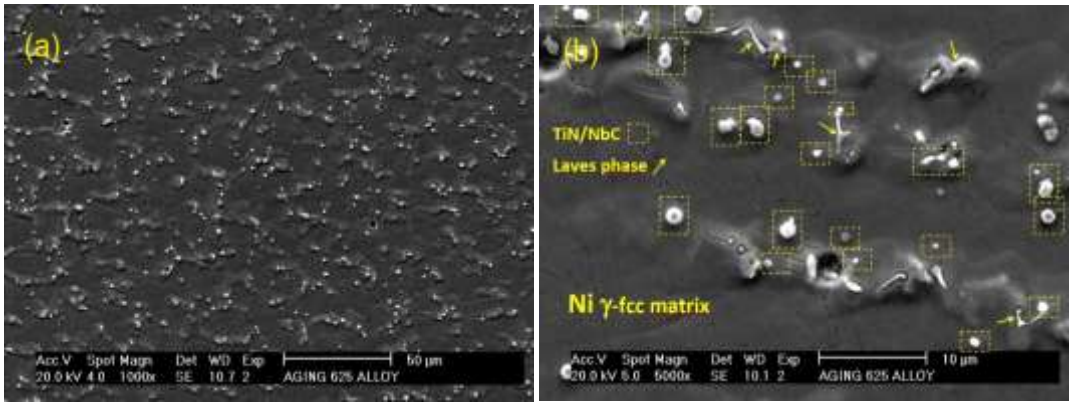

Figure 5. (a) Representative microstructure of the sample aged at 650^{o}C for 100 hours; (b) Detail decomposition of the Laves phase with significantly reduced dimensions, and where some cuboidal precipitates of carbides/nitrides can also be seen.

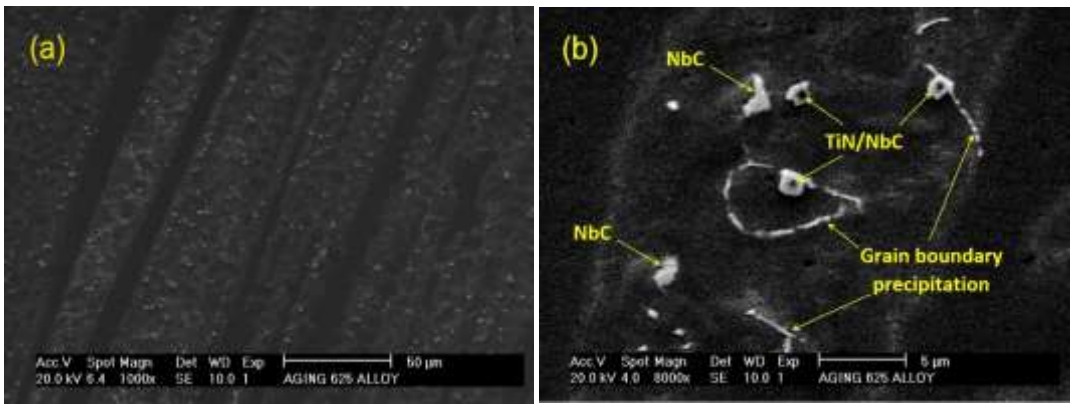

Figure 6. (a) Representative microstructure of the sample aged at 650 ^{o}C for 200 hours showing practically only NbTi carbides/nitrides; (b) Detail showing a small particle of Laves phase reminiscent of the incomplete decomposition.

A representative microstructure of the sample aged at 650°C for 10 hours is shown in Figure 4. There was a very low tendency for the dissolution of Laves phase particles. For the sample aged at 650°C for 100h, an intense dissolution of Laves phase is evident. The volume fraction of the phase reduced greatly compared to the initial conditions (Figure 5). The microstructure for the aged condition of 200 hours at a temperature of 650°C, there was almost a total dissolution of the Laves phase; only remnants were perceived in the microstructure, as shown in Figure 6. In this case, the microstructure consisted almost entirely of the γ-fcc matrix and the particles of cubic NbTi complex carbides/nitrides.

In addition, there was also a noticeable trend in the aged samples with further precipitation after 100 h and 200 h, especially along solidification grain boundaries and sub-grain boundaries. Figure 7a clearly shows the behavior of the precipitation for the 100 h aging condition, in which a discontinuous precipitation of very thin precipitates can be seen along

the grain boundaries. For the 200 h aging, a continuous thin film precipitate can be seen along the grain boundaries in Figure 7b.

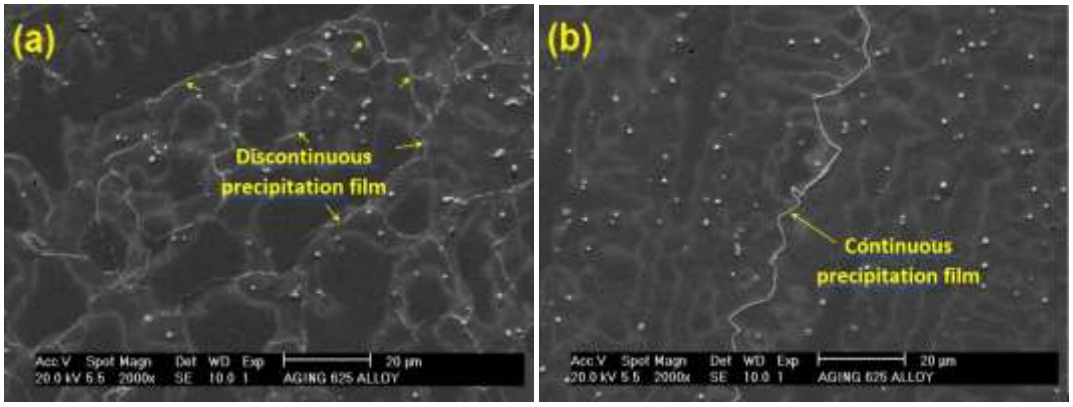

Figure 7. (a) Grain boundary precipitation in an early stage observed in the sample aged at 650 ^{o}C for 100 hours; (b) Grain boundary precipitation like continuous film observed in the sample aged at 650 ºC for 200 hours.

Using a low accelerating voltage in a SEM-FEG microscope, EDS analyses of some particles precipitated at the grain boundary were performed (Figure 8a). Unfortunately, due to the size of those particles precipitated along the grain boundary, the results of the EDS analysis were not conclusive. However, there was a slight increase in Cr in these particles and an intense peak of carbon and silicon in many cases (Figure 8b). This may indicate the formation of carbides such as (Cr_6C) and/or $(CrMo)_{23}C_6$. Also, there was a higher concentration of Nb in the matrix than in the interdendritic region, indicating an enrichment caused by Laves phase dissolution (Figure 8c).

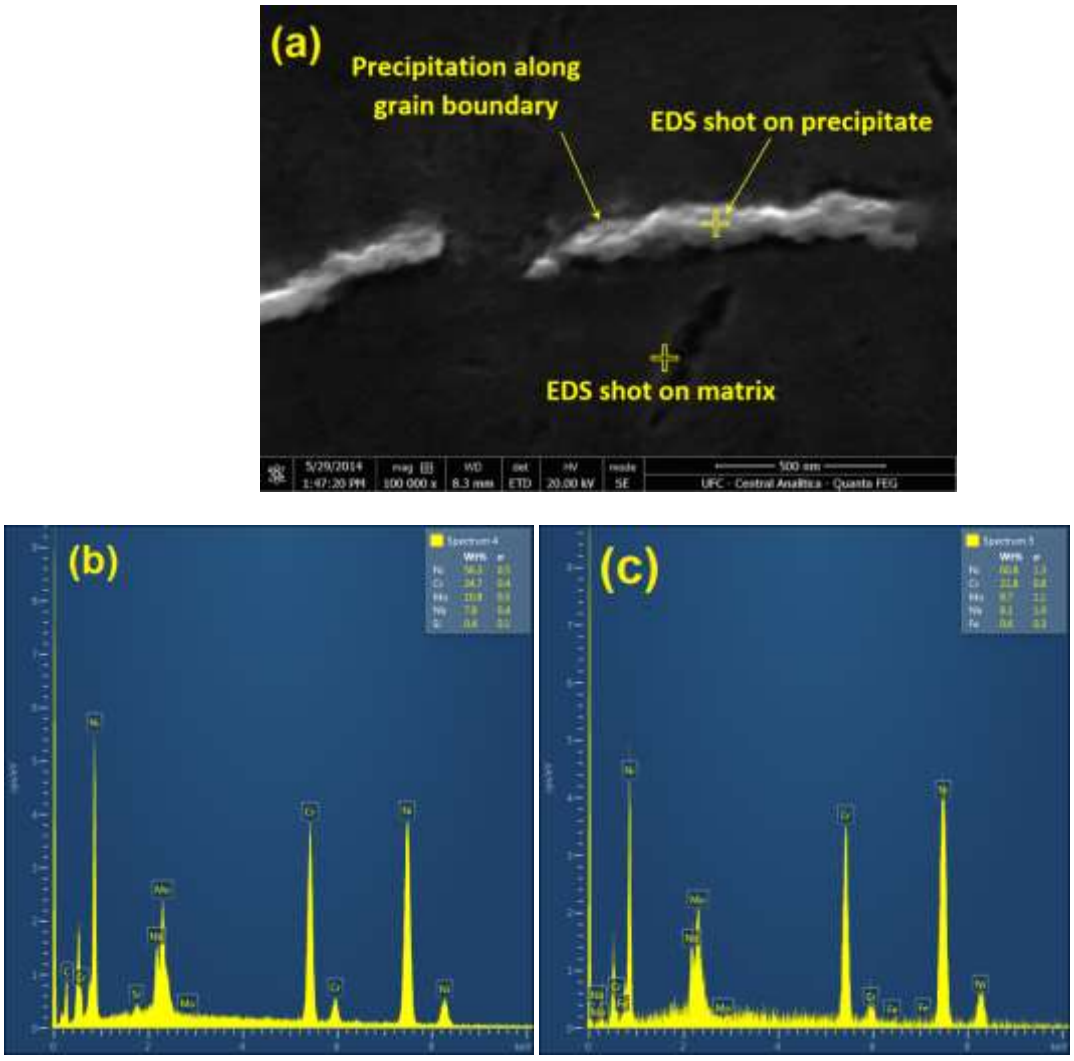

Figure 8. (a) Microchemical analysis of nano-sized precipitates along the grain boundary performed by EDS; (b) EDS spectrum of the particle; and (c) Spectrum of the matrix adjacent to the precipitate.

According to the Thermo-Calc analysis for the chemical composition of the weld metal evaluated by optical emission spectroscopy (Table 3), $M_{23}C_6$ is able to precipitate at all temperatures evaluated in this study (Figure 9). Therefore, $M_{23}C_6$ is considered a strong candidate to precipitate in grain boundaries as was found at 650 °C after 200 h.

However, the formation of M_6C carbides can not be discarded, since these carbides are frequently found in alloys containing chromium, molybdenum and niobium.[32] In addition, is reported that M_6C exhibit excellent temperature stability, however may undergo a transformation to $M_{23}C_6$ for long exposure time at high temperature (816°C - 927°C).[32] In addition, Figure 10 shows the presence of a very thin precipitation along the interdendritic region, together with grain boundary precipitation.

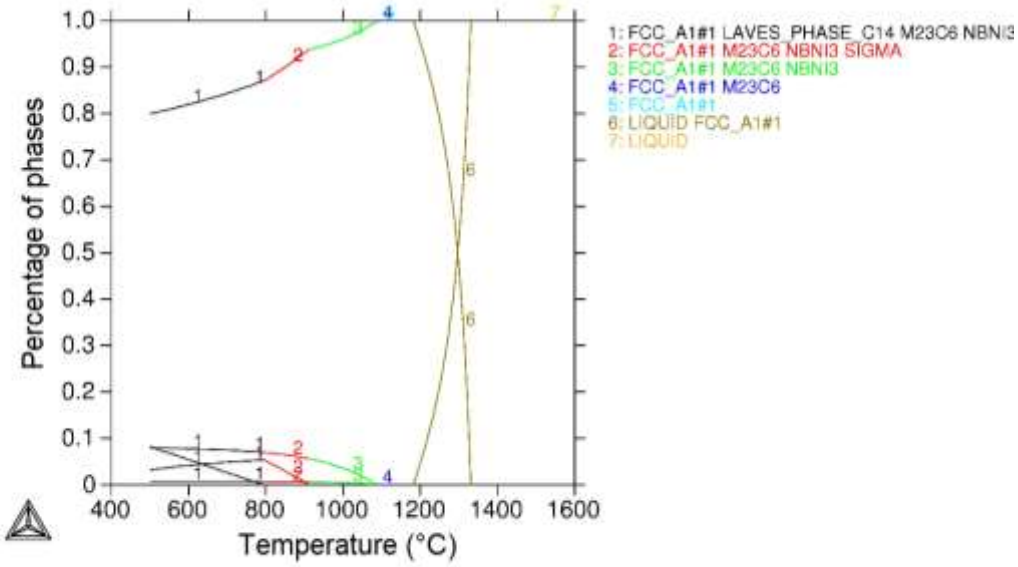

Figure 9. Phase diagram calculated by Thermo-Calc© based on the weld metal chemical composition.

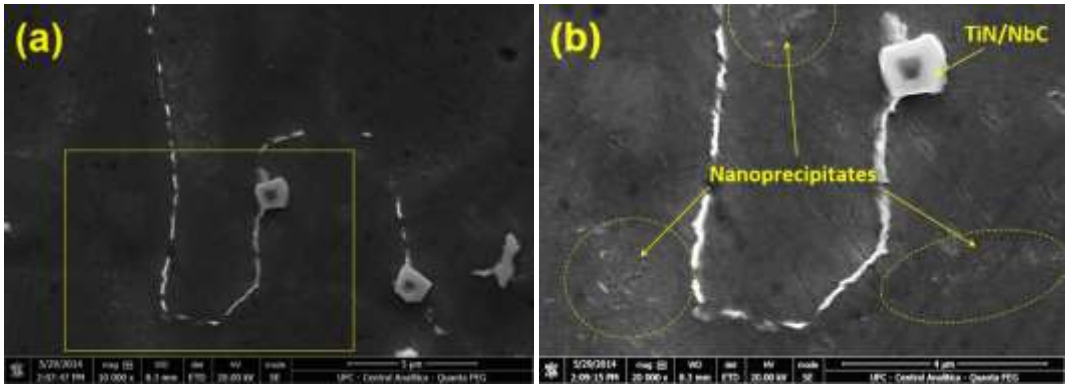

Figure 10. Precipitation along the grain boundary and a very thin precipitation dispersed into the interdendritic region which may be an indicative of the γ" (Ni_3Nb) phase.

On increasing the aging temperature from 650 to 950 °C, several microstructural changes were found. Figure 11 shows representative microstructures of the Inconel 625 alloy aged at 950 °C for 10 hours. In this case, the microstructure indicated the appearance of a new structure with needle morphology. As can be seen in Figure 12, the needles precipitated into the interdendritic region. Another observation is that Laves phase apparently dissolved to give needle phase.

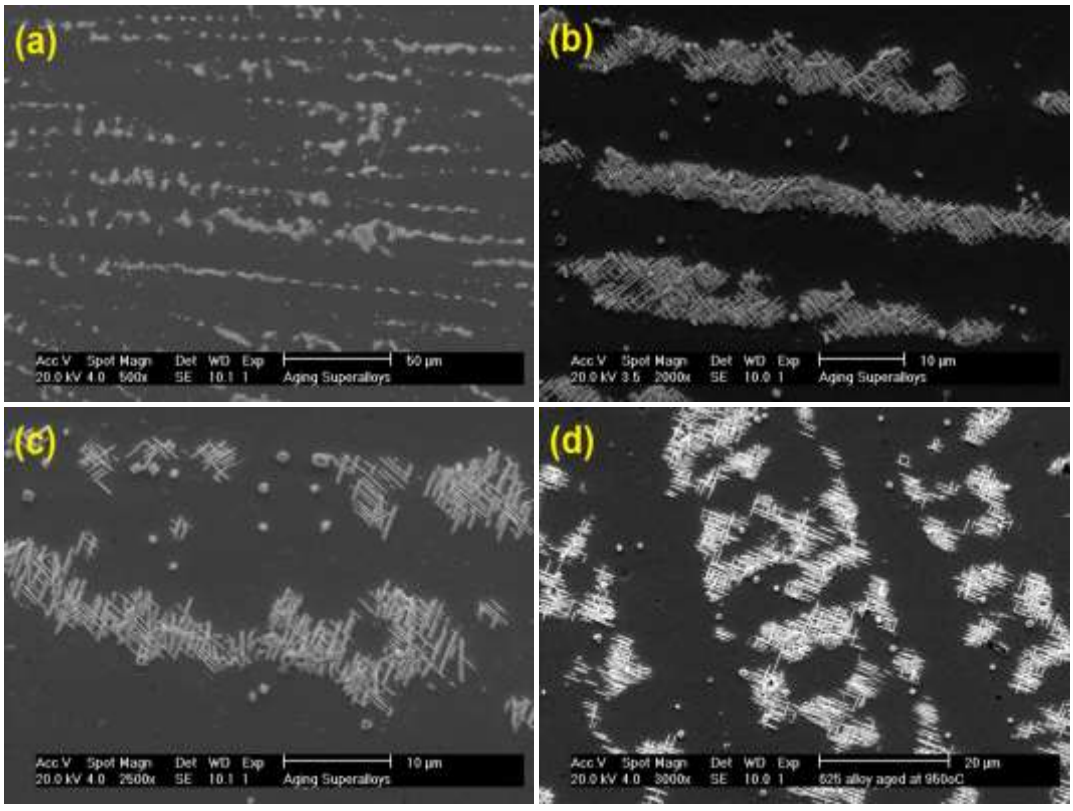

Figure 11. Examples of SEM micrographs using secondary electrons showing the aged microstructure at 950 °C for 10 hours taken from different positions.

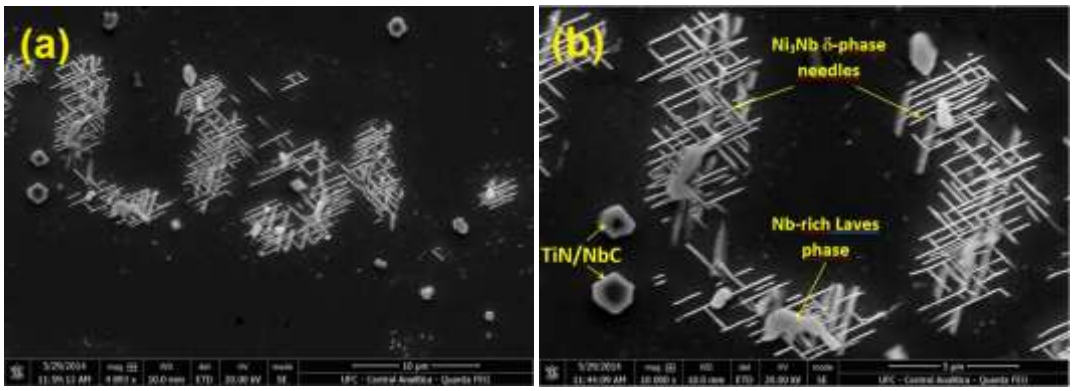

Figure 12. Details of TCP phases in the microstructure showing Ni_3Nb δ-phase needles together with Nb-rich Laves phases into the interdendritic region. Also a large cubic precipitate of NbTi complex carbide/nitrite was observed.

A chemical mapping acquired by EDS analysis for the main alloying elements is shown in Figure 13. The results indicated that the region where needles are precipitated is rich in Nb. This shows that the precipitation occurred preferably in the interdendritic region, since due to microsegregation, this zone is enriched in Nb. This region also has a high volume fraction of Laves phase rich in Nb, which is indicated in the Figure 13 by a dotted ellipse, and whose dissolution serves as a continuous supply of Nb to form the needle particles. No alterations were seen in the NbTi complex carbide/nitrides, or in the microstructure (indicated in the chemical maps by a dotted square).

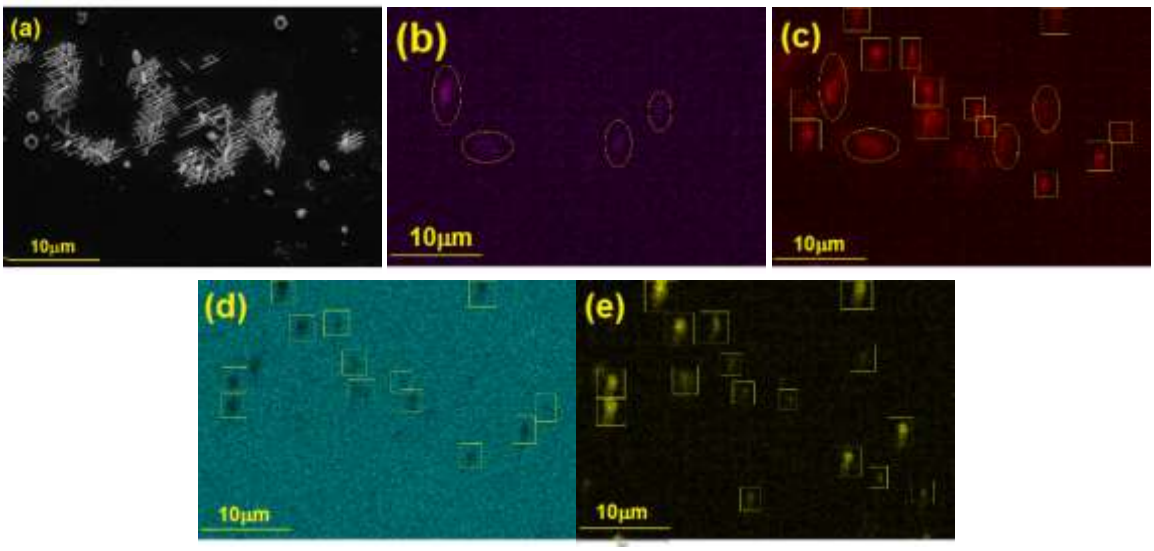

Figure 13. Chemical mapping obtained by EDS for the alloying elements: (a) SEM image, (b) Mo, (c) Nb, (d) Ni, and (e) Ti.

The 625 alloy weld metal showed a partial dissolution of the δ-phase up to 100 h aged at 950 °C, as can be seen in Figure 14a. In addition, several particles of the cubic complex carbides/nitrides and large blocks of NbC carbides that grow from preexisting carbides/nitrides can be seen. Also, but with a lower frequency, small particles of Laves phase were found, which were almost completely solubilized during the aging.

Figure 14b shows an early stage of nucleation of thin particles maidenly precipitated along grain boundaries and sub-grain boundaries. Figure 15a and 15b details the microstructure of the sample aged at 950 °C for 100h showing the apparent dissolution of the Ni_3Nb δ-phase needles and the presence of residual Nb-rich Laves phases in the interdendritic region. Also, some small cubic precipitates of the NbTi complex carbide/nitrite can be seen.

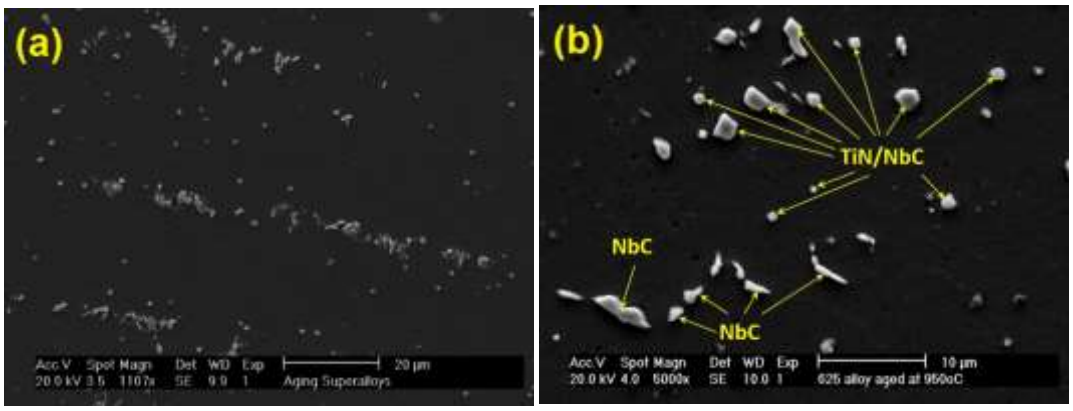

Figure 14. Examples of SEM micrographs using secondary electrons showing the aged microstructure at 950 °C for 100 hours taken from different positions.

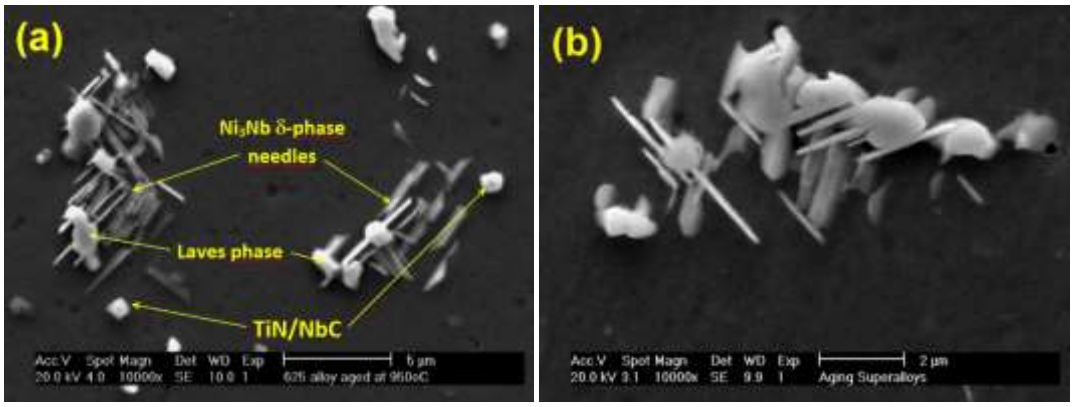

Figure 15. In detail, some secondary phases formed by Laves phase unsolved, δ-phase Ni_3Nb needle-like and some NbTi carbide/nitride cuboidal particles. Sample aged at 950 °C for 100h.

Figure 16a and Figure16b show representative micrographs of the treated material held at high temperatures for periods of up to 200 h. Here these Figures show an almost complete dissolution of the precipitates previously present in the microstructure. No precipitates with needled morphology can be seen, indicating that for this condition of aging, there was a complete dissolution of the δ-phase. Furthermore, Laves phase particles were not clearly observed, indicating also the complete dissolution of this phase. Therefore, for this condition of treatment, all TCP phases were dissolved and only cubic NbTi carbides/nitrides and large NbC carbides were present in the microstructure. In some regions, where there were

no large blocks of primary carbides (NbC), a fine precipitation along the grain boundaries and sub-grain boundaries together with the cubic NbTi carbides/nitrides can be seen, as shown in Figure 16c and Figure16d.

In order to increase the volume fraction of the analyzed material, increasing the peak intensities and to improve the identification of the phases formed in the weld metal, X-ray diffraction analyzes were performed on powder precipitates produced by the extraction technique in accordance with ASTM A923. XRD results showed the whole X-ray diffractogram recorded for the 10 h aged sample for the two temperatures, 650 and 950 °C (Figure 17). All the peaks were identified and indexed according to the standards, depending on the phases formed. For the sample aged at 650 °C for 10 h (Figure17a), the peaks corresponded to Laves phase, (Nb,Ti)C carbide and □-fcc matrix, which confirm the microstructural observations made by SEM. Some minor peaks were not associated to the phases and were indexed, for example, as iron oxide.

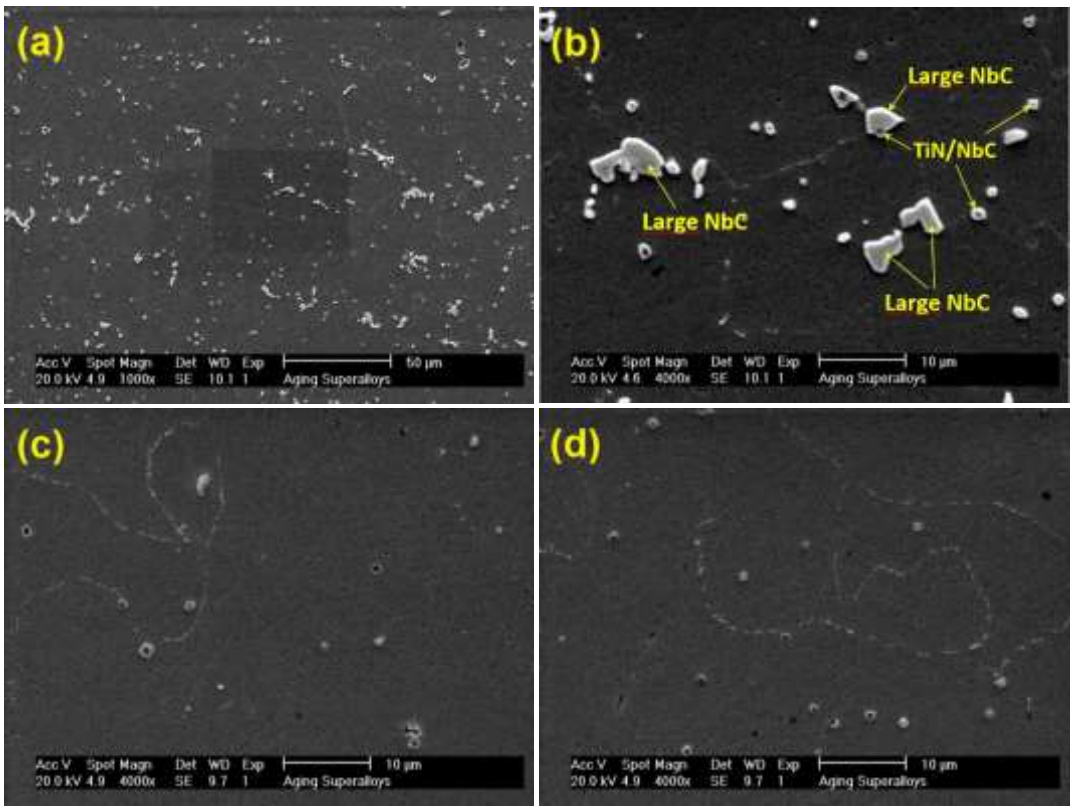

Figure 16. Examples of SEM micrographs using secondary electrons showing the aged microstructure at 950 °C for 200 hours taken from different positions. (a) and (b) Regions showing cubic NbTi carbides/nitrides and large NbC carbides; (c) and (d) Small cubic NbTi carbides/nitrides and a fine precipitation at the grain boundaries can be seen.

Figure 17b shows the diffractogram for the sample aged at 950 °C for 10 h. The peaks were identified and indexed as δ-phase, (Nb,Ti)C carbide and γ-fcc matrix, according to the ASTM A936 standard which covers the procedure for the isolation of TCP in nickel-based alloys. This result confirm that supposed Nb-rich needle-like phase is in fact δ-phase (Ni_3Nb).

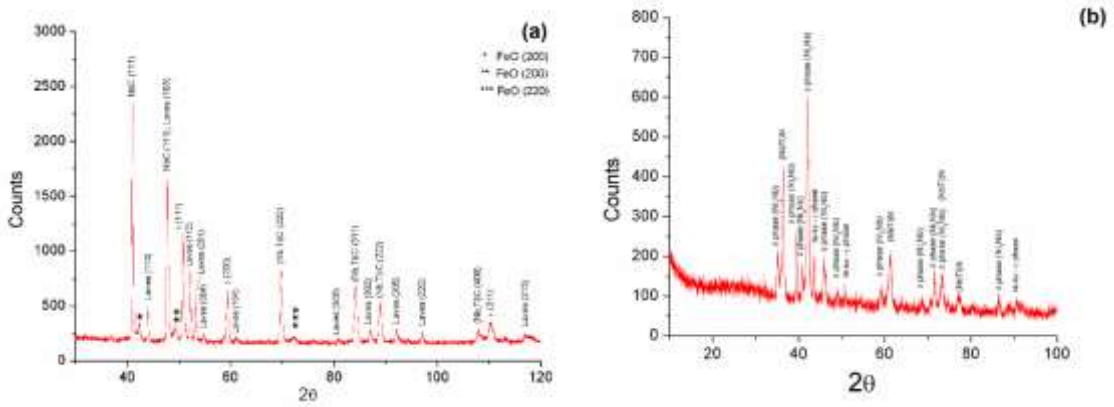

Figure 17. X-ray diffractograms from powder extraction concentrated in the secondary phases: (a) Sample aged at 650 °C for 10h; and (b) Sample aged at 950 °C for 10 h.

3.2 Mechanical properties evaluation

Figure 18 presents the results of the Charpy-V impact test. The analysis of variance (ANOVA) indicated that the absorbed energy in joules for both aging temperatures evaluated was significant, and varied as a function of aged time; the significance factor was below

0.00002 with a confidence of 95%. Table 4 shows that a high energy was absorbed for the as welded non-aged condition (0h), which was higher than 140 J. For the sample aged at 650 °C, there was a slight increase in toughness, from 142 to 151 J. On prolonging the aging time, there was a noticeable drop in the absorbed energy values for the times of 100 and 200 h. However, it is important to note that even after 200 hours of aging, the absorbed energy values were greater than 98 J. For the sample aged at 950 °C for 10 h aging time, there was a slight decrease in toughness, with a mean value of 121 J, while the energy absorbed for prolonged aging time (100h and 200h) increases again.

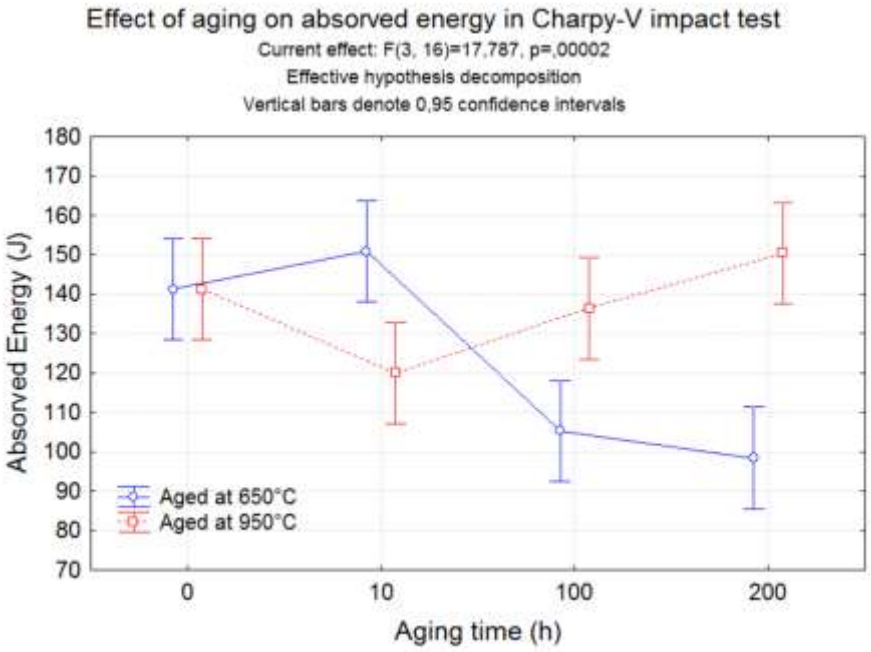

Figure 18. Results of the effect of aging temperature and time on the absorbed energy in the Charpy-V impact test, evaluated by analysis of variance.

Fractography analysis were performed on the surface of the Charpy-V impact test samples, in order to understand the details about the cracking behavior. The images were acquired using SEM operating in SE mode. Figure 19a and Figure 19b shows the

fractography images for the samples aged at 650°C for 10h and 200h, respectively. In both cases, ductile fracture characteristic was observed, with dimples structures.

Figure 20a and Figure 20b shows the fractography surface of the samples aged at 950°C for 10h and 200h, respectively. As observed in the fractography images of conditions aged at 650°C, the conditions aged at 950°C show the same ductile fracture characteristic.

An EDS mapping was obtained from the sample aged at 950 ° C for 200h, in order to detect the position of the secondary phases in relation with the fracture morphologies. The Figure 21 show the EDS mapping, which highlighted a high concentration of Nb and Ti into the dimples core, indicating thus the presence of precipitates in that region.

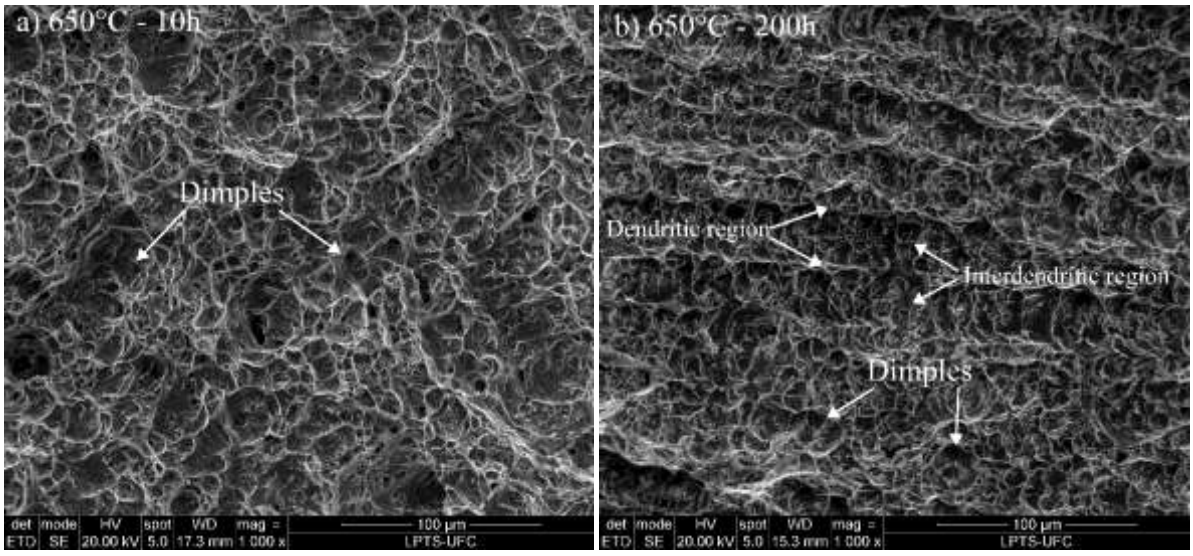

Figure 19. Fractography images of the conditions at 650°C for (a) 10h and (b) 200h.

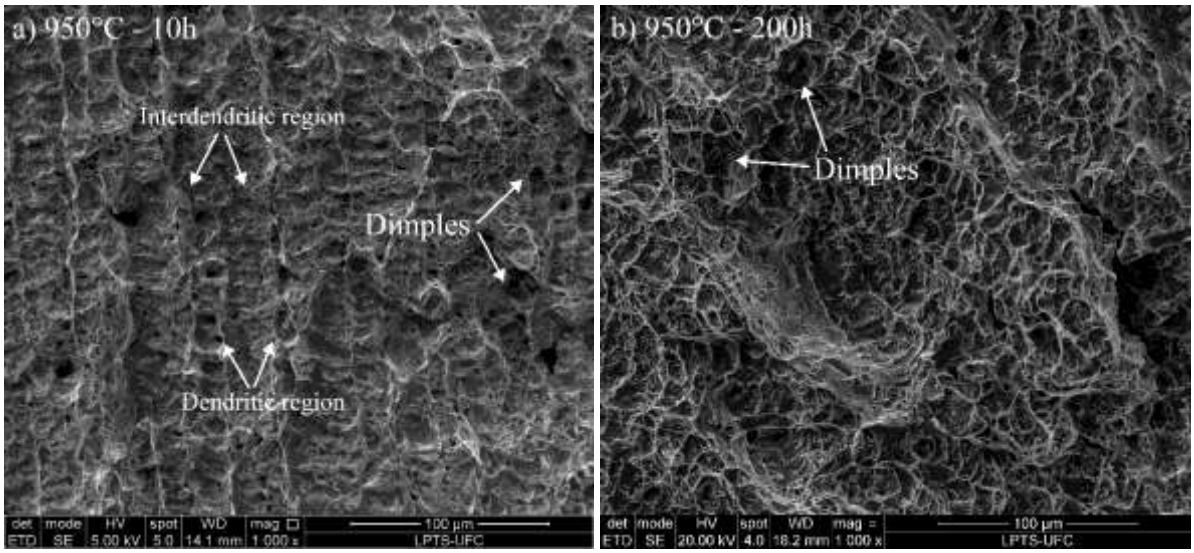

Figure 20. Fractography images of the conditions at 950°C for (a) 10h and (b) 200h.

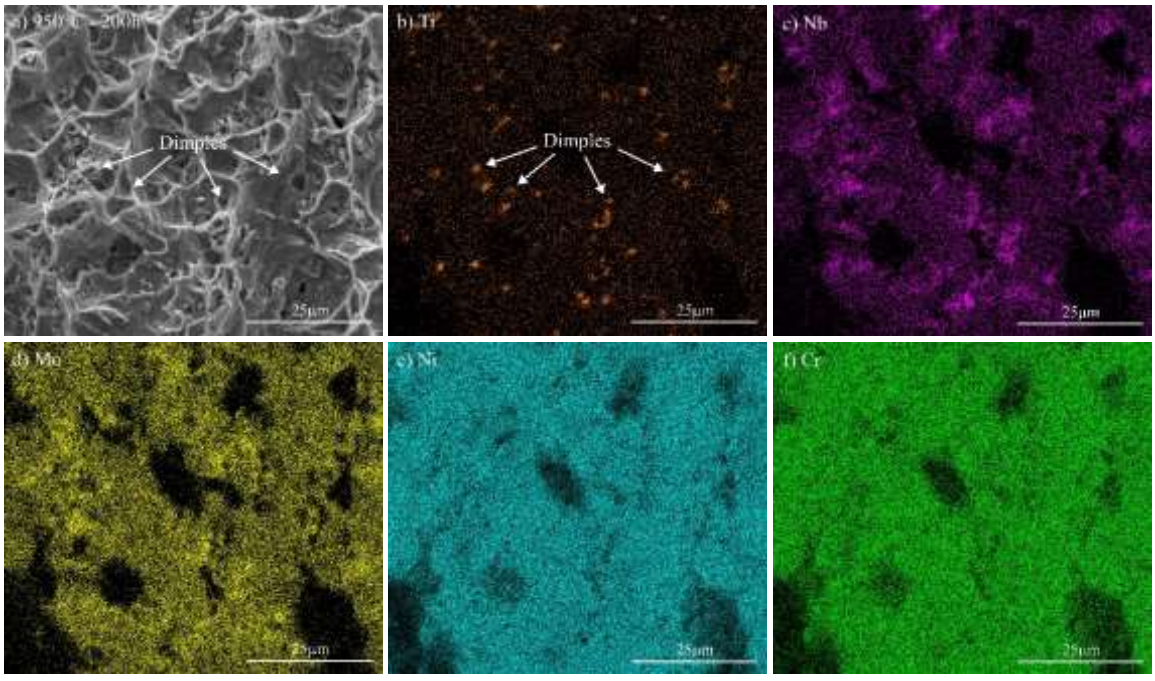

Figure 21. EDS mapping of the condition aged at 950°C for 200h. (a) Fracture surface image and yours respective chemical mapping of the elements (b) Ti, (c) Nb, (d) Mo, (e) Ni and (f) Cr.

The results of the micro hardness test were evaluated statistically by analysis of variance (ANOVA), see Figure 22. Again the statistical analysis shows that the hardness

varied with 95% confidence as a function of aged time, which is indicated by the significance factor below 0.00002. On evaluating the hardness curve for samples aged at 650 °C for a short period of time, no significant changes were found for the hardness, which remained at approximately 300 HV. However, increasing the exposure at high temperatures for long times such as 100h and 200 h, the hardness values rises to 437 HV and 443 HV, respectively. However, no difference in terms of hardness was found when the time of exposure was changed from 100h to 200 h. In addition to the statistical analysis, the variation in hardness was very significant in practice, since the difference from lower to higher values was almost 150 HV.

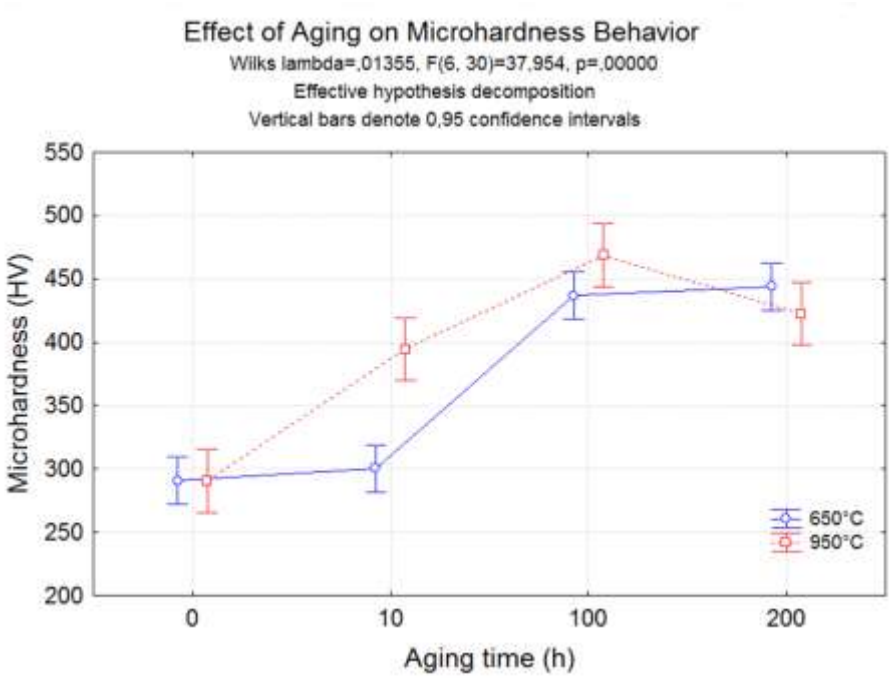

Figure 22. Results of the effect of aging temperature and time on the microhardness Vickers test evaluated by analysis of variance.

These results of hardness are in agreement with toughness behavior evaluated by the Charpy test. As shown in Figure 18, the samples aged at 650 °C during short times (0 and 10 h) had an impact energy between 140 to 150 J, whereas samples aged for 100 and 200 h

experienced a drop in this property. Since the hardness remained low for short aging times and underwent an increase for long times of exposure, the behavior of both properties are fully consistent, having a direct correlation, and indicate that a hardening mechanism took place during aging at 650 °C.

3.3 Physical properties evaluation

Albuquerque et al.,[25] presented the ultrasound velocities obtained using the transducers with frequencies of 4 and 5 MHz from the as-welded and aged at temperatures of 650 ºC for 10, 100 and 200 h samples, showing that ultrasound velocity decreased with the time of the aging heat treatment between 0 h (as-welded) and 100 h, and increased from 100 to 200 h. This behavior is more similar to results obtained by Charpy impact testing (Figure 18) and inversely proportional to hardness test (Figure 22).

However, Albuquerque et al.[25] did not consider inspection by ultrasound at temperatures of 950 ºC. Considering this to be important, Figures 23a and 23b present the results of ultrasonic velocity and attenuation, respectively. Based on these results, none significant modification of the ultrasonic measurements can be seen between the times of 0h to 200h. This behavior was completely different of the observed for microstructure, Charpy impact energy, see Table 4, as well as for hardness testing, Figure 22. We used the same conditions here as Albuquerque et al.[25]

According to measurements for 650°C aged conditions, non-destructive ultrasonic testing may be a promising tool for monitoring phase changes in the Inconel 625. Notwithstanding, based on 950°C aged condition it is demonstrated that this technique was sensitive to the microstructure. Therefore, it is clearly demonstrated that further studies on the application of non-destructive techniques for detection of microstructural changes in nickel-

based alloys by ultrasound should be developed to identify the technical capabilities and limitations.

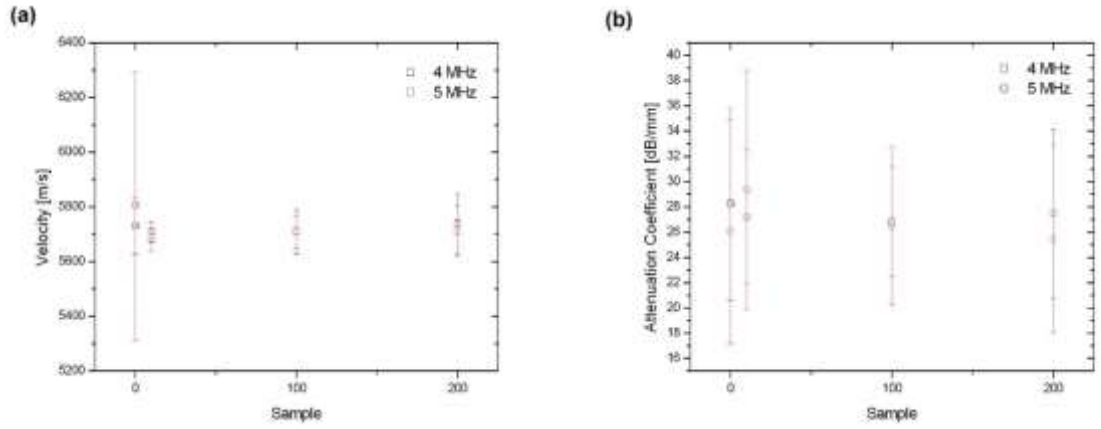

Figure 23. Ultrasonic a) velocity and b) attenuation measurements.

4. Discussion

Based on morphology and chemical composition performed by SEM-EDS analysis, the shapeless or eutectic particles were characterized as a TCP phase named Laves phase rich in Nb. These results are consistent with those reported by other authors evaluating the microstructure of the 625 alloy.[13,14,33]

In addition, the presence of cubic precipitates has been reported for the 625 alloy in the literature[33,34]. In another study, Silva et al.[33] confirmed by TEM analysis that these cubic precipitates observed in the microstructure, are a complex precipitate, consisting of a core with titanium nitride (TiN) surrounded by a niobium titanium carbide (NbTi)C.

Due to the high melting point of the NbTiN complex of carbides/nitrides (2,927 °C),[35] which is approximately twice the *liquidus* temperature of the 625 alloy, it is quite likely that they remain in the solid state within the volume of the liquid pool, differently of Laves phases which have a low melting point and are formed during the solidification reaction.

516 The microstructural evolution due to thermal aging was evaluated. Based on results is
517 clearly shows the formation of a discontinuous precipitation of very thin precipitates along the
518 grain boundaries for the sample aged at 650 °C for 100 h, whereas for the 200 h aging, a
519 continuous thin film precipitate along the grain boundaries has been observed. Chakravartty et
520 al.[16] evaluated a tube exposed to high temperatures ranging from 650 to 680 °C after
521 100,000h in service, and reported the formation of a thin layer of discrete carbide particles at
522 the grain boundaries, which were identified by TEM as $M_{23}C_6$ carbide. In addition, they found
523 large chunky $M_{23}C_6$ carbide particles at the grain boundaries.

524 Evans et al.[36] performed a series of creep testing of foils in air at 750 °C, and among
525 several significant changes in microstructure, they reported that the grain boundaries became
526 heavily decorated with precipitates, the majority of which were rhombohedral μ phase.
527 Additionally, a significant fraction of the grain boundary precipitates were found to be a Si-
528 rich variant of M_6C.

529 For the samples thermal aged at 950 °C the microstructural analysis shows the
530 presence of a new type of precipitation. The evaluation of the characteristics of this new phase
531 of needle particles, and their comparison with information reported in literature, showed that
532 these needles are most probable an ordered phase, whose stoichiometric composition is Ni_3Nb
533 and whose crystallographic structure is orthorhombic.[37,38] This phase is commonly observed
534 in Ni-based alloys containing Nb, such as 625 and 718 alloys, and can precipitate in a wide
535 range of temperatures and with various morphologies.[39]

536 As mentioned before, the interdendritic region is enriched in Nb due to
537 microsegregation during solidification, which makes the precipitation of phases rich in this
538 element possible. In fact, based on the results presented before, the δ-phase needles are
539 formed due to the favorable microchemistry in the dendritic region, having a high
540 concentration of Nb, which is the main element of δ-Ni_3Nb. However, this formation is

different from what has been observed for Ni-based superalloys with the addition of Nb in annealing conditions, when the δ-phase forms due to the decomposition of γ" phase, since both phases have the same stoichiometry but different crystal structures.

In this study, it was proven that Laves phase formed due to microsegregation during solidification which acts as a niobium reserve for the formation of the delta phase, and its dissolution over time, which acts as a necessary supply of the said element to the system, in order to have a continuous formation of the δ-phase.

According to Delueme et al.,[38-40] there are two kinds of δ-phases depending on the precipitation temperature. Phases formed in the temperature range (900 ºC–1000 °C) are named δ_{HT} and are characterized by coarse spheroidized or platelet formation. When the δ-phase is precipitated at lower temperatures (around 750 °C) during the ageing heat treatment, the phase is named δ_{LT}, precipitating in the form of a film or continuous strings along the grain boundaries.

Mittra et al.[18] suggested that lath-shaped δ-phases form in Alloy 625 when the alloy is held isothermally at 850°C. Since, this temperature is the nose temperature of the "C" curve corresponding to the δ-phase of Alloy 625; the presence of this ordered phase is expected in all the samples.

The literature reports that the formation of the δ-phase in significant quantities can be harmful to the mechanical properties for precipitation hardening Ni-based alloys.[39-41] In the case of the 625 alloy, which is a solid-solution strengthened alloy, the precipitation of the δ-phase is produced after long time exposure at high temperatures from the solid solution supersaturated. Precipitation of the δ-phase leads to reduced ductility.[40-42]

Another study showed that both hardness and tensile strength decreased with an increase in ageing temperature due to the precipitation and coarsening of the delta-phase.[41-43]

565 Therefore, the precipitation of the δ-phase in weld metal of the 625 alloy aged at 950 °C
566 found in this study may have a harmful effect on the mechanical properties.

567 According the detailed microscopic analysis performed for samples thermal aged at
568 950 °C, was found that many particles remain in microstructure even for longest time of
569 exposure. This behavior indicates that the aging conditions (time and temperature) were not
570 favorable to dissolve completely the TCP phases. Cai et al.,[42-44] studied the dissolution
571 kinetics of the δ-phase in the 718 alloy, which has additional Nb, and mentions that the δ-
572 phase can be fully dissolved into the matrix after a heat treatment at 1020 °C for more than
573 2h. However, when held at 980 and 1000 °C, a certain amount of δ-phase was still found in
574 the alloy, even after more than 6h. In this case, the chemical inhomogeneity due to
575 microsegregation and the formation of Nb-rich phases during solidification makes the
576 precipitation and dissolution kinetics of the δ-phase different in the 625 nickel-based weld
577 metals.

578 Xing et al.[43-45] evaluated the effect of post-weld heat treatment temperature on the
579 microstructure of Inconel 625 and found that at 950 °C, the γ" phase and the δ phase
580 disappeared, similar to the behavior observed in this study. In addition, the authors reported
581 that small amounts of blocky secondary phases appeared at the grain boundaries, which were
582 identified by TEM analysis as M_6C-type carbide, with a face-centered cubic (fcc) structure
583 and lattice parameter of 1.12 nm. Thomas & Tait[19] also reported some precipitates at grain
584 boundaries. The EDS analysis of those particles indicated that they were rich in molybdenum
585 and niobium, which has led the authors to conclude that they were carbides of the M_6C type.
586 Similar results were found by Ferrer et al.[44-46] and Burke & Miller.[45-47] This reinforces the
587 suspicions that the thin precipitation along the grain boundaries are particles of M_6C carbides.

In addition, the results obtained by XRD analysis were consistent with the ones reported in literature.[46-48] This result confirms that most probably the whole volume of Laves phase were consumed during the aging treatment, providing the niobium necessary for the formation the of δ-phase. This behavior is in agreement with the microstructural observations performed by SEM.

Evaluating the results obtained in Charpy-V impact test for 650 °C aged condition was found that energy absorbed varied as a function of aged time. As reported by Thomas & Tait,[19] the heat treatment at comparatively modest temperatures ranging from 650 to 700°C and for reasonable times of 6-12 h proved beneficial in regenerating the toughness of some alloys.

Notwithstanding, the behavior exhibited by the post aging material was consistent with the microstructural changes previously reported. From the as-welded sample to 10 h aged sample, a small dissolution of Laves phase was observed, this implicated in an increase in toughness. For longer times of exposures (100 - 200 h), the main microstructural changes were the dissolution of the Laves phase and precipitation of nanometric particles at grain boundaries. If on one hand the decrease in the volume fraction of Laves phase has proved interesting to improve the impact resistance, on the other hand the precipitation of finely dispersed nanosized particles at grain boundaries and sub-grain boundaries was found to be harmful to toughness (impact test).

Also for 100 and 200 h of exposure at 650 °C the presence of large blocks of NbC carbides and cubic NbTi complex were found, which remained from solidification. However, these particles probably have low or no effect on toughness, since in another study, carried out by Silva et al.[48-49] evaluating the effect of the interpass temperature on mechanical properties in weld metal of 625 alloy, these particles were found. The results of the Charpy-V impact test at cryogenic temperature (-196 °C) showed no significant differences among the

weld conditions and the level of energy absorbed was higher than 100 J. Therefore, it is believed that the harmful effect on impact strength was due to the precipitation along the grain boundaries.

For the conditions aged at 950 °C, a different behavior was observed. There was a significant drop in fracture toughness for the sample with 10 h treatment. Then, it was perceived an increasing toughness, returning at about the same level as-welded condition. This drop in the impact strength for the sample of 950 °C and 10 h may be attributed to precipitation of the delta phase needles precipitated in interdendritic regions. This indicates a detrimental effect of precipitation. For 100h treatment at 950 °C, there was a significant reduction in the amount of the delta phase, which resulted in a recovery of the impact resistance. For 200 h treatment, as reported above, a microstructure consisting of only large blocks of Nb carbides and cubic precipitates of NbTi carbides/nitrides was found. Although nanometric precipitation along the grain boundaries has been reported, this was less intense compared to those observed for aging at 650 °C. Therefore, the results of impact resistance indicate that this microstructural condition was not detrimental to the weld properties.

According Mittra et al.,[18] the ductility of which alloy after 1200 h of aging at 540°C (813 K) is seen to be much higher than that of all samples aged at 700°C (973 K) and 850°C (1123 K). The formation of large plate-shaped δ phases at 850°C (1123 K) results in lower strength and ductility compared to that of 700ºC (973 K). A considerable amount of δ formation after 1200 h of isothermal holding is also seen to produce {111} plane facets. However, fine micro-dimples of uniform size are seen along the facets of the fractograph. Since the ductility and toughness of the Ni-fcc matrix is very high, the reduction in impact strength was lower than expected for aged conditions, but its influence was enough to observe the behavior that was directly linked with the microstructural changes.

Thomas & Tait[19] confirmed that the improvement in properties after heat treatment at 650-700 °C was most successful for the recovery of some toughness as observed in the as-received material. However, the toughness still remained low compared to new material. It is possible that this was due to the formation of the orthorhombic δ phase. Another works[49-50] has found that a reduction in Charpy impact energy to around 180 to J/cm^2 occurred as a result of intermediate temperature ageing, which was attributed primarily to the formation of the orthorhombic δ phase.

About fractography images of the conditions aged at 650°C, it was observed that the changes in toughness do not reflected in the fractography behavior. The ductile characteristic observed in the recovered condition aged for 10h was the same noted for the worst toughness condition, which was aged for a long period of exposure (200h). For all conditions aged at 950°C were observed a ductile fracture, even for 10h of treatment that show the lowest impact toughness. According to Mittra et al.,[18] the most cases of heat treatment performed on Inconel 625, the nickel matrix hold the ductile fracture characteristic even for significant changes in the microstructure, since the nickel matrix holding the resistant to impact test.

As shown previously, the fractographies indicates the presence of some small particles into the cavities of the dimples. In addition, the fracture features reveled some similarity with microstructure, in which the crack propagation pattern and dimples were aligned along a specific direction (Figures 19b and 20a), similar to dendrite growth orientation assumed during solidification.

The presence of precipitates located into the dimples cores suggest that the interdendritic regions observed in microstructure were the prefer region to open cavities under deformation. In this case, the precipitates acted as pinning points, blocking the movement of dislocations and preventing the plastic deformation of the Ni matrix, which is in accordance

with reported by Sheng et al.[51] On the other hand, the dendrite core regions are precipitate free and show an impoverishment of solid solution elements such as Mo, Nb and Ti, when compared with the interdendritic regions, due to the microsegregation phenomena,[33] which probably reduced the mechanical strengthening and improve the ductility of the dendrites formed by γ-fcc matrix.

The EDS mapping in the sample aged at 950°C for 200h, highlighted the presence of Nb-rich carbides and cubic precipitates of NbTi carbides/nitrides located mainly in the dimples cores, giving thus the support to the hypothesis that the precipitates act as barrier to movement of dislocations.

Thus, is possible to correlate the fracture surface with microstructure, assuming that the dimples arise from small precipitates into interdendritic regions, and the dendrite core which is precipitate free, is necked and sheared during further yielding.

Concerning to the micro hardness test, the results were also evaluated and its behavior was statistically significant, which varied as a function of aged time. Thomas & Tait[19] evaluated the hardness of an aged 625 alloy and found 230 HV_{30} to annealed material conditions, while for samples aged at 650 °C after 3, 6 and 12 hours resulted in hardness values ranging from 303 to 317 HV_{30}. In fact, the 10 h aged sample achieved hardness similar to that found by Thomas & Tait[19] for aged materials (300 HV). Nonetheless, the materials studied were not weld metals, therefore the initial precipitation of Laves phase due to solidification would probably make the hardness higher if compared to annealing conditions. In addition, the authors reported that the results of hardness for a pipe that had been in service for approximately 50,000 h at 500 °C, a value of 444 HV_{30} was found. Kirman and Warrington[50, 52] also reported that the aged material at 650 °C achieved a peak hardness of 400 HV after about 500 h. Therefore, the hardness values measured for samples aged at 650

°C for higher time of exposure evaluated in this study (100 and 200 h) are in agreement with those in the literature.

Considering the samples aged at 950 °C, the hardness measures increased continuously from 0 until 100 h, going up from 291 HV (0 h) to 395 HV (10 h) and 469 HV for aging times of 100 h. However, on increasing the aging time to 200 h, the hardness decreased to 422 HV. This behavior shows that intense δ-Ni_3Nb phase precipitation after 10h exposure, produces an increment of 100 HV approximately, compared to the as-welded condition (0h).

Nevertheless, the maximum value of hardness was achieved when the 625 alloy weld metal was exposed to 950 °C for 100 h. For this particular condition, the microstructure shows a significant reduction in the amount of δ-phase precipitated. Also for 200 h of exposure, the hardness value does not drop significantly, even experiencing an expressive microstructural variation, denoted by a complete delta-phase dissolution and a very low amount of particles precipitated, according to SEM analysis.

Comparing the hardness values with the toughness results obtained in the Charpy-V impact test, it was possible to observe that the δ-phase, whose precipitation was quite intense and highlighted an embrittlement effect denoted by a drop in impact resistance, did not cause any significant effect on hardness. On the other hand, for the condition of maximum hardness in the treatment of 950 °C (100h), the microstructure had a very smaller amount of delta phase and experienced a higher impact resistance when compared to the 10 h aged condition. Thereby, it was not possible to establish a direct correlation between hardness and impact resistance for the 625 alloy aged at 950 °C.

Unfortunately, the microstructural changes that have caused the hardness behavior were not observed by microscopic techniques used in this study. The main microstructural change from 0 and 10 h to 100 and 200 h at 650 °C was the Laves phase dissolution and δ-Ni_3Nb precipitation followed by dissolution together Laves phase at 950°C, which may supply for example the Nb necessary to precipitation of another phase such as γ" (Ni_3Nb).

As the analytical techniques used are not able to confidently identify other precipitates one should not assume the probable formation of γ', γ" or $Ni_2(Cr,Mo)$ dispersion strengthening phases. Based on Kumar et al.[37-53], who studied a service tube of Inconel 625 alloy exposed to ~600 °C for ~60,000 h, a short duration aging at 650 ºC up to 10 h caused a dissolution of the $Ni_2(Cr,Mo)$ phase. When the alloy was aged at 850 ºC for 1 h, there was a complete dissolution of both γ" and $Ni_2(Cr,Mo)$ precipitates.

There was no evidence of any other phase present in the SEM analysis, such as Laves, γ' or γ". However, phases such as γ' and γ" cannot be identified by XRD due to their small size. Therefore, the possibility that there was formation of these phases cannot be discarded, since, as is well established by numerous studies, that these phases are formed together with Laves and delta phases in aged conditions ranging from 600 °C to 900 °C[43-47]. Therefore, as previously mentioned, it is believed that some γ" may have precipitated, which would justify the increase in hardness.

4. Conclusions

Based on the results obtained experimentally in this study about the effect of aging temperature and exposure time on the microstructure and mechanical properties of 625 alloy weld metal, the following conclusions can be pointed out:

731 (1) The microstructural evolution at 650 °C revealed that the Laves phase rich in Nb produced
732 by microsegregation during solidification was continuously dissolved with the increase of
733 exposure time and an intense precipitation of nanosized particles along the grain boundaries
734 was observed. For the TiNb complex carbides/nitrides found in the as-welded condition, no
735 change was observed.
736 (2) For the aging temperature of 950 °C for a short exposure time, there was an intense
737 precipitation of Ni_3Nb δ-phases along the interdendritic region, and the Laves phase was
738 partially dissolved and replaced by δ-phases. For the longest exposure times, the δ-phases
739 were completely dissolved, and only the TiNb complex carbides/nitrides remained together
740 with a very fine precipitation along γ-fcc matrix grain boundaries.
741 (3) In terms of the Charpy-V impact test results, the energy absorbed for 0 and 10 h samples
742 aged at 650 °C was kept almost the same; however there was a decrease for the longer
743 exposure times such as 100 and 200 h. When the aging temperature was increased to 950 °C,
744 the impact energy absorbed fell at 10h exposure but increased for longer exposure times. The
745 impact energy values achieved were regarded as very good, and in general were higher than
746 100 J.
747 (4) The aging effect at 650°C on the hardness behavior showed a good correlation with the
748 response of impact resistance, since when there was an increment in hardness there was a
749 drop in the impact energy absorbed. The same behavior was not found for the treatment at
750 950 °C, in which the lower impact energy did not correspond to the maximum hardness
751 condition.
752 (5) The non-destructive techniques for detection of microstructural changes in nickel-based
753 alloys based on ultrasound signals was not able to identify the microstructural changes for the
754 temperature of 950 ºC, but demonstrated to be a very promising technique for monitoring

phase changes in the nickel-based alloys for temperature of 650 ºC. Thus, requires further studies to identify the technical capabilities and limitations for temperatures above 650 ºC.

Acknowledgments

All authors are also grateful for the support given by the following laboratories of the Federal University of Ceará: Welding Research & Technology Laboratory (LPTS-UFC), Materials Characterization Laboratory (LACAM), Center of Non-Destructive Testing (CENDE), X-ray Difraction Laboratory (LRX-UFC), Analytical Central - UFC/CT-INFRA/MCTI-SISNANO/Pró-Equipamentos CAPES. The authors would also like to thank the financial support given by the National Council for Research and Development (CNPq), Research and Projects Financing (FINEP), Coordination for the Improvement of People with Higher Education (CAPES) and finally to Petróleo Brasileiro S/A (Petrobras) in Brazil. Victor Hugo C. de Albuquerque received support from the CNPq via grants #470501/2013-8 and #301928/2014-2.

References

[1] F.G. Hodge: JOM, 2006, vol. 58, pp. 28–31.

[2] C.T. Sims, N.S. Stoloff, W.C. Hagel. Superalloys II. John Wiley & Sons, New York, USA, 1987.

[3] J. N. Dupont, S. Babu, S. Liu: Metall. Mater. Trans. A, 2016, vol. 44, pp 3385–3410.

[4] P.M. Mignanelli, N.G. Jones, K.M. Perkins, M.C. Hardy, H.J. Stone: Mater. Sci. Eng. A, 2015, vol 621, pp. 265–271.

778 [5] E. M. Miná, Y. C. da Silva, J. Dille, C. C. Silva: Metall. Mater. Trans. A, 2016, vol. 47A,
779 pp 6138–6147.

780 [6] M. Sundararaman, L.Kumar,G. Eswara Prasad, P. Mukhopadhyay, S. Banerjee: Metall.
781 Mat. Trans. A, 1999, vol. 30A, pp. 41–52.

782 [7] S.S. Hosseono, S. Nategh, A.A. Ekrami: J. Alloys Compd., 2012, vol. 512, pp. 340–350.

783 [8] L. M. Suave, J. Cormier, P. Villechaise, A. Soula, Z. Hervier, D. Bertheau, J. Laigo:
784 Metall. Mater. Trans. A, 2014, Vol. 45A, pp 2963–2982.

785 [9] Y.J. Zhang, Y.J. Huang, L. Yang, J.G. Li: J. Alloys Compd., 2013, vol. 570, pp. 70–75.

786 [10] C.C. Silva, C.R.M. Afonso, A.J. Ramirez, M.F. Motta, H.C. Miranda, J.P. Farias: J.
787 Alloys Compd., 2016, vol. 684, pp. 628-642.

788 [11] D. Verdi, , M.A. Garrido, C.J. Múnez, P. Poza: Mater. Des., 2015, vol. 67, pp. 20–27.

789 [12] T.E. Abioye, D.G. McCartney, A.T. Clare, Laser cladding of Inconel 625 wire for
790 corrosion protection, J. Mater. Process. Technol. 217 (2015) 232-240.

791 [13] J.N. Dupont, Solidification of an Alloy 625 Weld Overlay, Metall. Mater. Trans. A. 27A
792 (1996) 3612-3620.

793 [14] M. J. Cieslak, T. J. Headley, T. Kollie, A. D. Romig: Metall Trans A, 1988, vol. 19A,
794 pp. 2319-2331.

795 [15] J. N. DuPont, C. V. Robino, J. R. Michael, M. R. Notis, A. R. Marder: Metall Mater
796 Trans A, 29A (1998), pp. 2785-2796.

[16] J. K. Chakravartty, J. B. Singh, M. Sundararaman: Mater. Sci. Technol. 2012, vol. 28, pp. 702-710.

[17] P. Liu, J.O. Nilsson: Mater. Sci. Technol. 1990, vol. 6, pp. 764-771.

[18] J. Mittra, S. Banerjee, R. Tewari, G.K. Dey: Mater. Sci. Eng. A., 2013, vol. 574, pp. 86-93.

[19] C. Thomas, P. Tait: Int. J. Press. Vessels Pip.: 1994, vol. 59, pp. 41–49.

[20] S. Floreen, G.E. Fuch, W.J. Yang. In: E.A. Loria (Ed.), Superalloys 718, 625, 706 and Various Derivatives, TMS, Warrendale, PA (1994), pp. 13–37.

[21] J. J. Schirra, R. H. Caless, R. W. Hatala. In: E. A. Loria (Ed.), Superalloys 718, 625, 706 and Various Derivatives, TMS, Warrendale, PA (1991), pp. 375–388.

[22] V.H.C. Albuquerque, C.C. Silva, T.I.S. Menezes, J.P. Farias, J.M.R.S. Tavares: Microsc. Res. Tech., 2011, vol. 74, pp. 36-46.

[23] V. L. A. Freitas, V. H. C. Albuquerque, E. M. Silva, A. A. Silva, J. M. R. S. Tavares: Mater. Sci. Eng. A: 2010, vol. 527, pp. 4431-4437.

[24] E.M. Silva, V.H.C. Albuquerque, J.P. Leite, A.C.G. Varela, E.P. Moura, J.M.R.S. Tavares: Mater. Sci. Eng. A., 2009, vol. 516, pp. 126-130.

[25] V. H. C. Albuquerque, C. C. Silva, P. G. Normando, E. P. Moura, J. M. R. S. Tavares: Mater. Des., 2012, vol. 36, pp. 37-47.

[26] T. M. Nunes, V. H. C. Albuquerque, J. P. Papa, C. C. Silva, P. G. Normando, E. P. Moura, J. M. R. S. Tavares: Expert Syst. Appl., 2013, vol. 40, pp. 3096-3105.

817 [27] V.H.C. Albuquerque, C.V. Barbosa, C. C. Silva, E.P. Moura, P.P. Rebouças Filho, J.P.
818 PAPA, J.M.R.S. Tavares: Sensors, 2015, vol. 15, pp. 12474-1249.

[28] F.E. Silva, F.N.C. Freitas, H.F.G. Abreu, L.L. Gonçalves, E.P. Moura, M.R. Silva: J. Mater. Sci., 2011, vol. 46, pp. 3282-3290.

819 [29] E. M. Silva, J. P. Leite, F. A. França Neto, W. M. L. Fialho, V. H. C. Albuquerque, J. M.
820 R. S. Tavares: J. Test. Eval., 2016, vol. 44, pp. 2003-2013.

821 [30] P. G. Normando, E. P. Moura, J. A. Souza, S. S. M. Tavares, L. R. Padovese: Mat. Sci.
822 Eng. A, 2010, vol. 527, pp. 2886-2891.

823 [31] ASNT 147/147WCD, Nondestructive Testing Handbook, 3rd ed., vol. 7, Ultrasonic
824 Testing, American Society for Nondestructive Testing, 2007.

825 [32] C.T. Sims, N.S. Stoloff, W.C. Hagel (Eds.) Superalloys II. Wiley, New York (1987).

826 [33] C. C. Silva, H. C. Miranda, M. F. Motta, J. P. Farias, C. R. M. Afonso, A. J. Ramirez: J.
827 Mater. Res. Tech., 2013, vol. 2, pp. 228–237.

828 [34] C. C. Silva, C. R. M. Afonso, A. J. Ramirez, M. F. Motta, H. C. Miranda, J. P. Farias:
829 Sold. Insp., 2012, vol. 17, pp. 251-263.

830 [35] W. Lengauer. Transition metal carbides, nitrides and carbonitrides. R. Riedel (Ed.),
831 Handbook of ceramic hard materials, vol. 1Wiley–VCH, Weinheim (2000), pp. 202–252.

832 [36] N.D. Evans, P.J. Mazias, J.P. Shingledecker, Y. Yamamoto: Mater. Sci. Eng. A, 2008,
833 vol. 498, pp. 412–420.

834 [37] M. Sundararaman, P. Mukhopadhyay, S. Banerjee: Metall. Trans. A, 1988, vol. 19A, pp.
835 453-465.

836 [38] S.H. Zhang, H.-Y. Zhang, M. Cheng: Mater. Sci. Eng. A: 2011, vol. 528, pp. 6253–6258.

837 [39] N. Kashaev, M. Horstmann, V. Ventzke, S. Riekehr, N. Huber: J. Mater. Res. Tech.,
838 2013, vol. 2, pp. 43-47.

839 [40] J. Deleume, J.-M. Cloué, E. Andrieu: J. Nucl. Mater, 2008, vol. 382, pp. 70–75.

840 [41] D.D. Krueger. In: Loria EA, editor. Superalloy 718 - metallurgy and application. TMS;
841 1989. p. 279–96.

842 [42] V. Shankar, M. Valsan, K. Bhanu Sankara Rao, S.L. Mannan: Scripta Mater, 2001, vol.
843 44, pp. 2703–2711.

844 [43] M.D. Mathew, K. Bhanu Sankara Rao, S.L. Mannan: Mater. Sci. Eng. A, 2004, vol. 372,
845 pp. 327–333.

846 [44] D. Cai, W. Zhang, P. Nie, W. Liu, M. Yao: Mater. Charact. 2007, vol. 58, pp. 220–225.

847 [45] X. Xing, X. Di, B. Wang: J. Alloys Compd., 2014, vol. 593, pp. 110–116.

848 [46] L. Ferrer, B. Pieraggi, J.F. Uginet: *Superalloys 718, 612 and Various Derivatives*, E. A.
849 Loria, ed., TMS, Warrendale, PA, 1991.

850 [47] M.G. Burke, M.K. Miller: *Superalloys 718, 612 and Various Derivatives,* E. A. Loria,
851 ed., TMS, Warrendale, PA, 1991.

852 [48] C.B. Shoemaker, A.H. Fox, D.P. Shoemaker: Acta Cryst. 1960, vol. 13, pp. 585-587.

853 [49] C.C. Silva, H.C. Miranda, M.F. Motta, D.C.F. Ferreira, R.R. Marinho, G. Dalpiaz:
854 Mater. Sci. Forum, 2014, vol. 783-786, pp. 2816-2821.

855 [50] M. Kohler: *Superalloys 718, 612 and Various Derivatives,* E. A. Loria, ed., TMS,
856 Warrendale, PA, 1991.

857 [51] J. Sheng, S. Huang, J.Z. Zhou, Z.W. Wang: Eng. Fract. Mech. 2017, vol. 169, pp. 99-
858 108.

859 [52] I. Kirman, D.H. Warrington: Metall. Trans. A., 1970, pp. 2667-2675 .

860 [53] A. Kumar, V. Shankar, T. Jayakumar, K.B.S. Rao, B. Raj: In: Proc. Europ. Conf.
861 Nondestr. Test., J. Serrano, ed., Barcelona, Spain, 2002.

862

863

864

865

866

867

868

869

870

FIGURE CAPTIONS

Figure 20. Experimental setup used in the welding process: (a) robotic system, (b) GTAW guide wire feed and torch.

Figure 21. Schematic diagram showing: (a) the location and orientation of the Charpy-V specimens taken from the weld cladding; (b) dimensions of the Charpy impact specimens.

Figure 22. (a) SEM micrographs using secondary electrons showing the Ni-fcc matrix and the secondary phases of the sample as-welded, (b) In detail, an agglomerate formed by a cuboidal precipitate of NbC/TiN wrapped by Nb-rich Laves phase, (c) EDS spectrum of Laves phase, (d) EDS spectrum of NbC/TiN cuboidal precipitate.

Figure 23. (a) Representative microstructure of the sample aged at 650^{o}C for 10 hours; (b) Detail of the Eutectic-like Laves phase and some cuboidal precipitates of NbTi carbides/nitrides.

Figure 24. (a) Representative microstructure of the sample aged at 650^{o}C for 100 hours; (b) Detail decomposition of the Laves phase with significantly reduced dimensions, and where some cuboidal precipitates of carbides/nitrides can also be seen.

Figure 25. (a) Representative microstructure of the sample aged at 650 ^{o}C for 200 hours showing practically only NbTi carbides/nitrides; (b) Detail showing a small particle of Laves phase reminiscent of the incomplete decomposition.

Figure 26. (a) Grain boundary precipitation in an early stage observed in the sample aged at 650 ^{o}C for 100 hours; (b) Grain boundary precipitation like continuous film observed in the sample aged at 650 ºC for 200 hours.

Figure 27. (a) Microchemical analysis of nano-sized precipitates along the grain boundary performed by EDS; (b) EDS spectrum of the particle; and (c) Spectrum of the matrix adjacent to the precipitate.

TABLE CAPTIONS

Table 1. Chemical composition in percent weight of the weld metal/coating and base metal.

Table 2. Results of the chemical composition analysis performed by SEM/EDS on: (a) Laves phase and (b) Complex NbTi carbide/nitride.

Table 3. Mean weld metal chemical composition in % wt.

Table 4. Impact strength of as-welded and aged condition obtained by the Charpy-V impact test.

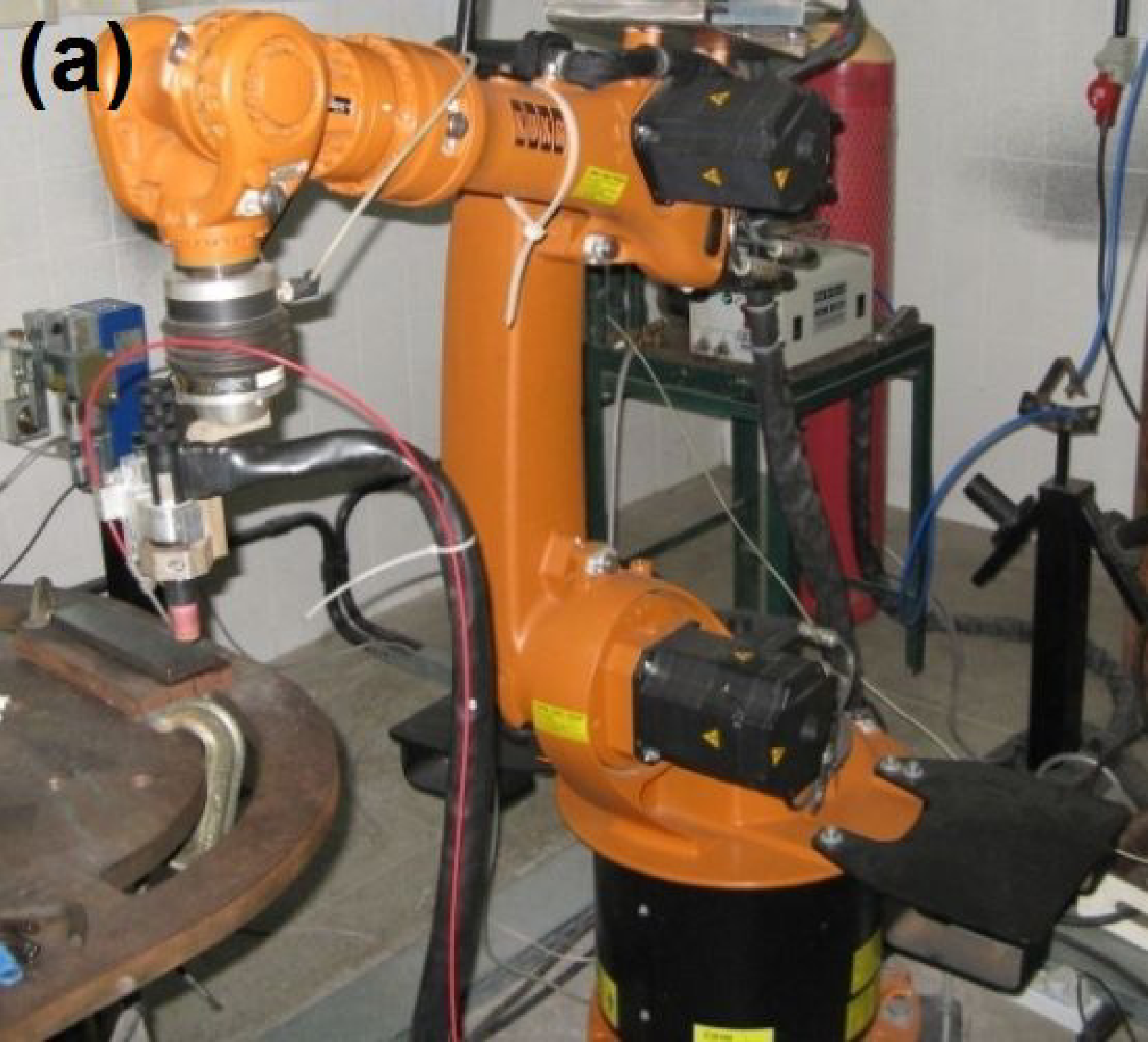
(a)


(b)

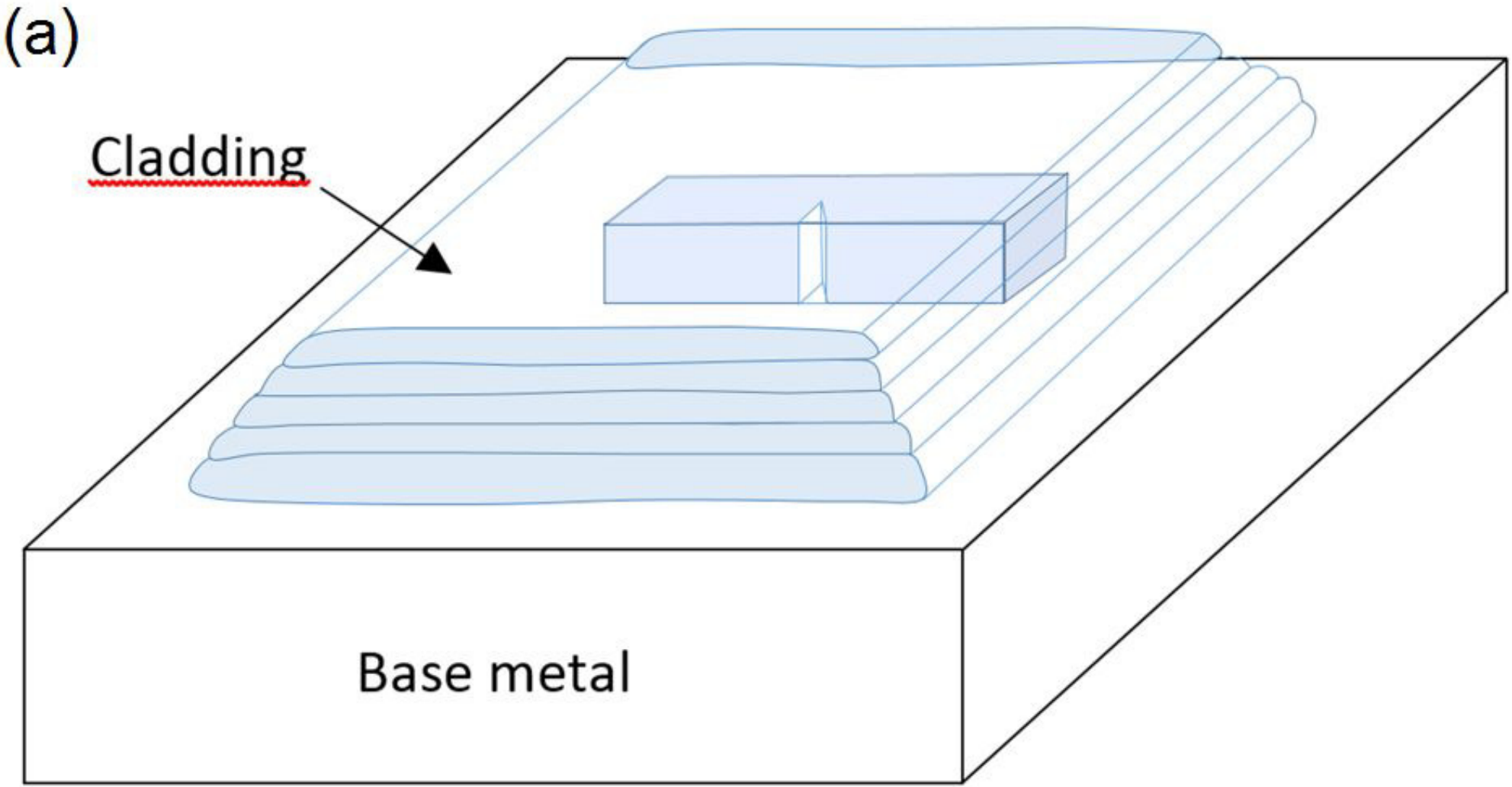
(a)
Cladding
Base metal

(b)

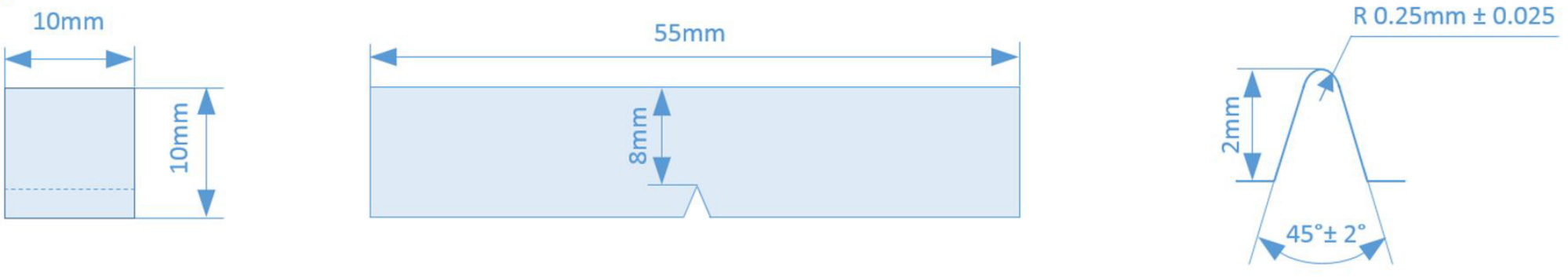

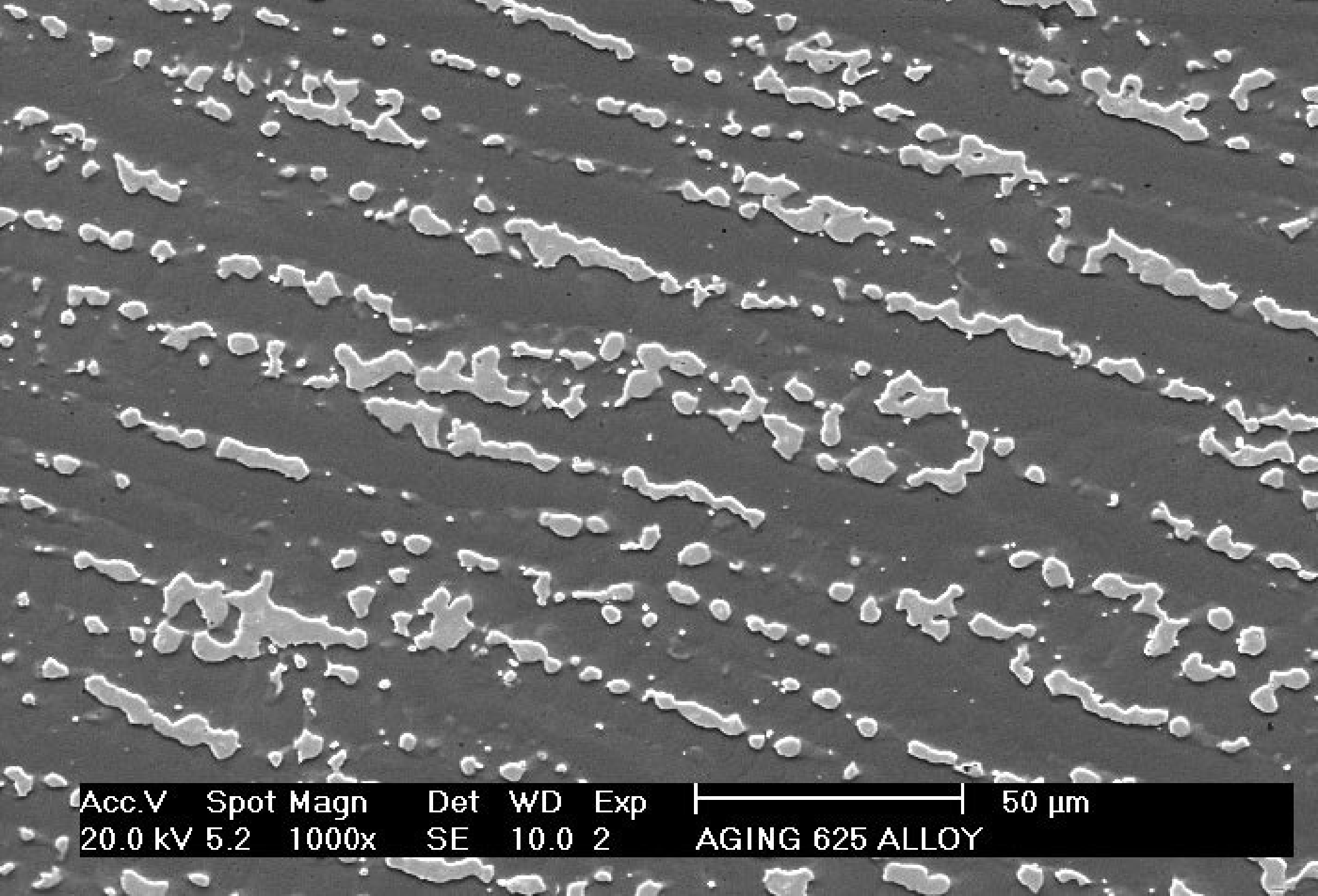
Acc.V Spot Magn Det WD Exp
50 µm
20.0 kV 5.2 1000x SE 10.0 2 AGING 625 ALLOY

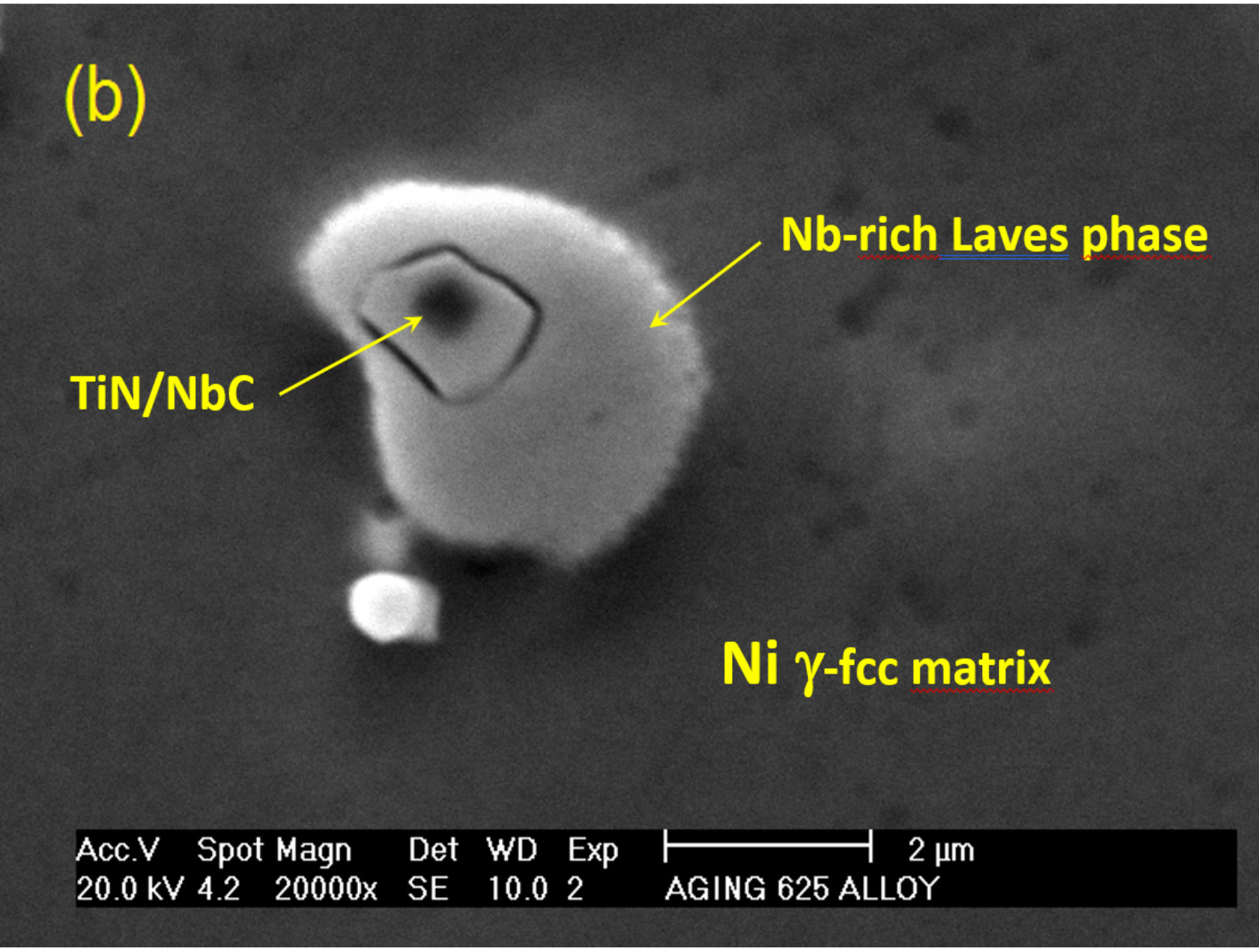
(b)
Nb-rich Laves phase
TiN/NbC
Ni γ-fcc matrix
Acc.V Spot Magn Det WD Exp
20.0 kV 4.2 20000x SE 10.0 2
2 µm
AGING 625 ALLOY

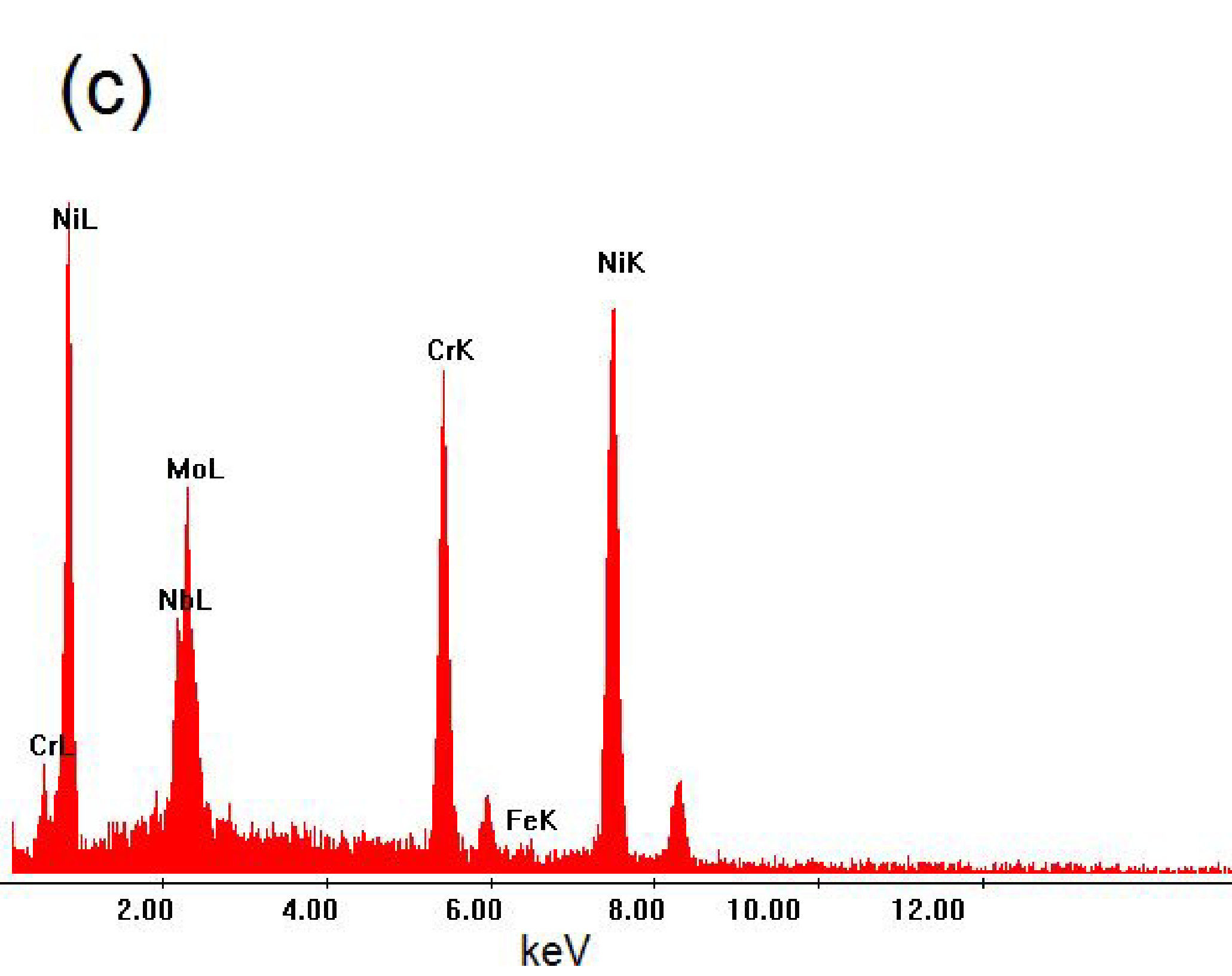
(c)
NiL
NiK
CrK
MoL
NbL
CrL
FeK
2.00
4.00
6.00
8.00
10.00
12.00
keV

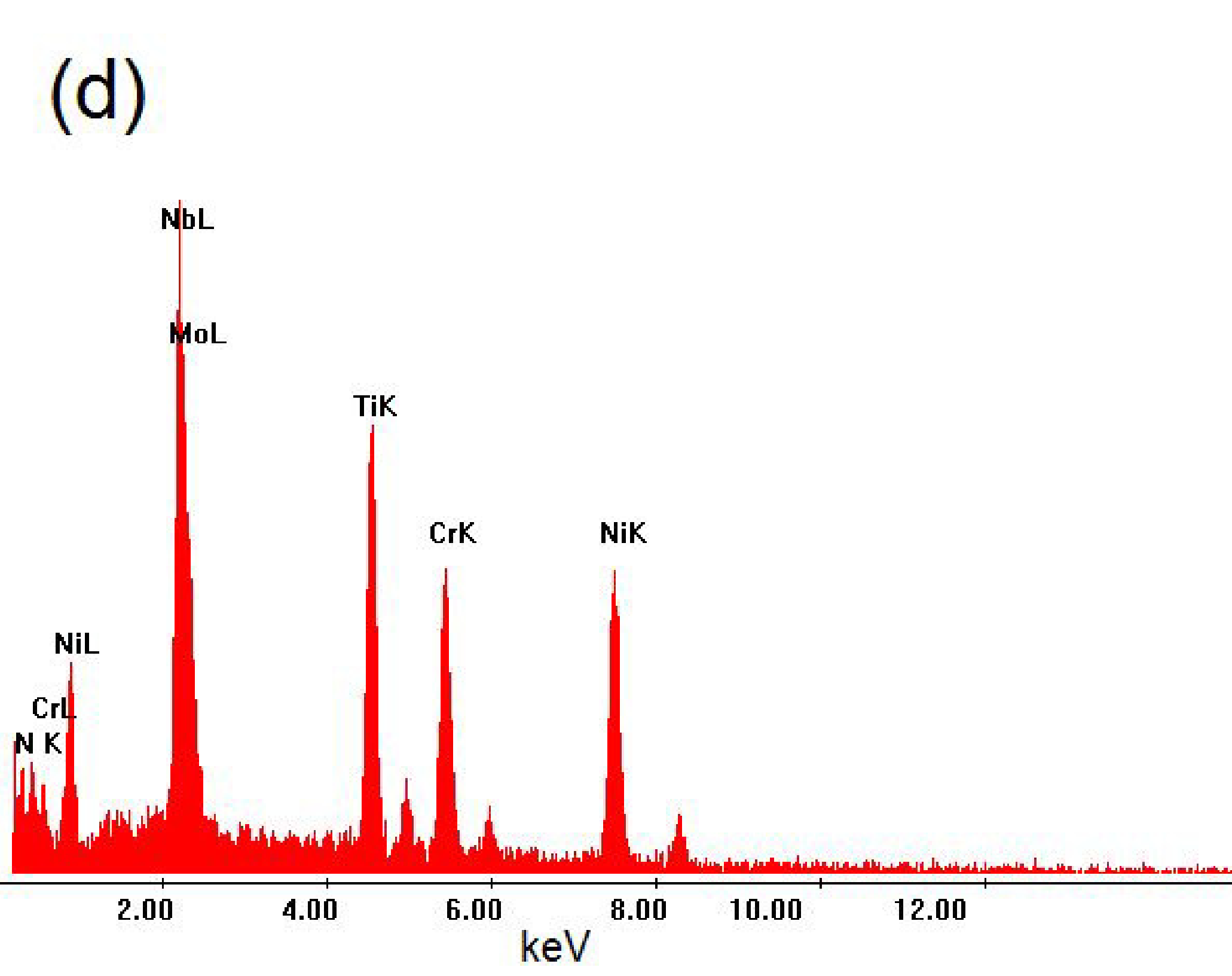
(d)
NbL
MoL
TiK
CrK
NiK
NiL
CrL
N K
2.00
4.00
6.00
8.00
10.00
12.00
keV

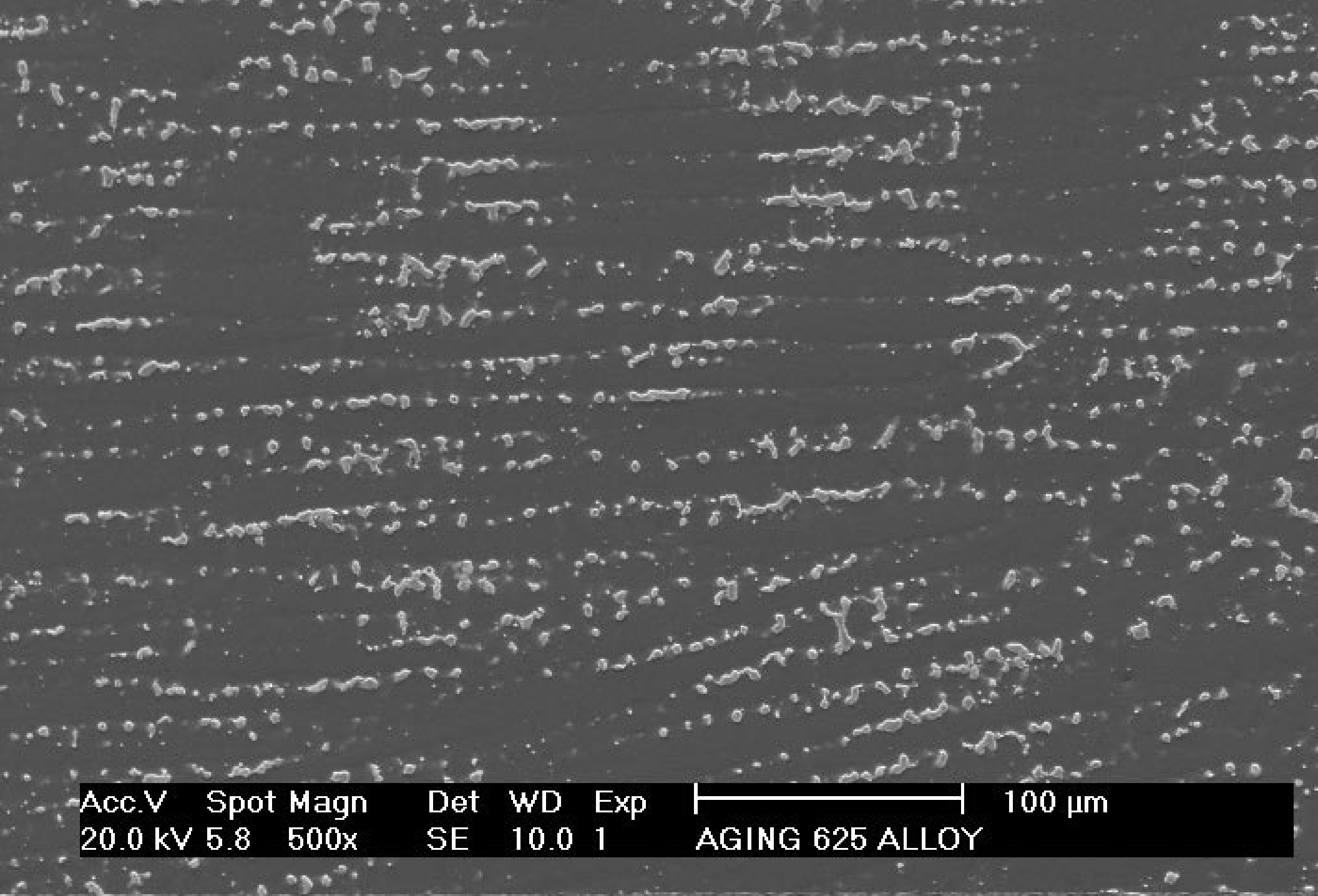
Acc.V Spot Magn Det WD Exp
100 µm
20.0 kV 5.8 500x SE 10.0 1 AGING 625 ALLOY

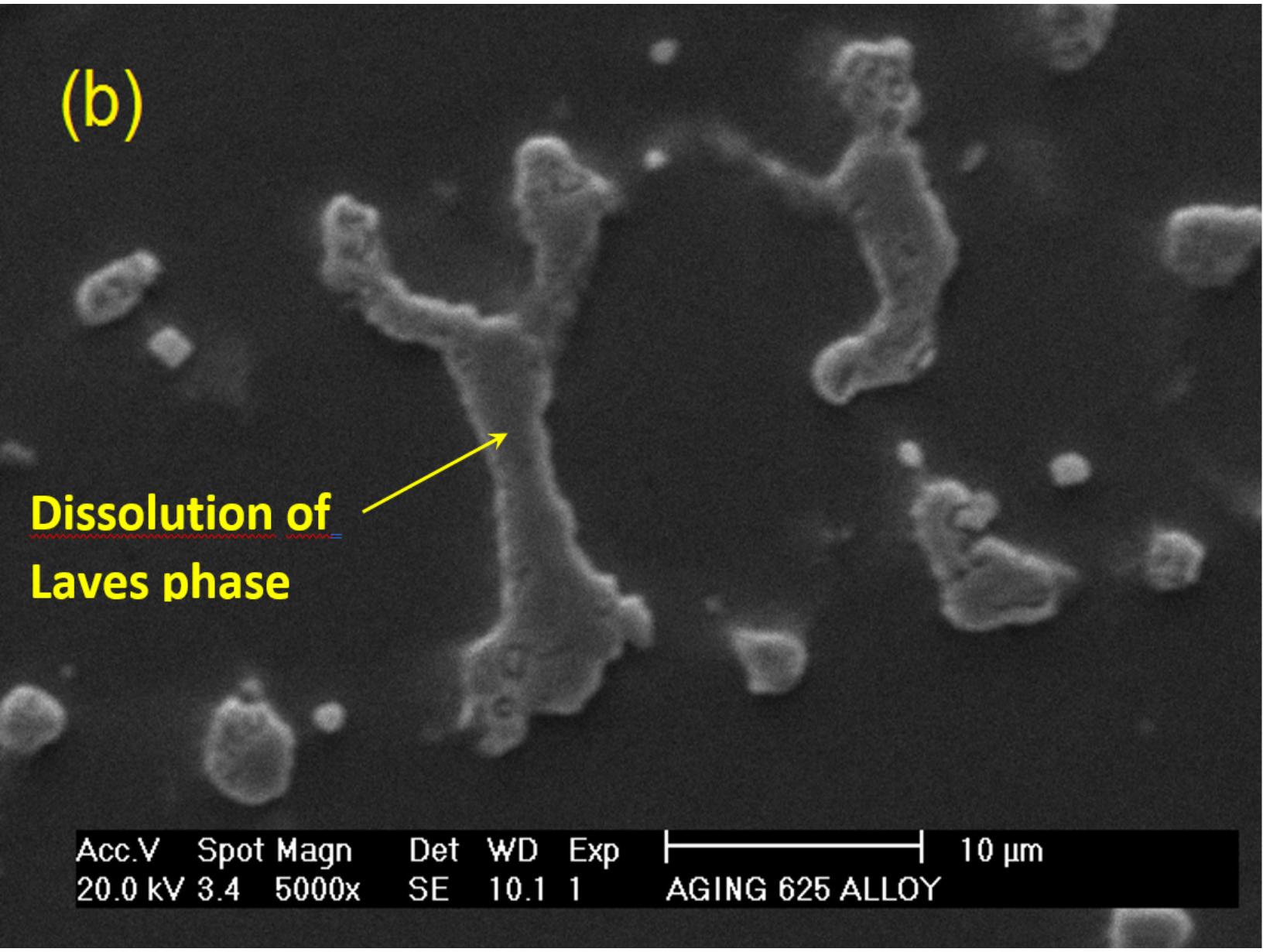
(b)
Dissolution of
Laves phase
Acc.V Spot Magn Det WD Exp 10 µm
20.0 kV 3.4 5000x SE 10.1 1 AGING 625 ALLOY

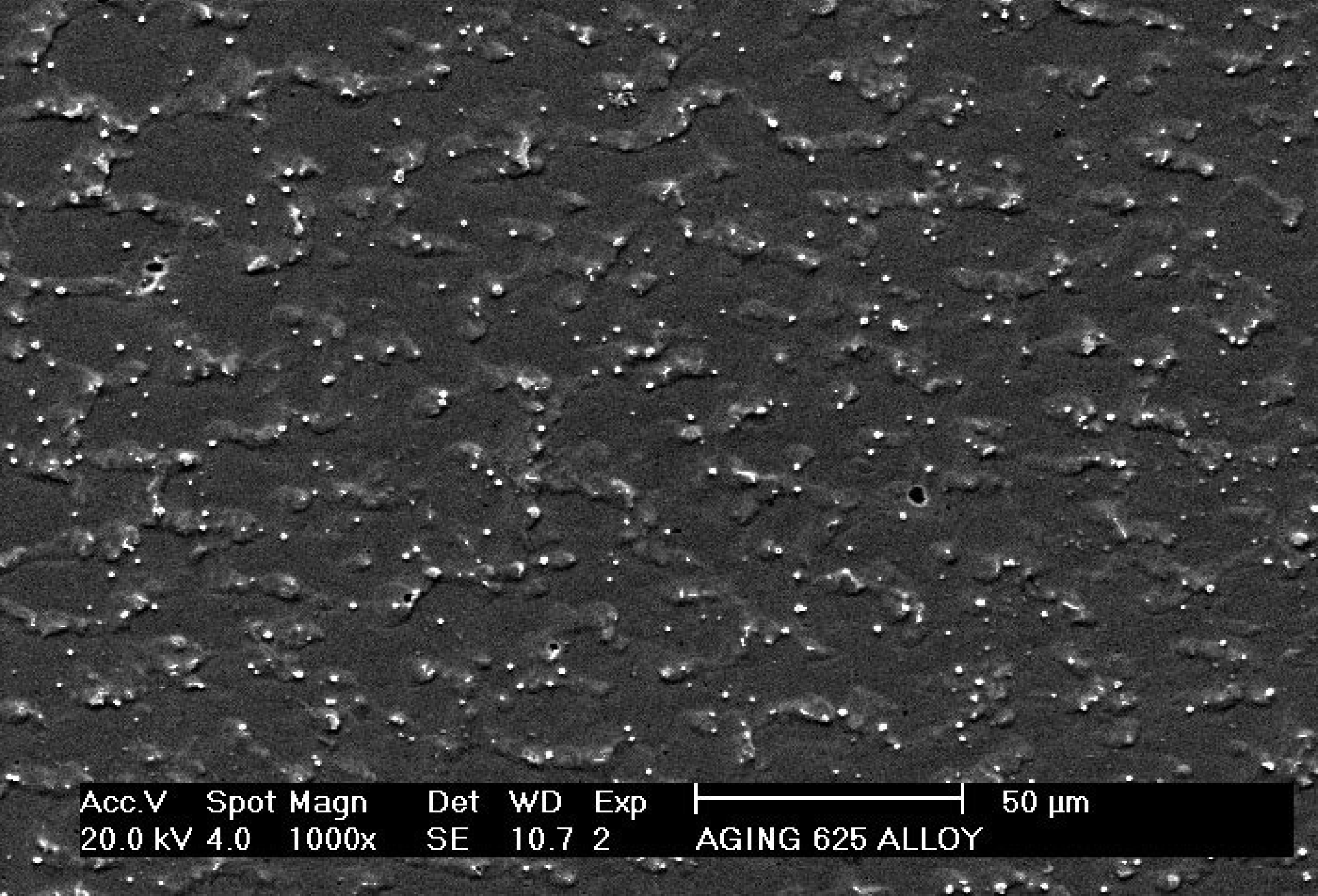
Acc.V Spot Magn Det WD Exp
50 µm
20.0 kV 4.0 1000x SE 10.7 2 AGING 625 ALLOY

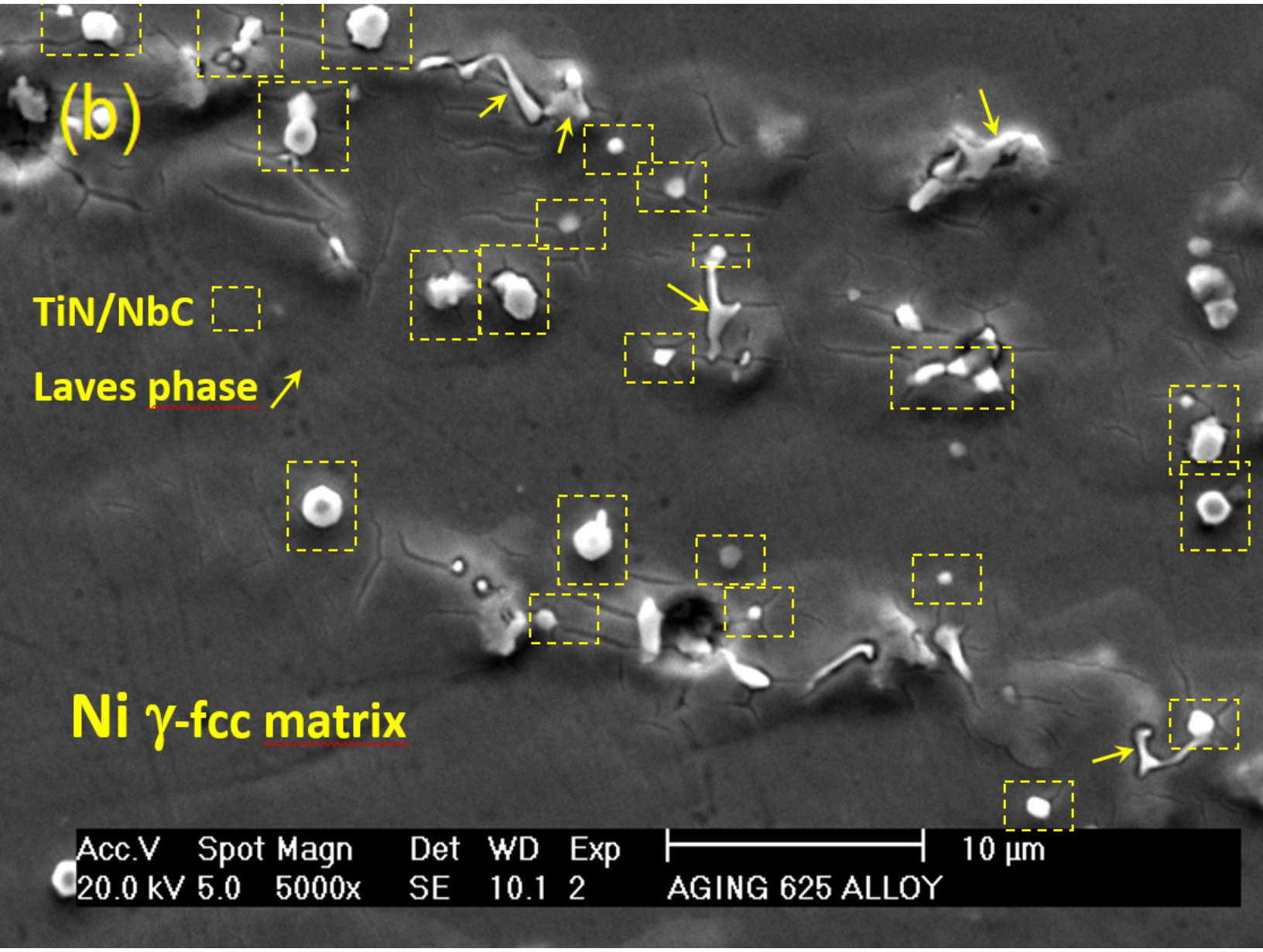
(b)
TiN/NbC
Laves phase
Ni γ-fcc matrix
Acc.V Spot Magn Det WD Exp
20.0 kV 5.0 5000x SE 10.1 2
10 µm
AGING 625 ALLOY

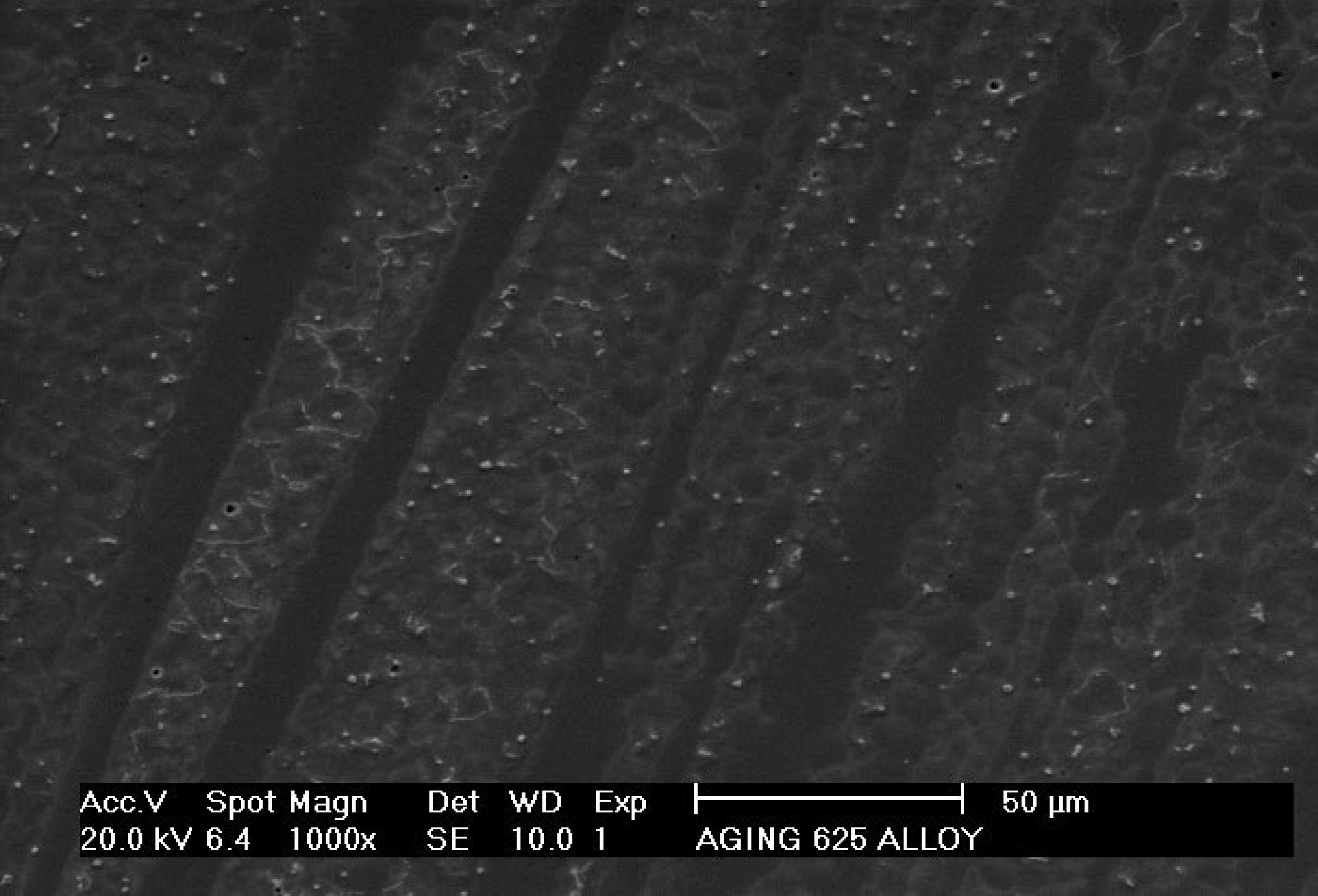
Acc.V Spot Magn Det WD Exp
50 µm
20.0 kV 6.4 1000x SE 10.0 1 AGING 625 ALLOY

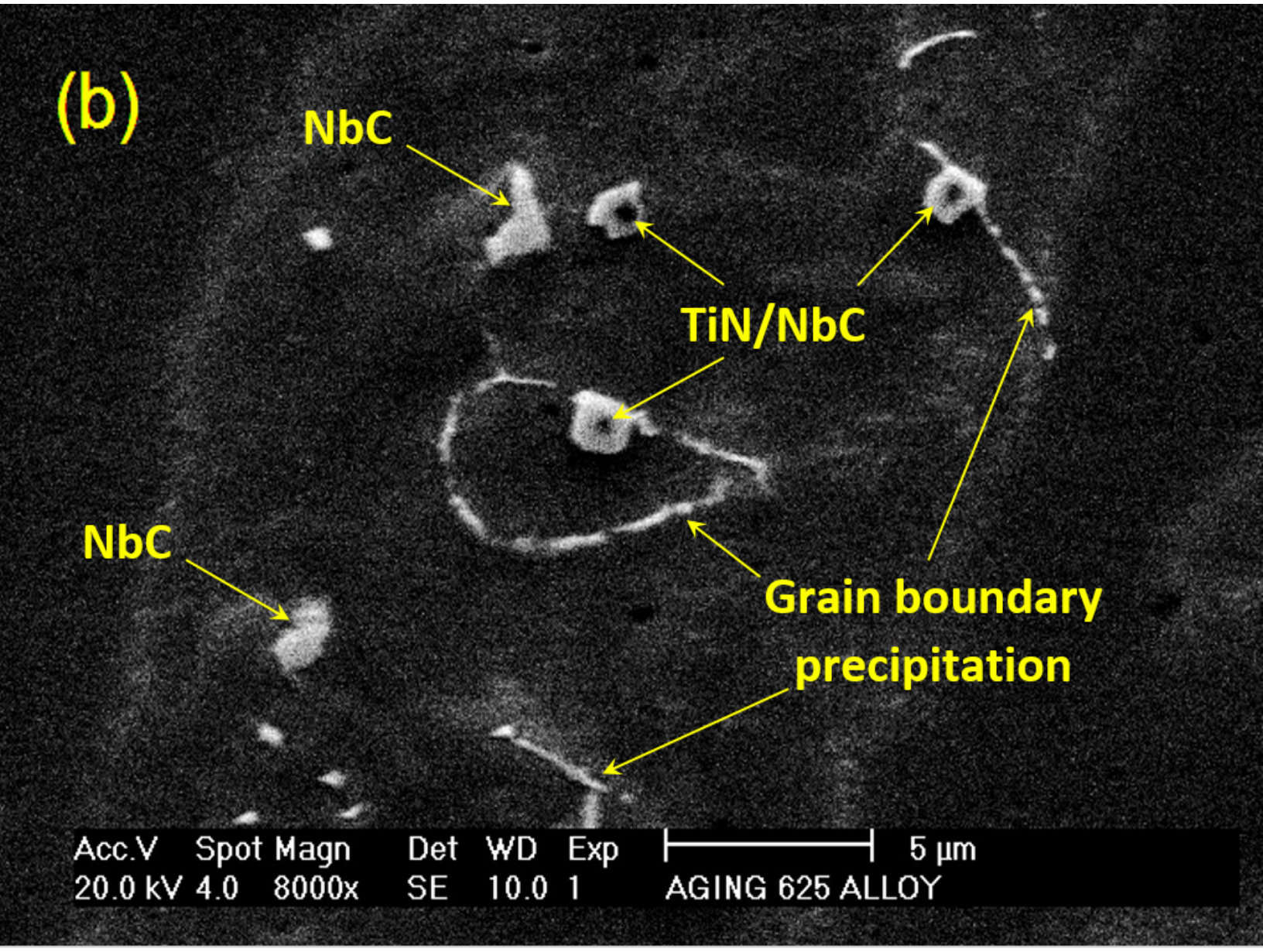
(b)
NbC
TiN/NbC
NbC
Grain boundary
precipitation
Acc.V Spot Magn Det WD Exp 5 µm
20.0 kV 4.0 8000x SE 10.0 1 AGING 625 ALLOY

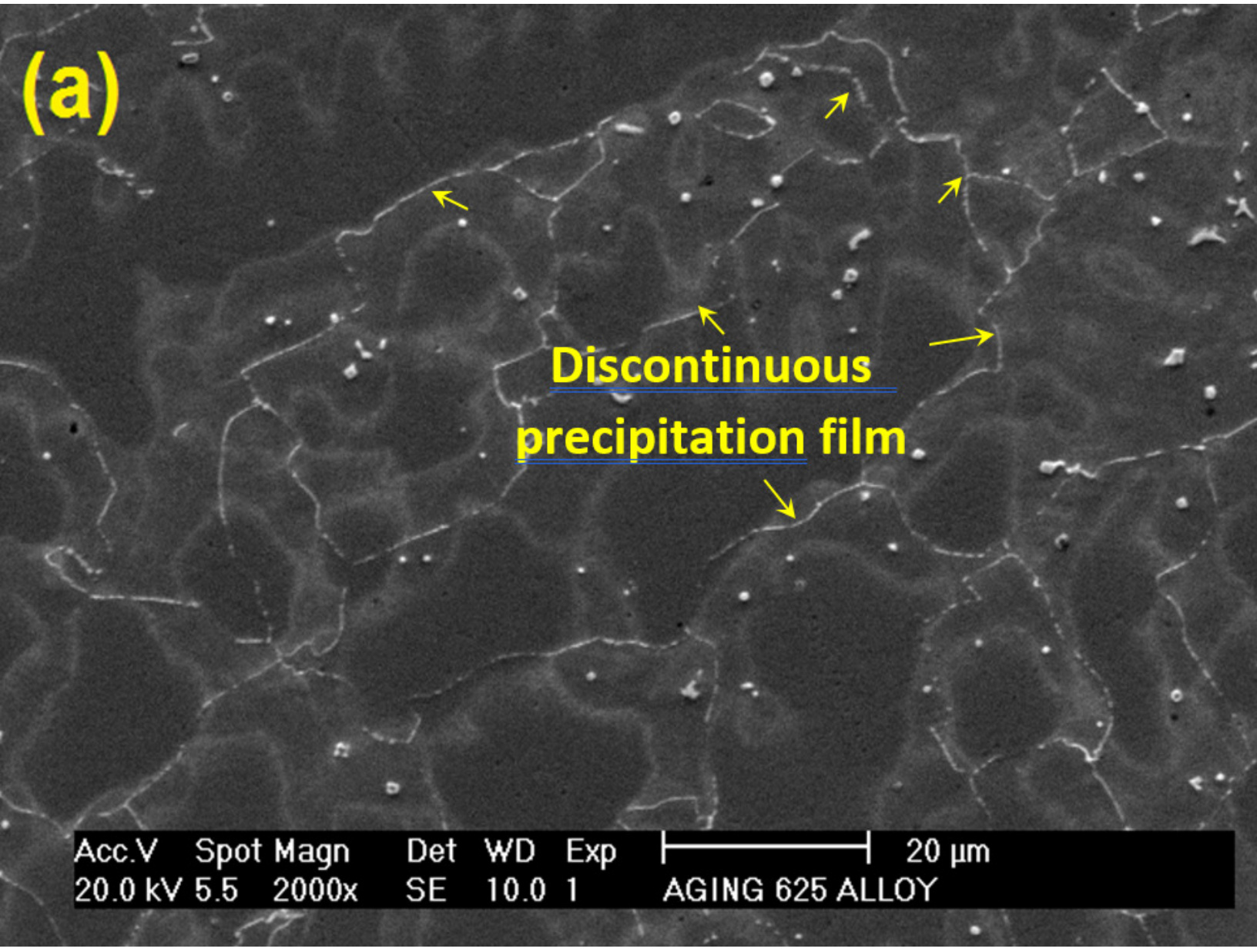
(a)
Discontinuous
precipitation film
Acc.V Spot Magn Det WD Exp 20 µm
20.0 kV 5.5 2000x SE 10.0 1 AGING 625 ALLOY

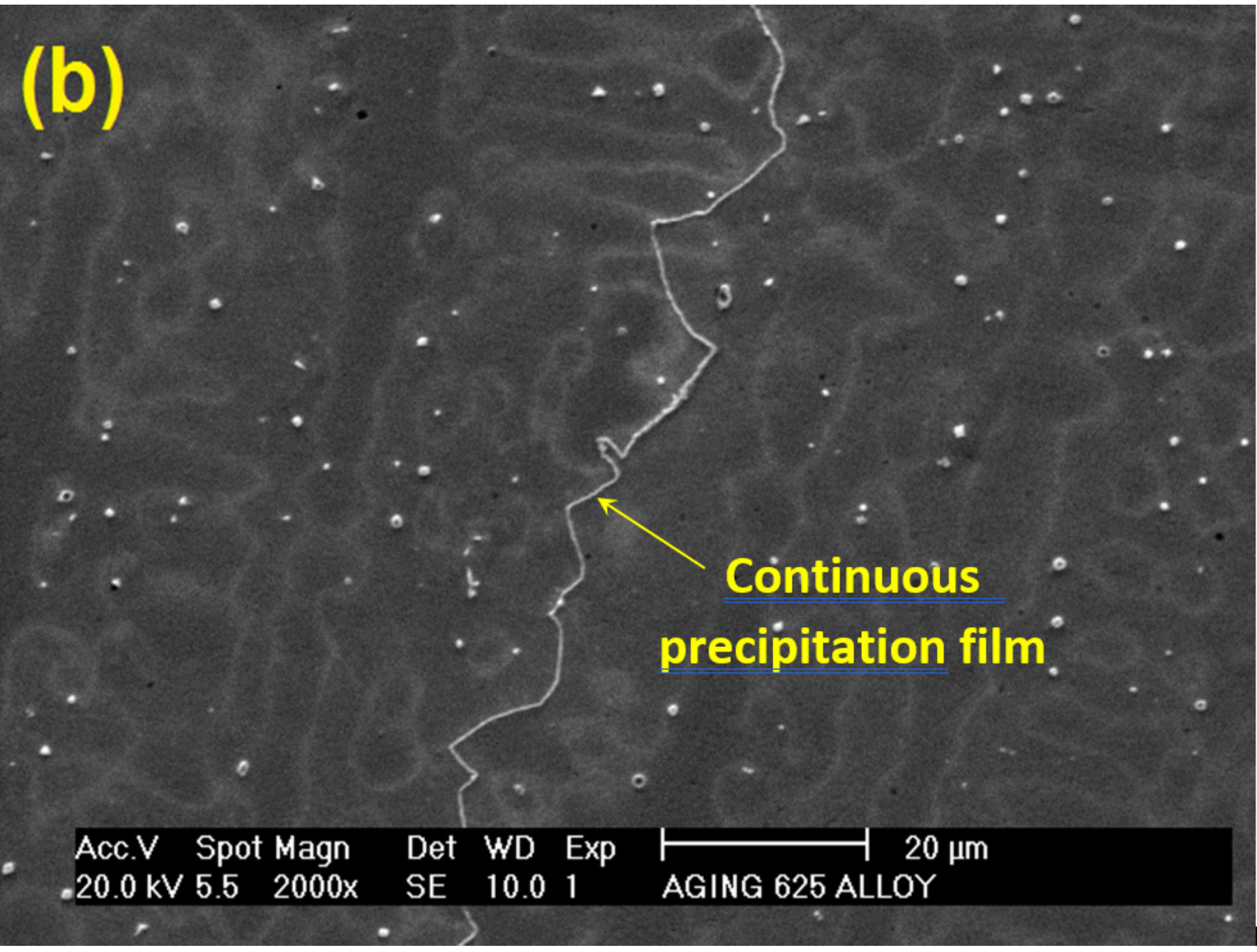
(b)
Continuous
precipitation film
Acc.V Spot Magn Det WD Exp 20 µm
20.0 kV 5.5 2000x SE 10.0 1 AGING 625 ALLOY

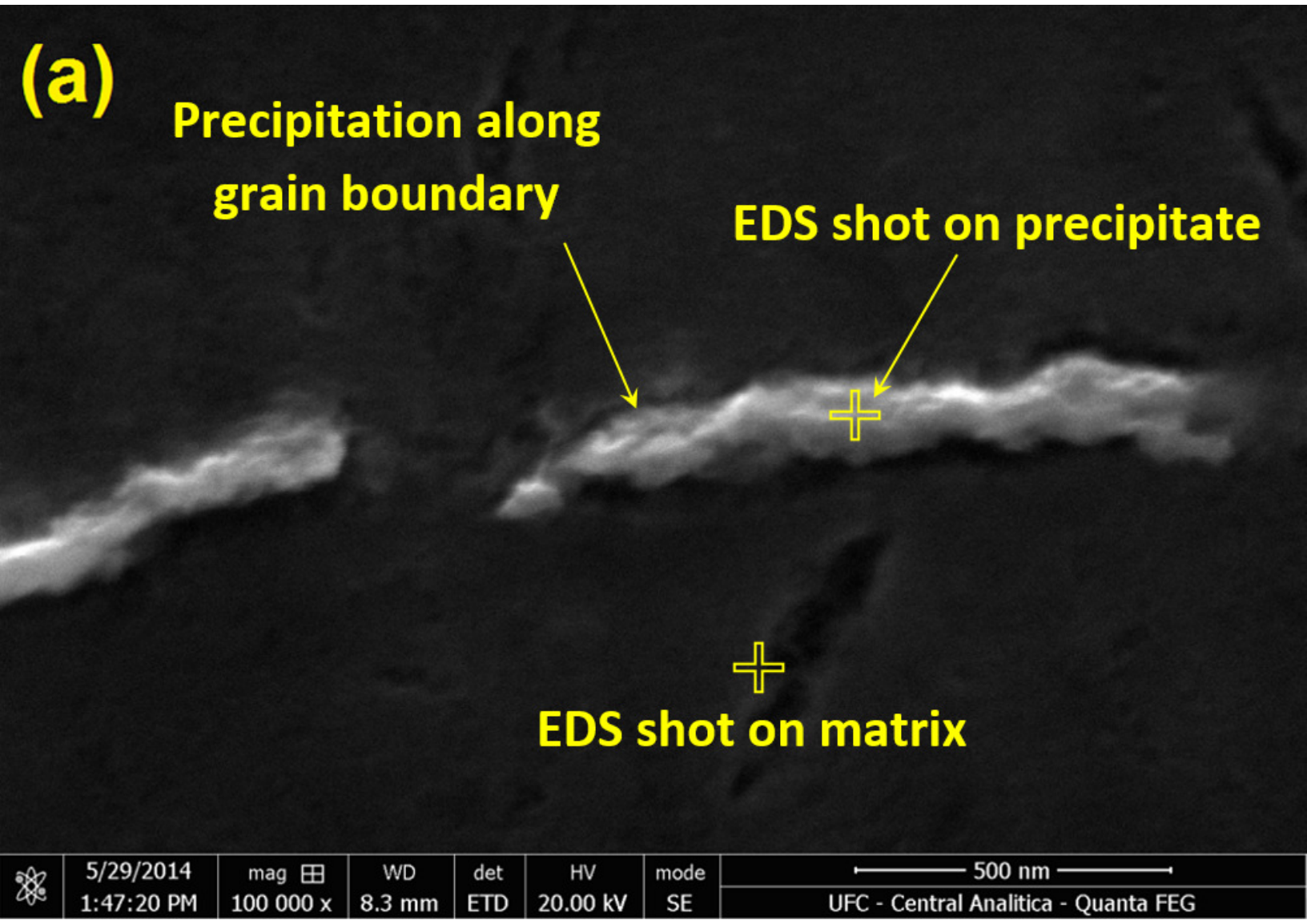
(a)
Precipitation along grain boundary
EDS shot on precipitate
EDS shot on matrix
5/29/2014
1:47:20 PM
mag
100 000 x
WD
8.3 mm
det
ETD
HV
20.00 kV
mode
SE
500 nm
UFC - Central Analitica - Quanta FEG

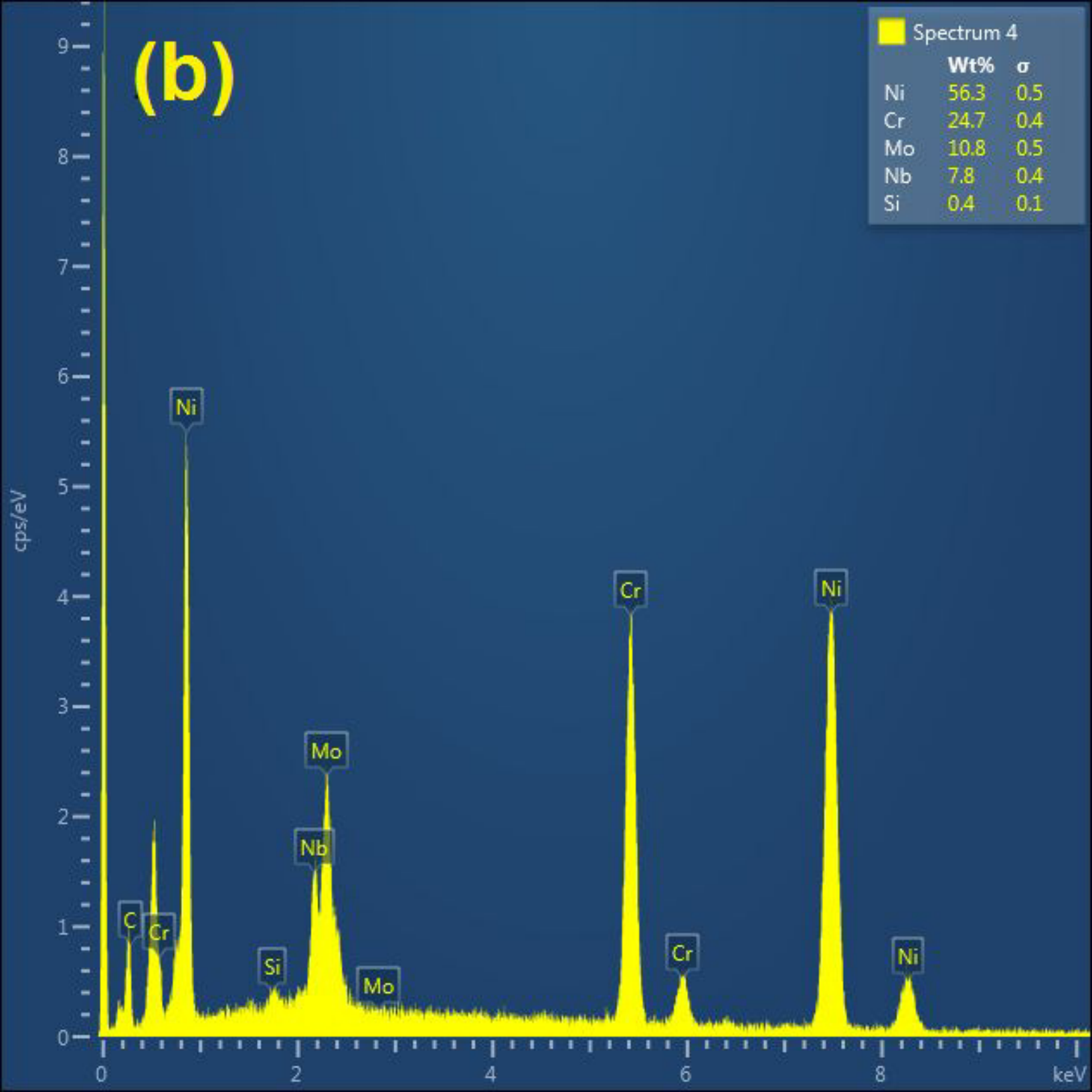
(b)
Spectrum 4
Wt% σ
Ni 56.3 0.5
Cr 24.7 0.4
Mo 10.8 0.5
Nb 7.8 0.4
Si 0.4 0.1
cps/eV
keV
C
Cr
Ni
Si
Mo
Nb
Mo
Cr
Cr
Ni
Ni

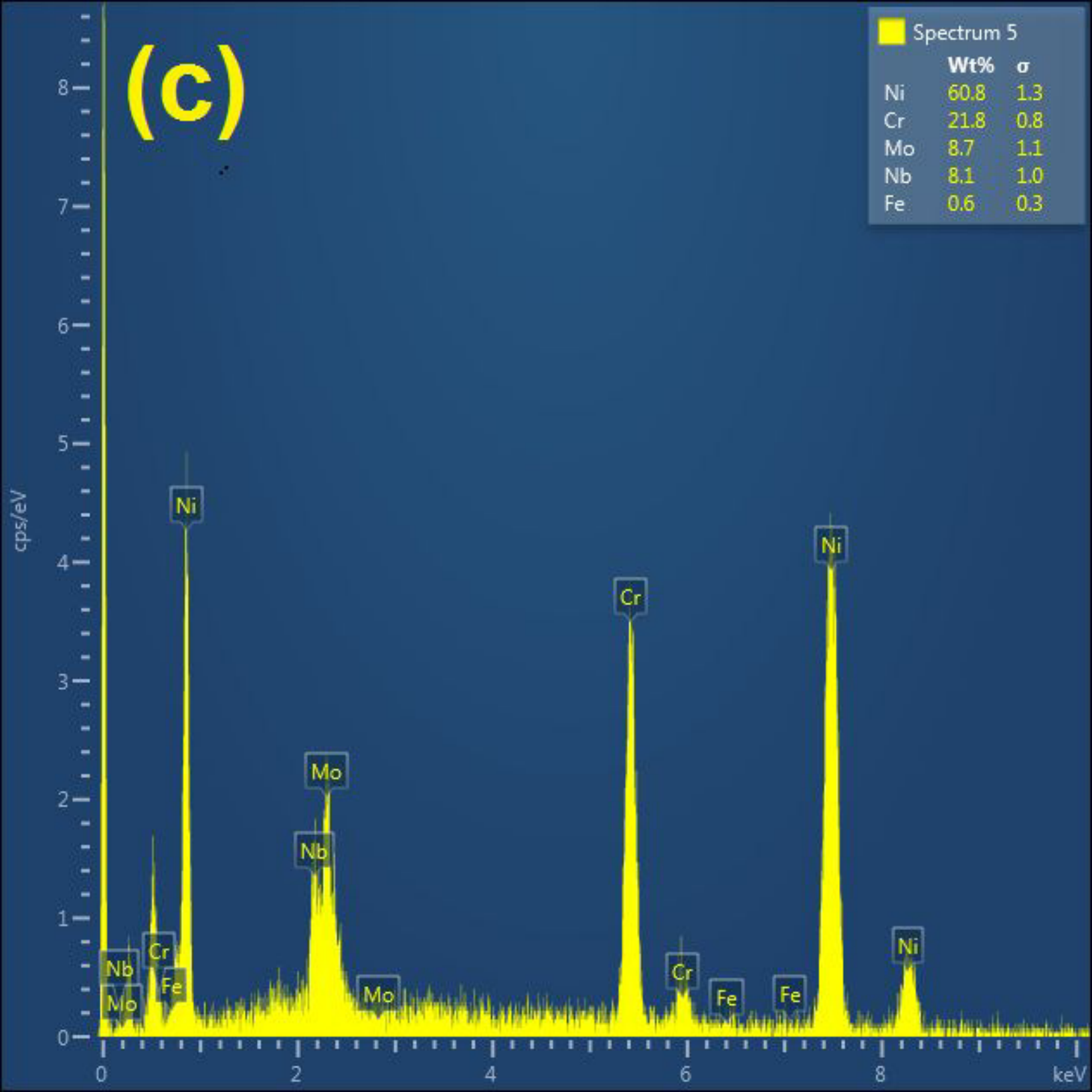
(c)
Spectrum 5
Wt% σ
Ni 60.8 1.3
Cr 21.8 0.8
Mo 8.7 1.1
Nb 8.1 1.0
Fe 0.6 0.3
cps/eV
keV
Ni
Cr
Mo
Nb
Fe

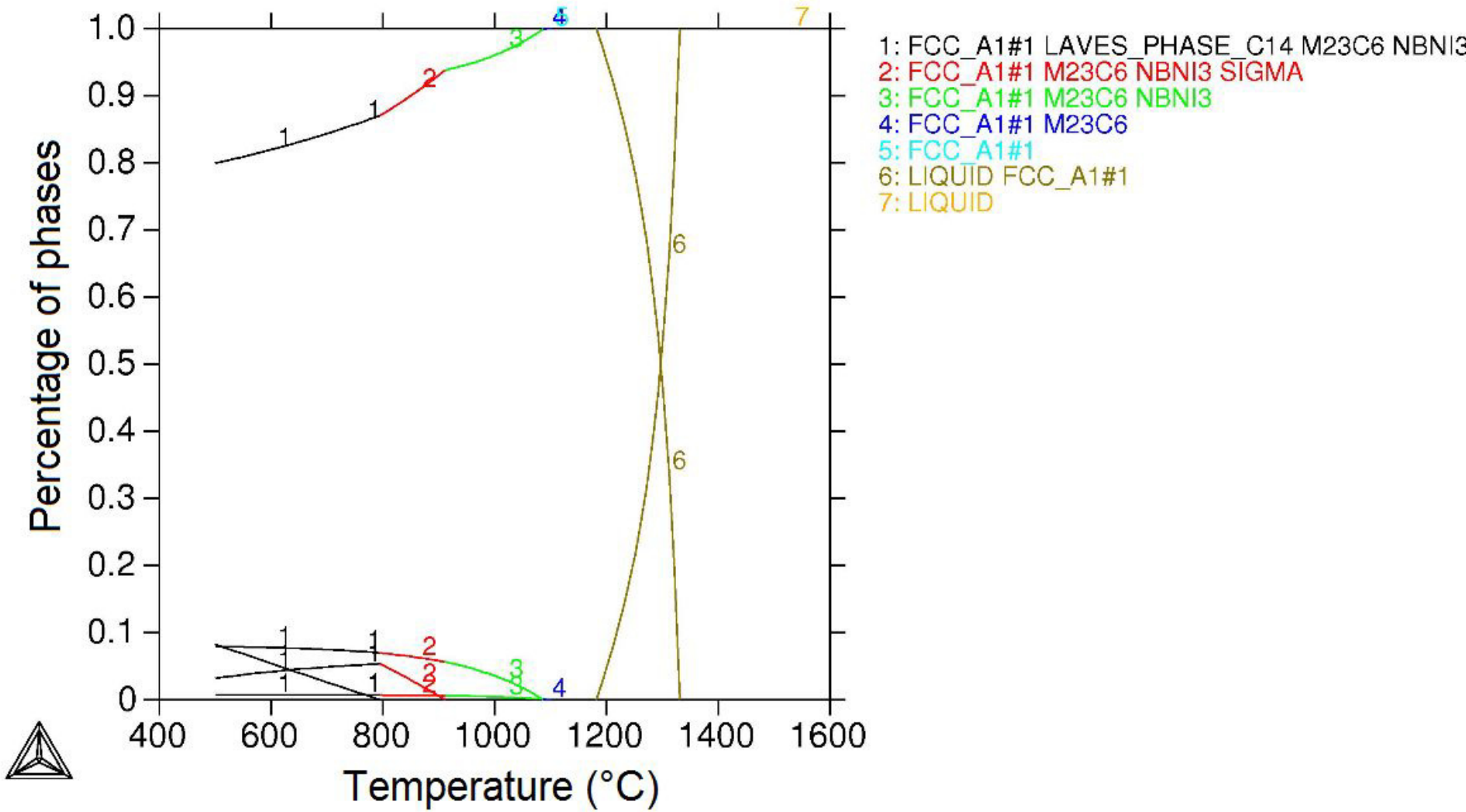
Percentage of phases
Temperature (°C)
1.0
0.9
0.8
0.7
0.6
0.5
0.4
0.3
0.2
0.1
0
400
600
800
1000
1200
1400
1600
1: FCC_A1#1 LAVES_PHASE_C14 M23C6 NBNI3
2: FCC_A1#1 M23C6 NBNI3 SIGMA
3: FCC_A1#1 M23C6 NBNI3
4: FCC_A1#1 M23C6
5: FCC_A1#1
6: LIQUID FCC_A1#1
7: LIQUID

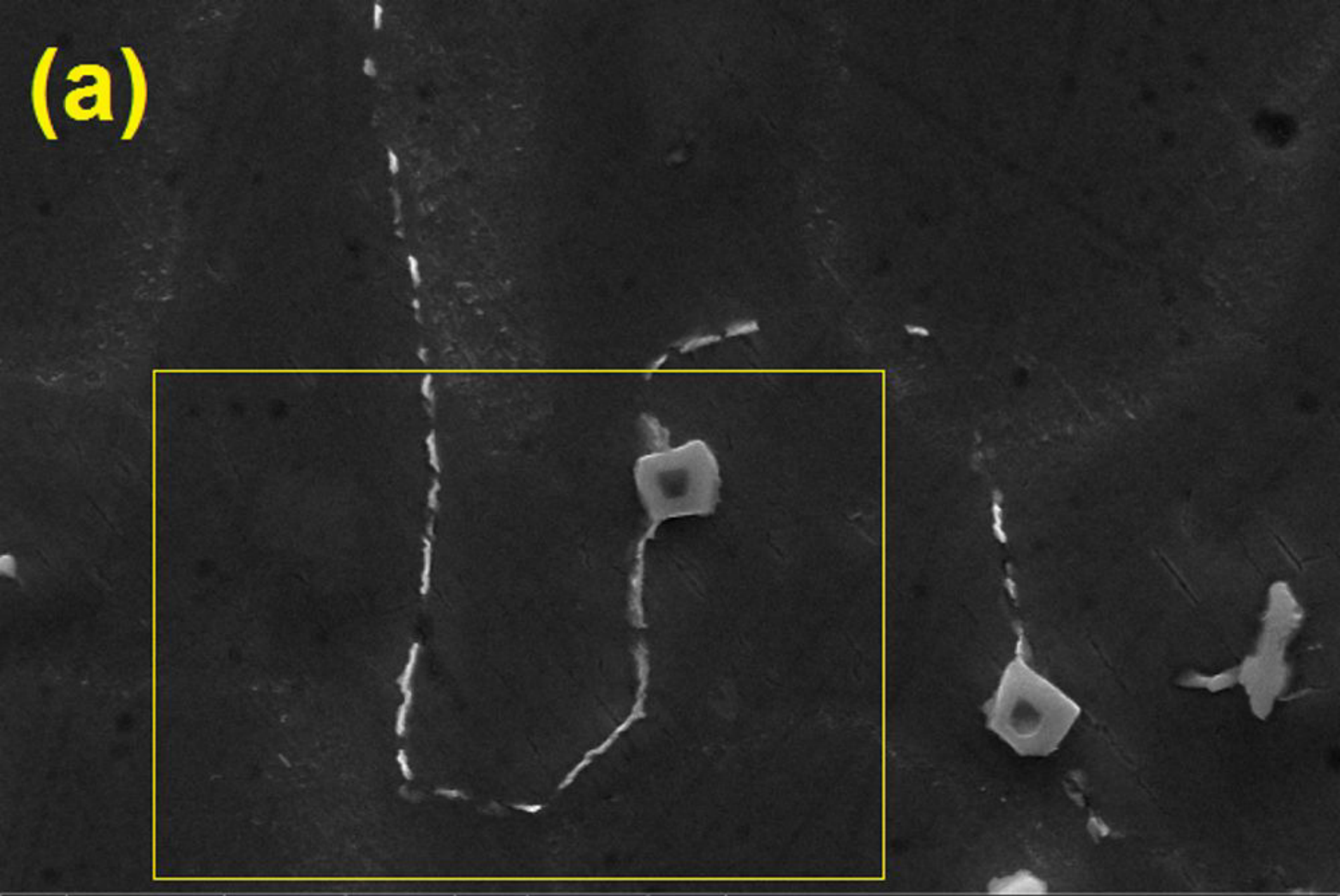
(a)
5/29/2014
2:07:47 PM
mag
10 000 x
WD
8.3 mm
det
ETD
HV
20.00 kV
mode
SE
5 µm
UFC - Central Analitica - Quanta FEG

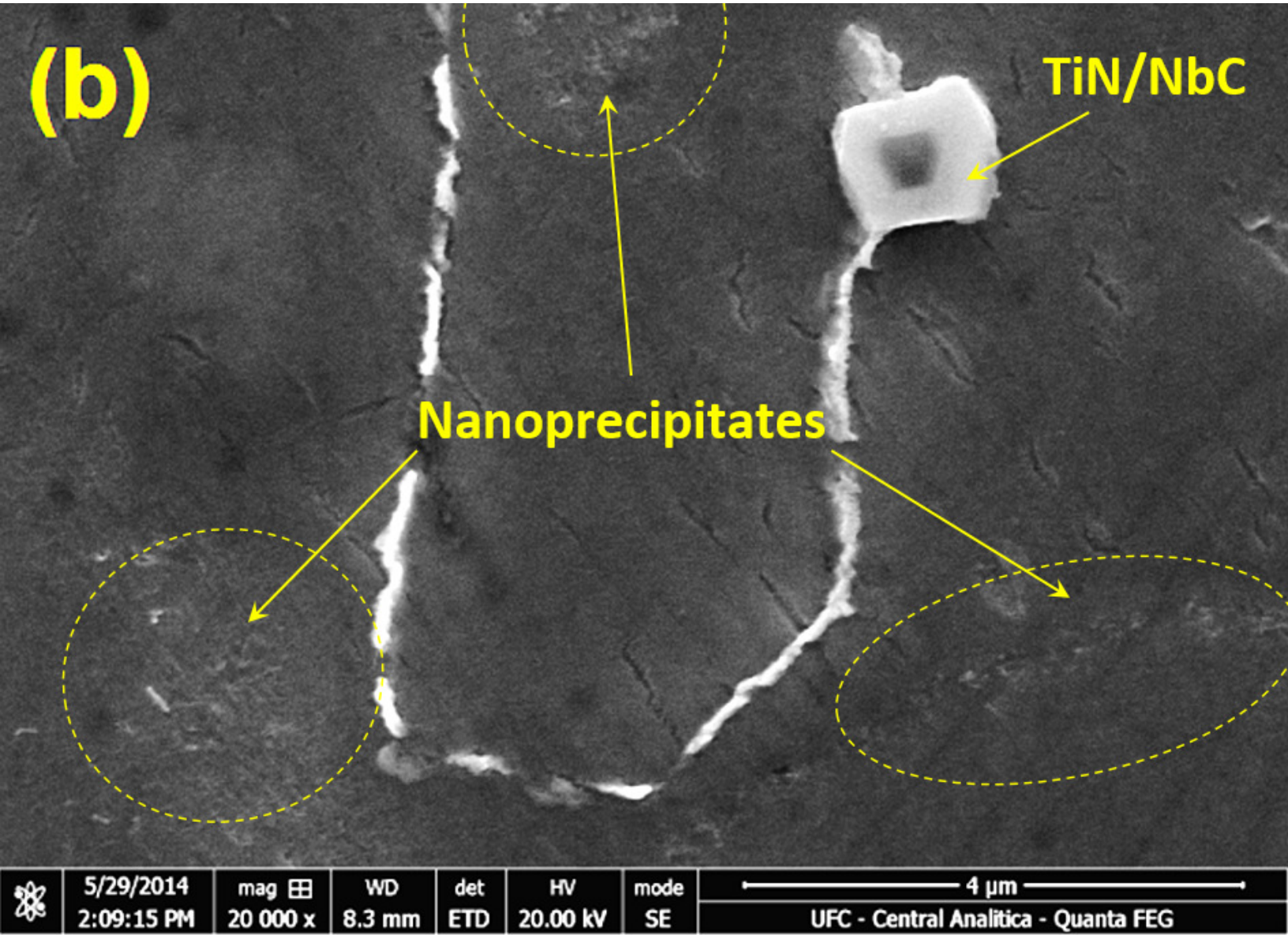
(b)
TiN/NbC
Nanoprecipitates
5/29/2014
2:09:15 PM
mag
20 000 x
WD
8.3 mm
det
ETD
HV
20.00 kV
mode
SE
4 µm
UFC - Central Analitica - Quanta FEG

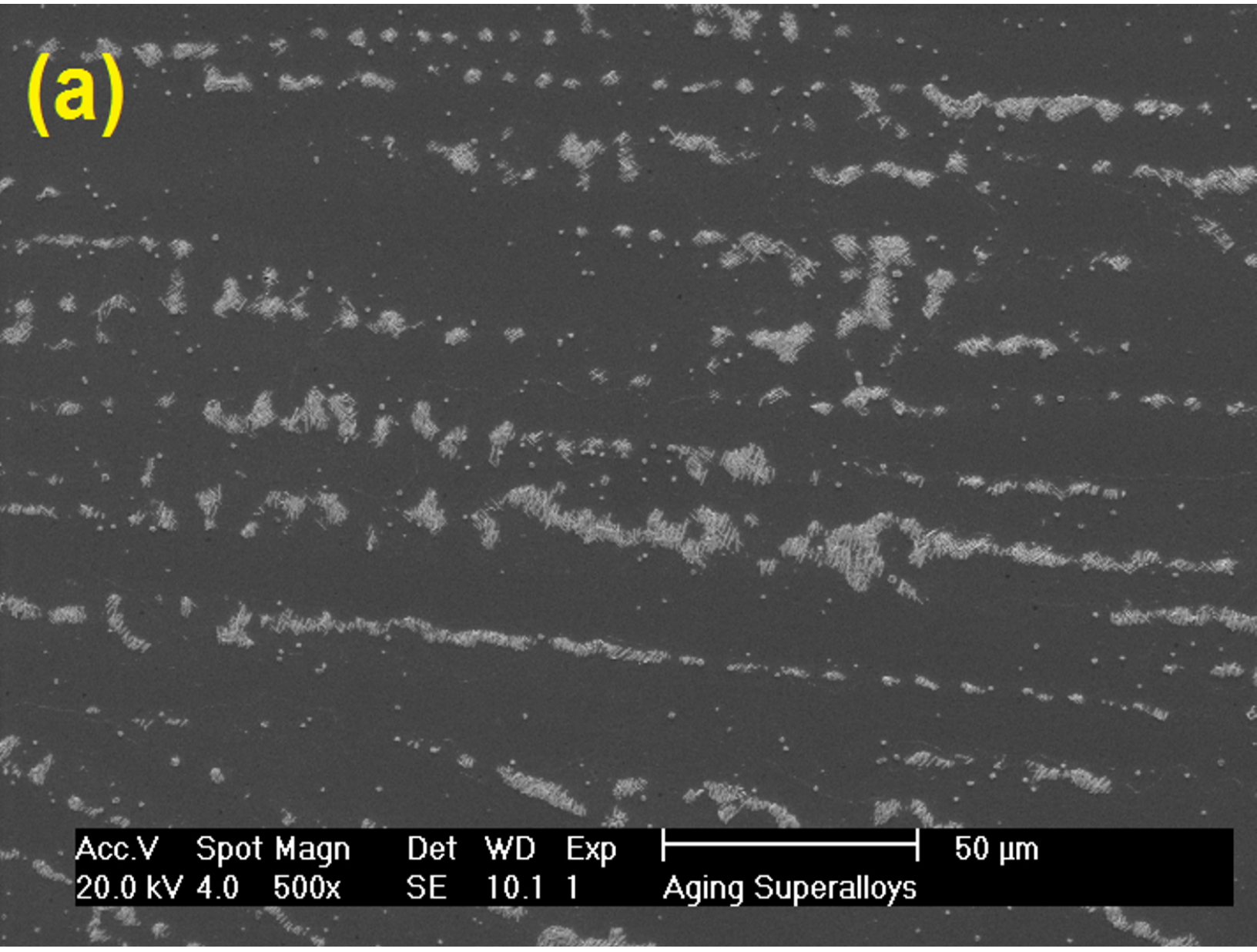
(a)
Acc.V Spot Magn Det WD Exp
20.0 kV 4.0 500x SE 10.1 1
50 µm
Aging Superalloys

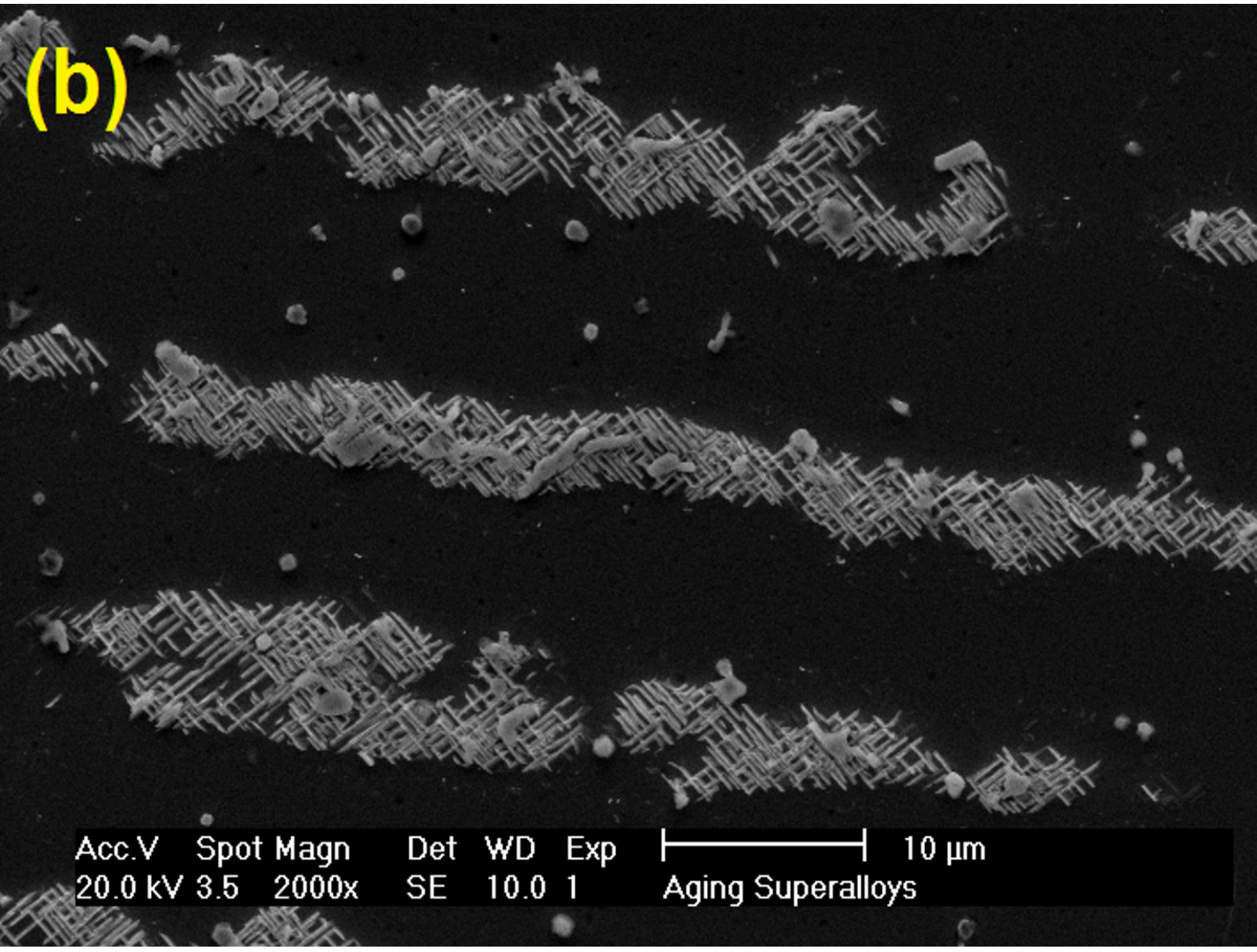
(b)
Acc.V Spot Magn Det WD Exp
10 µm
20.0 kV 3.5 2000x SE 10.0 1
Aging Superalloys

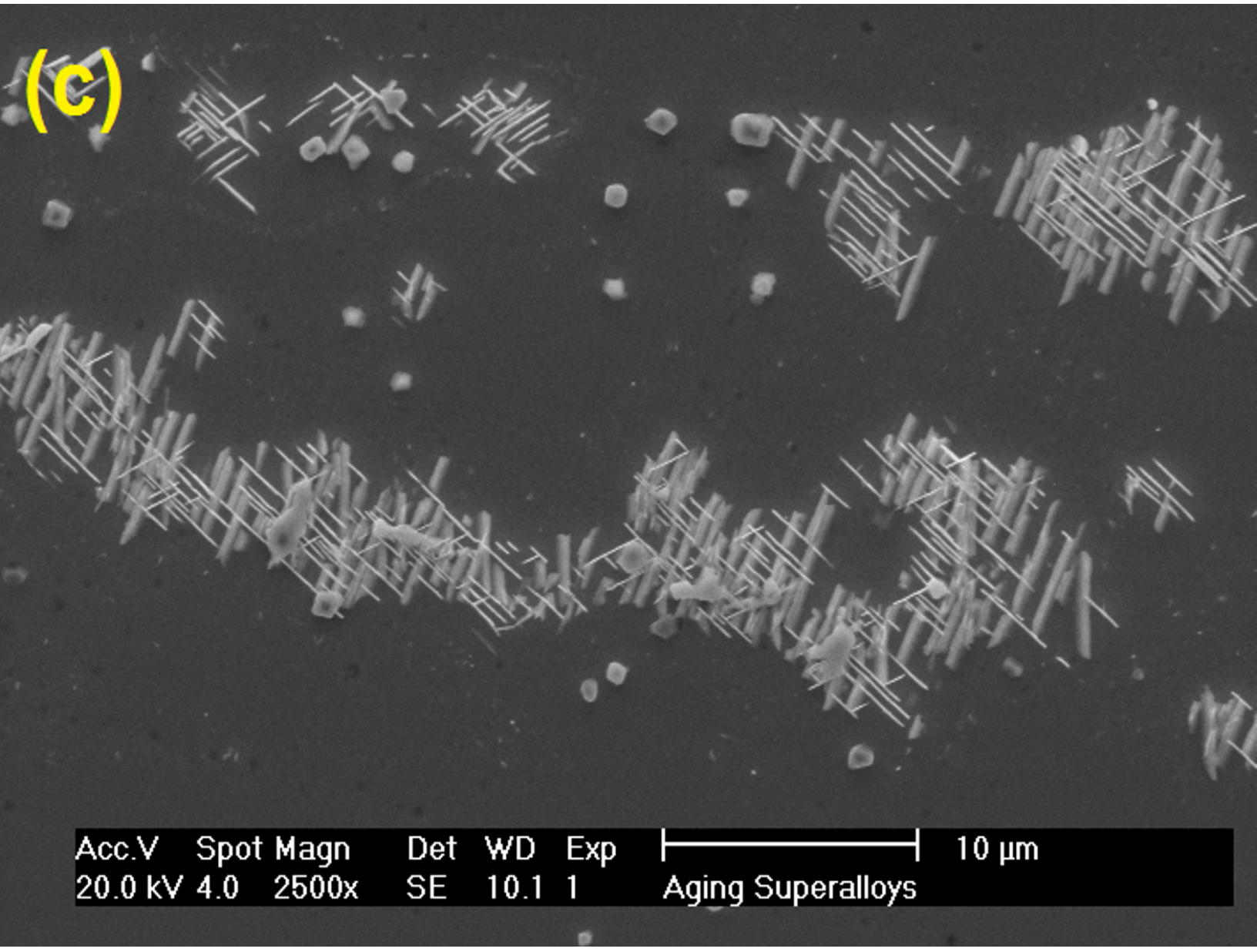
(c)
Acc.V Spot Magn Det WD Exp
20.0 kV 4.0 2500x SE 10.1 1
10 µm
Aging Superalloys

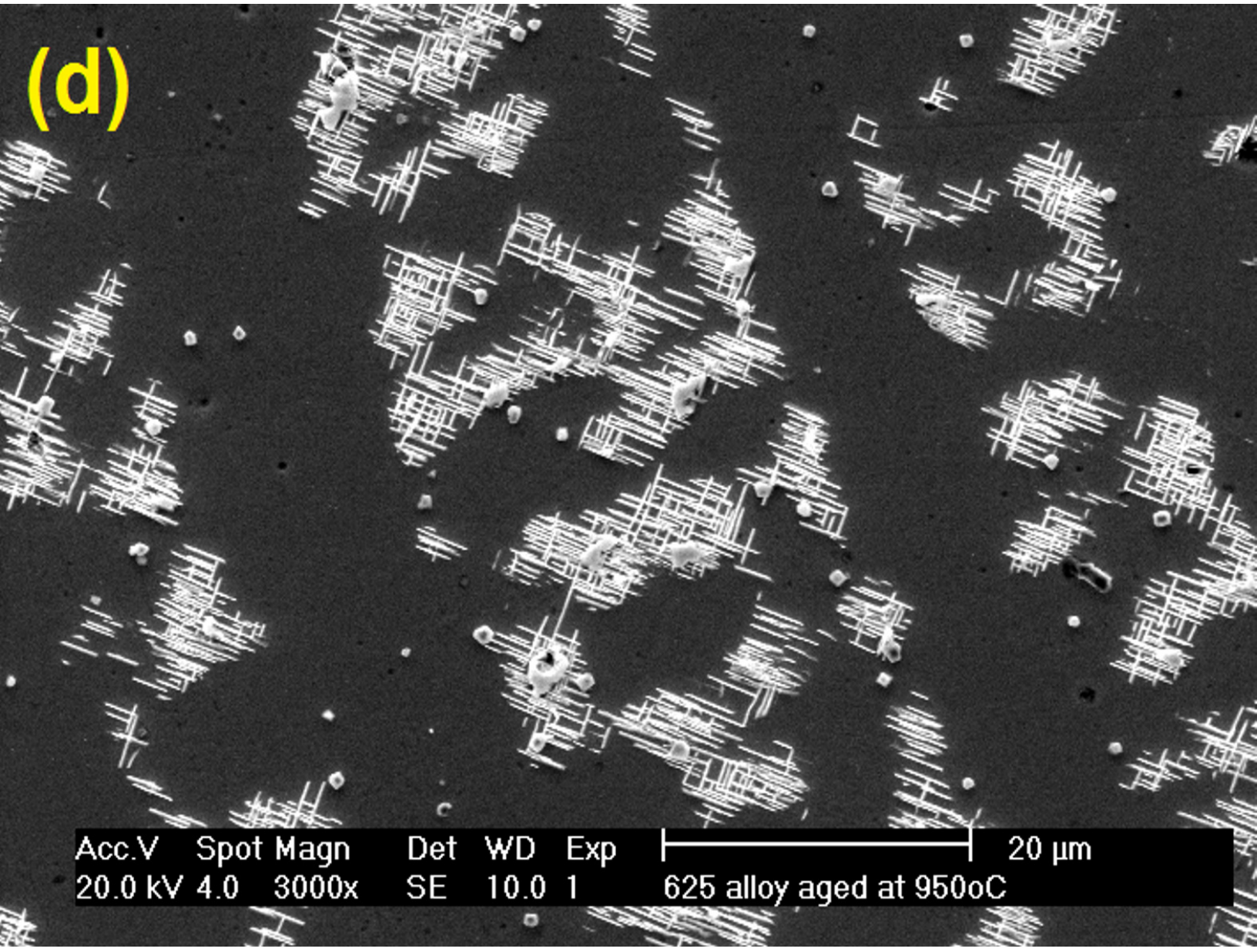
(d)
Acc.V Spot Magn Det WD Exp
20.0 kV 4.0 3000x SE 10.0 1
20 µm
625 alloy aged at 950oC

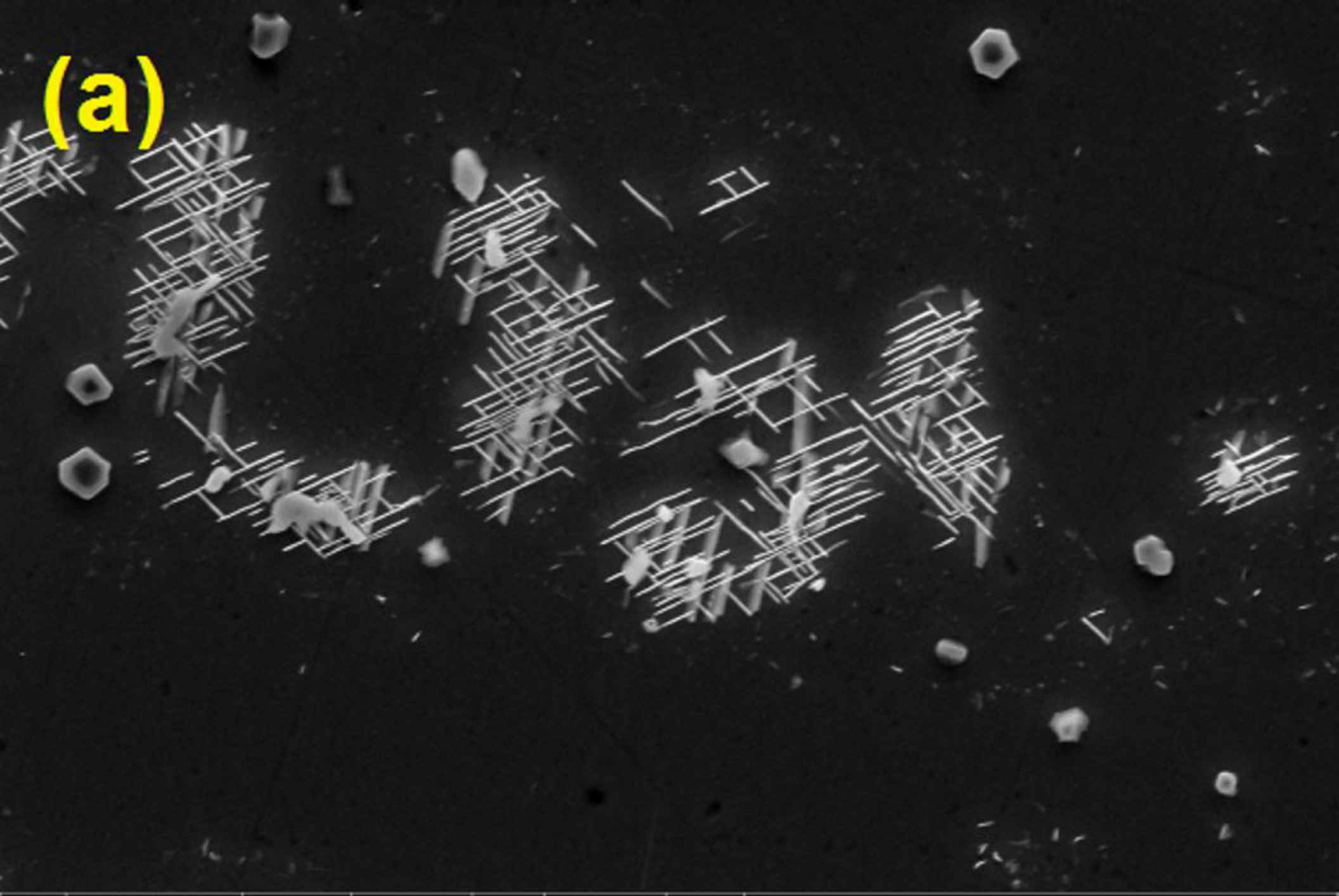
(a)
5/29/2014
11:59:12 AM
mag
4 893 x
WD
10.0 mm
det
ETD
HV
20.00 kV
mode
SE
10 µm
UFC - Central Analitica - Quanta FEG

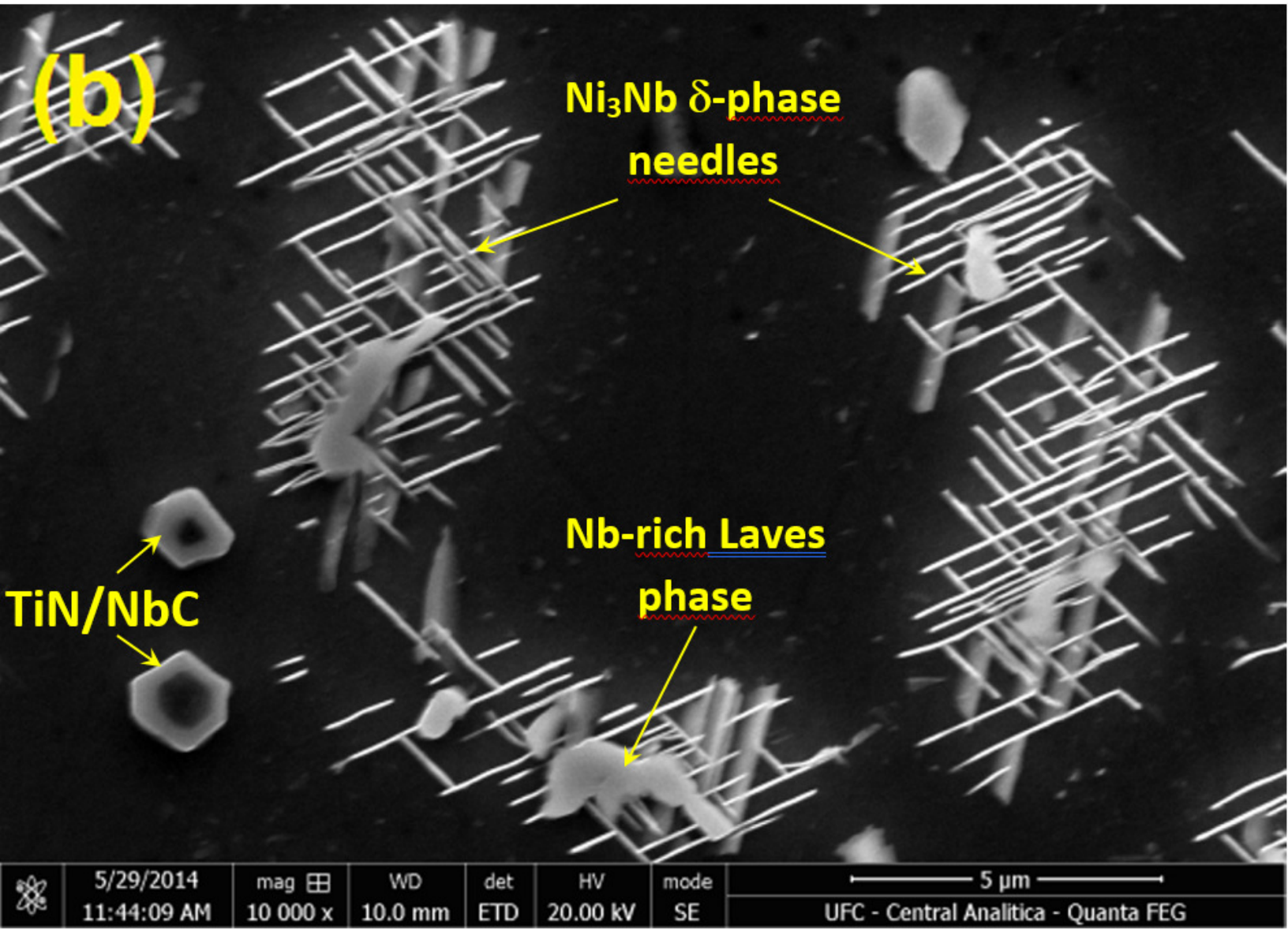
(b)
Ni3Nb δ-phase needles
Nb-rich Laves phase
TiN/NbC
5/29/2014
11:44:09 AM
mag
10 000 x
WD
10.0 mm
det
ETD
HV
20.00 kV
mode
SE
5 µm
UFC - Central Analitica - Quanta FEG

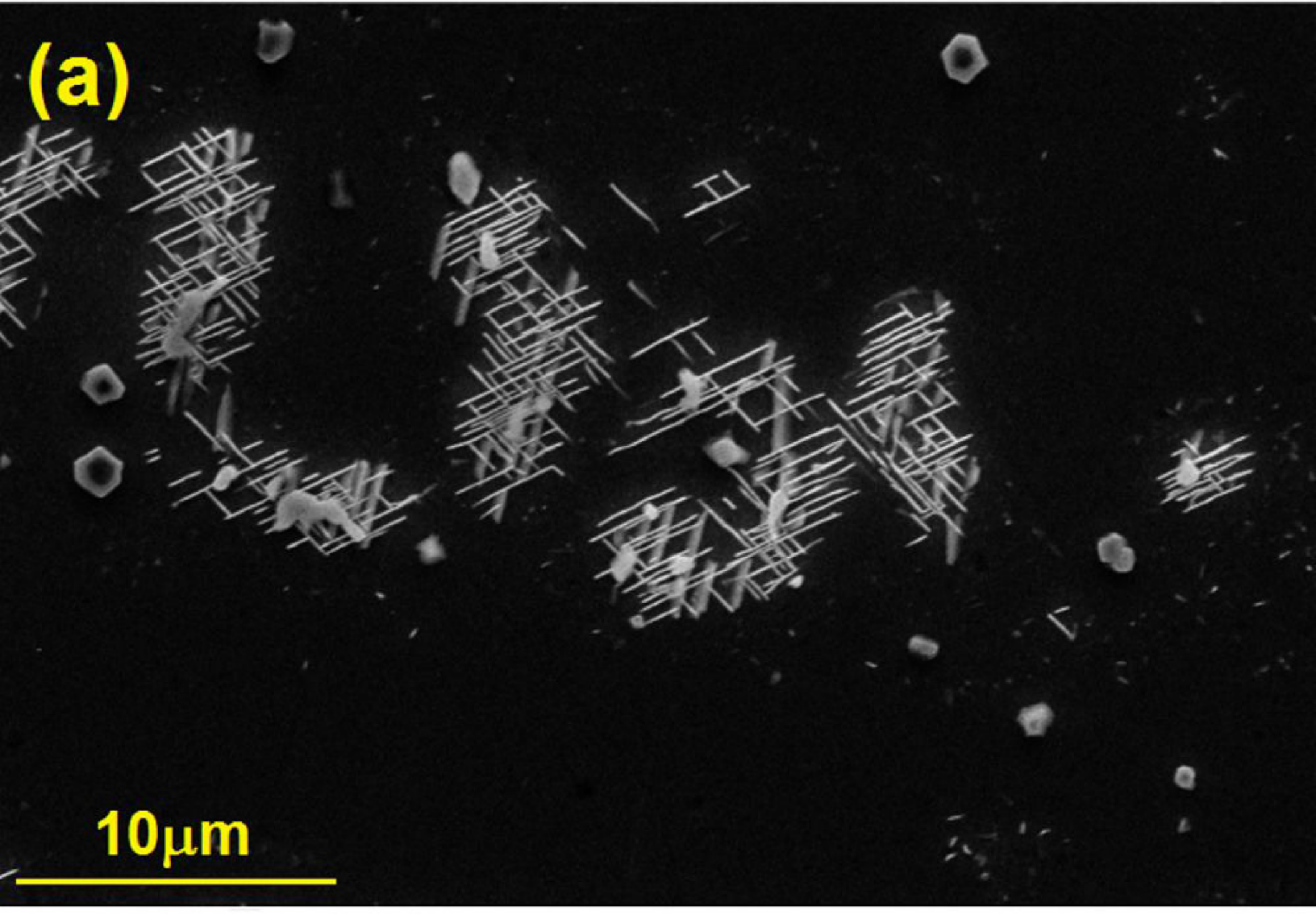
(a)
10μm

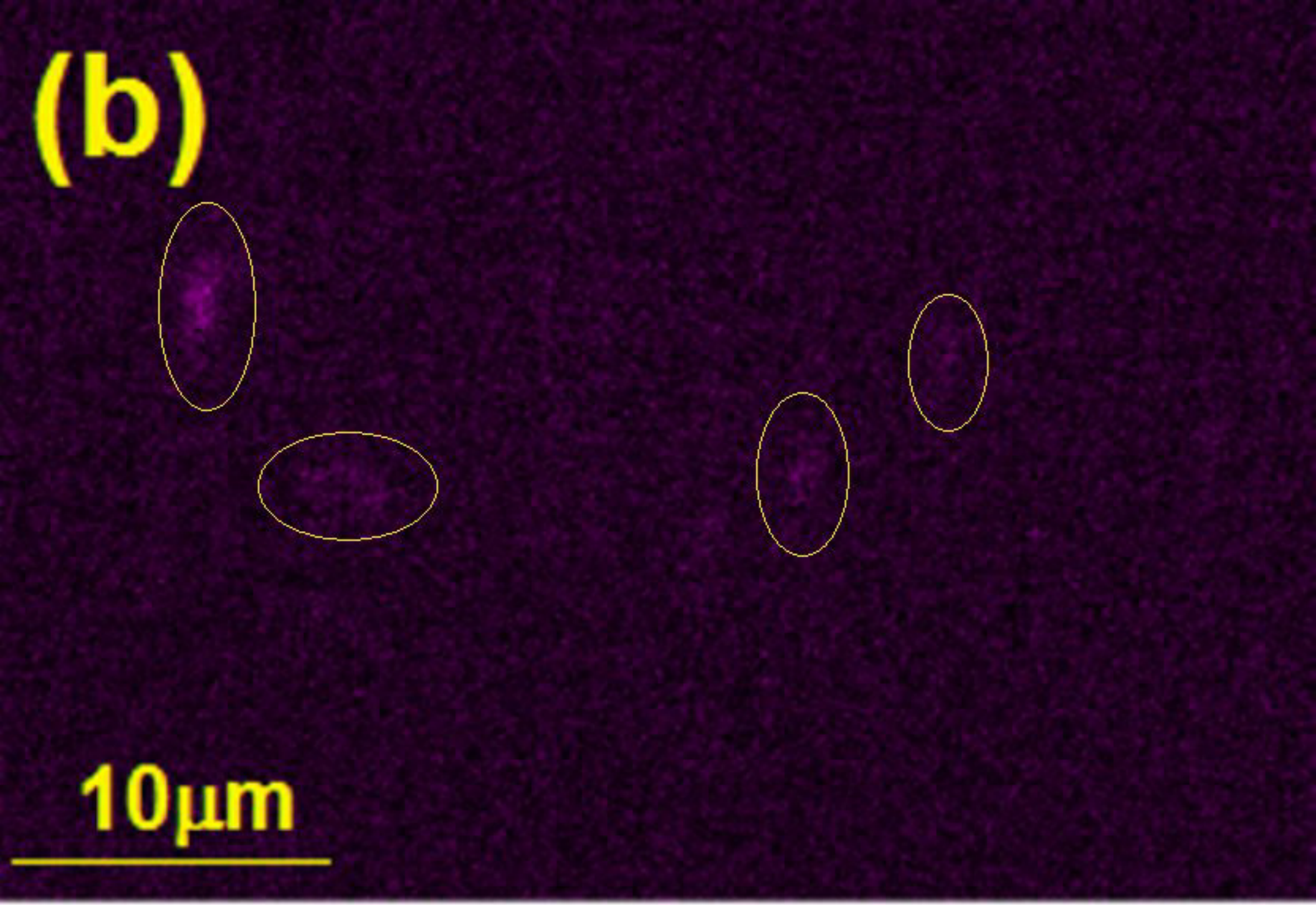
(b)
10μm

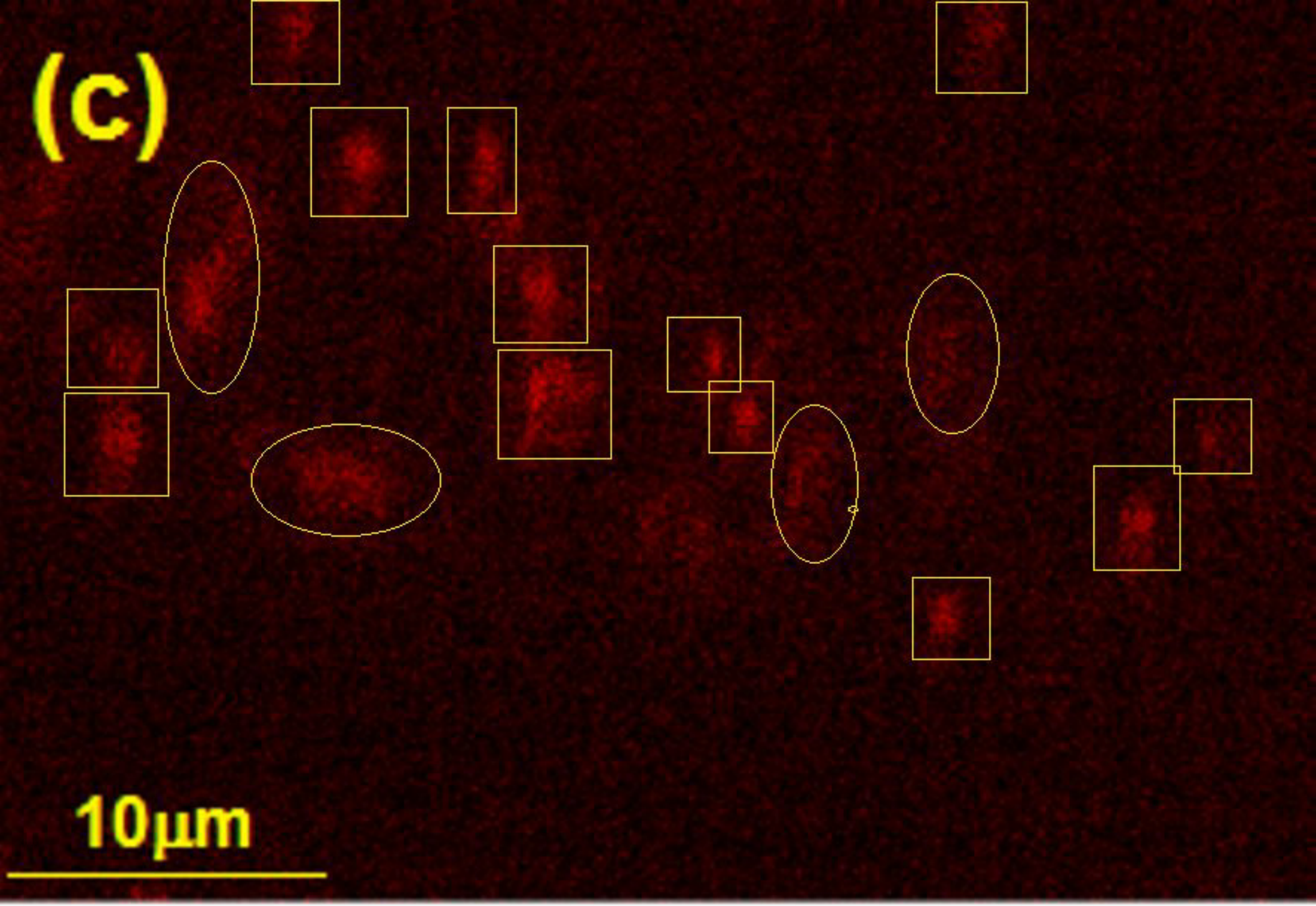
(c)
10μm

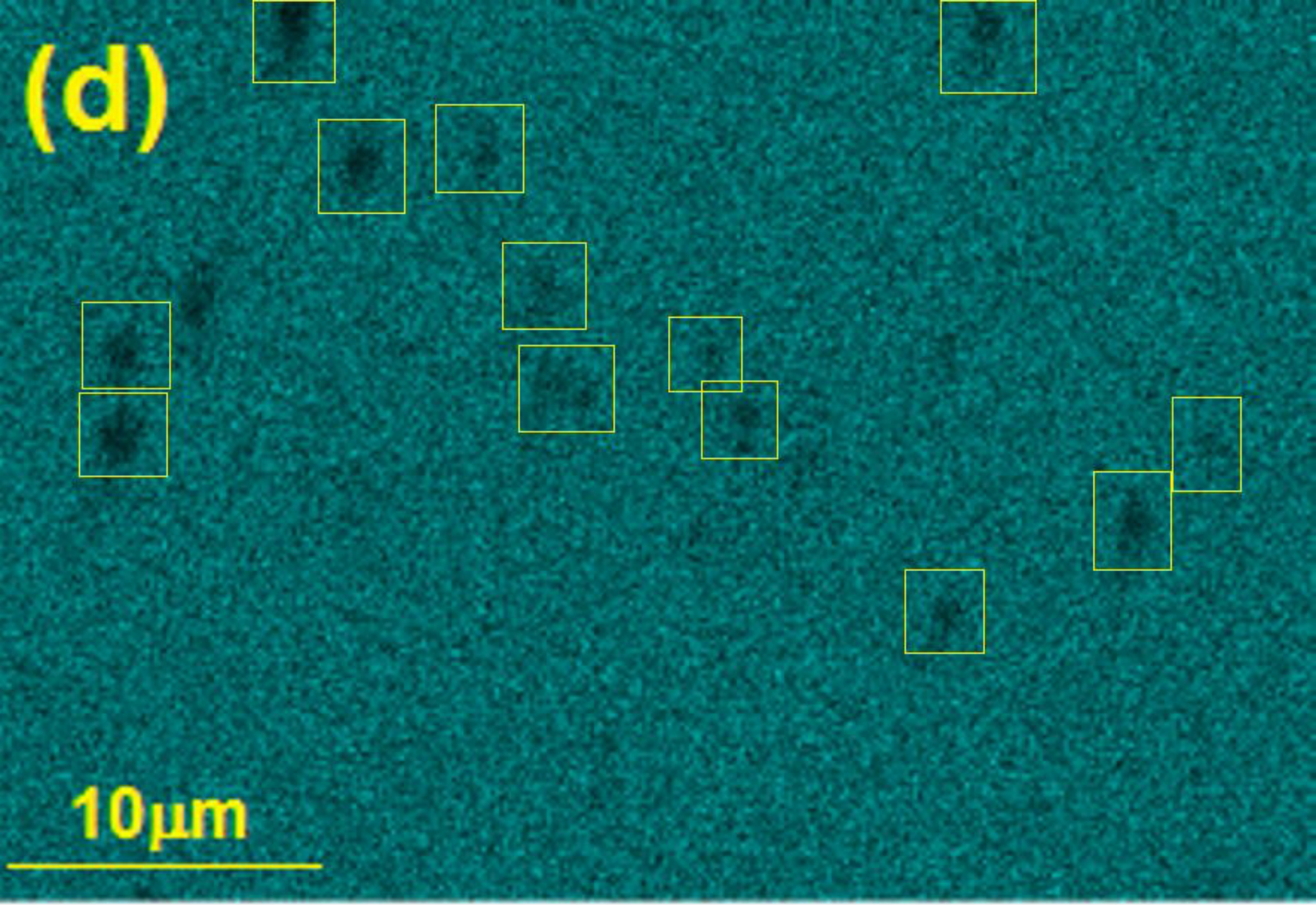
(d)
10μm

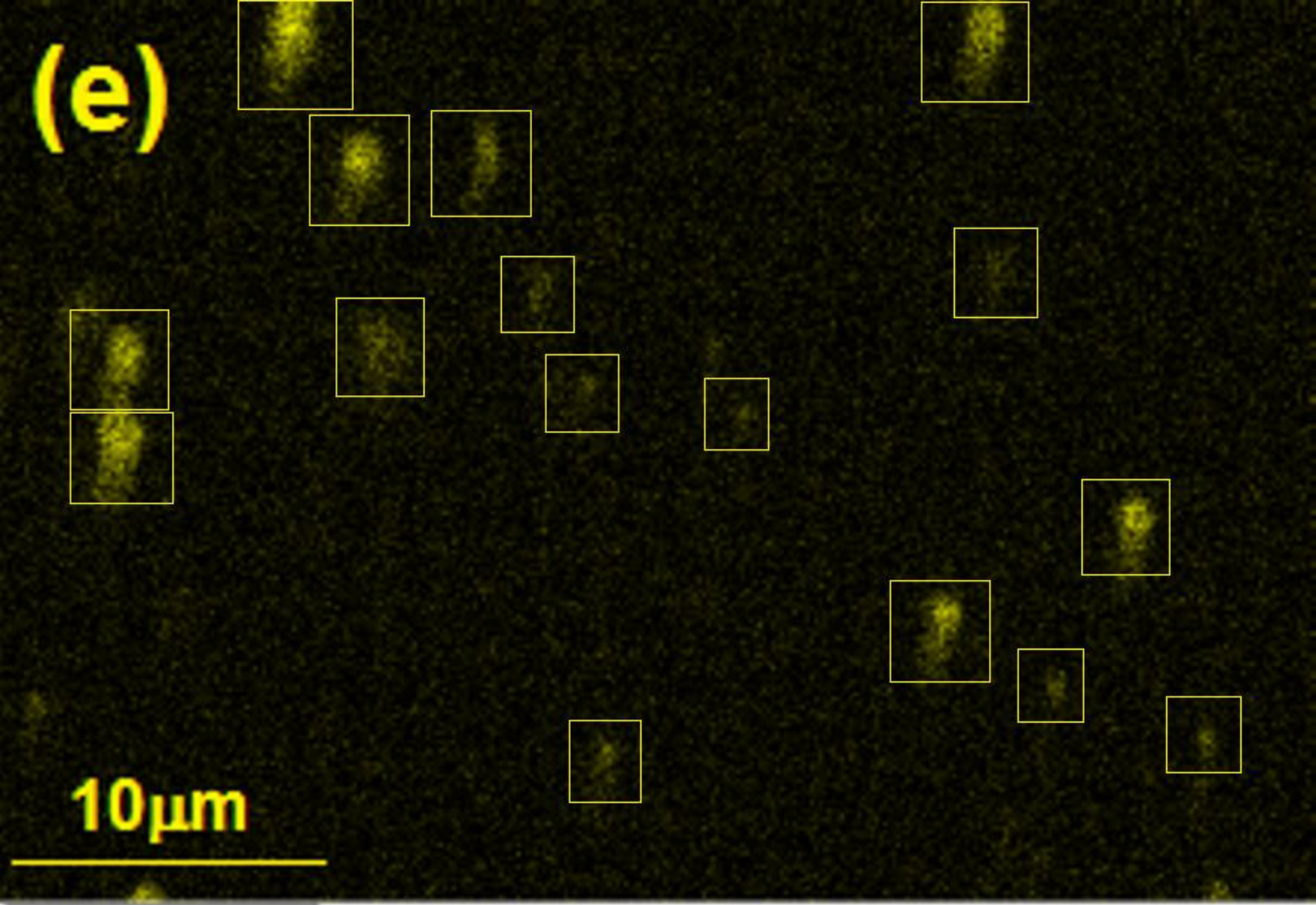
(e)
10μm

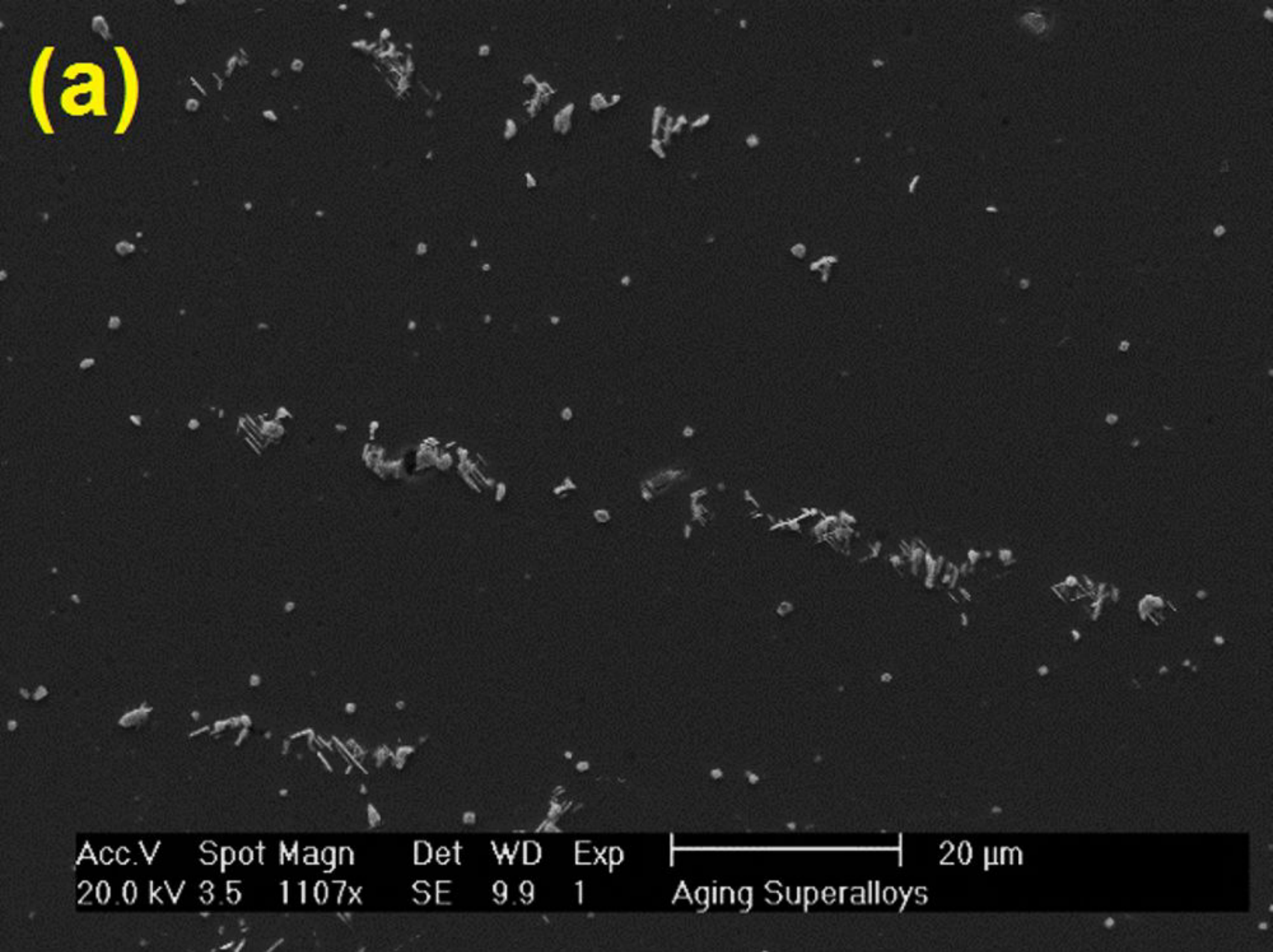
(a)
Acc.V Spot Magn Det WD Exp
20.0 kV 3.5 1107x SE 9.9 1
20 µm
Aging Superalloys

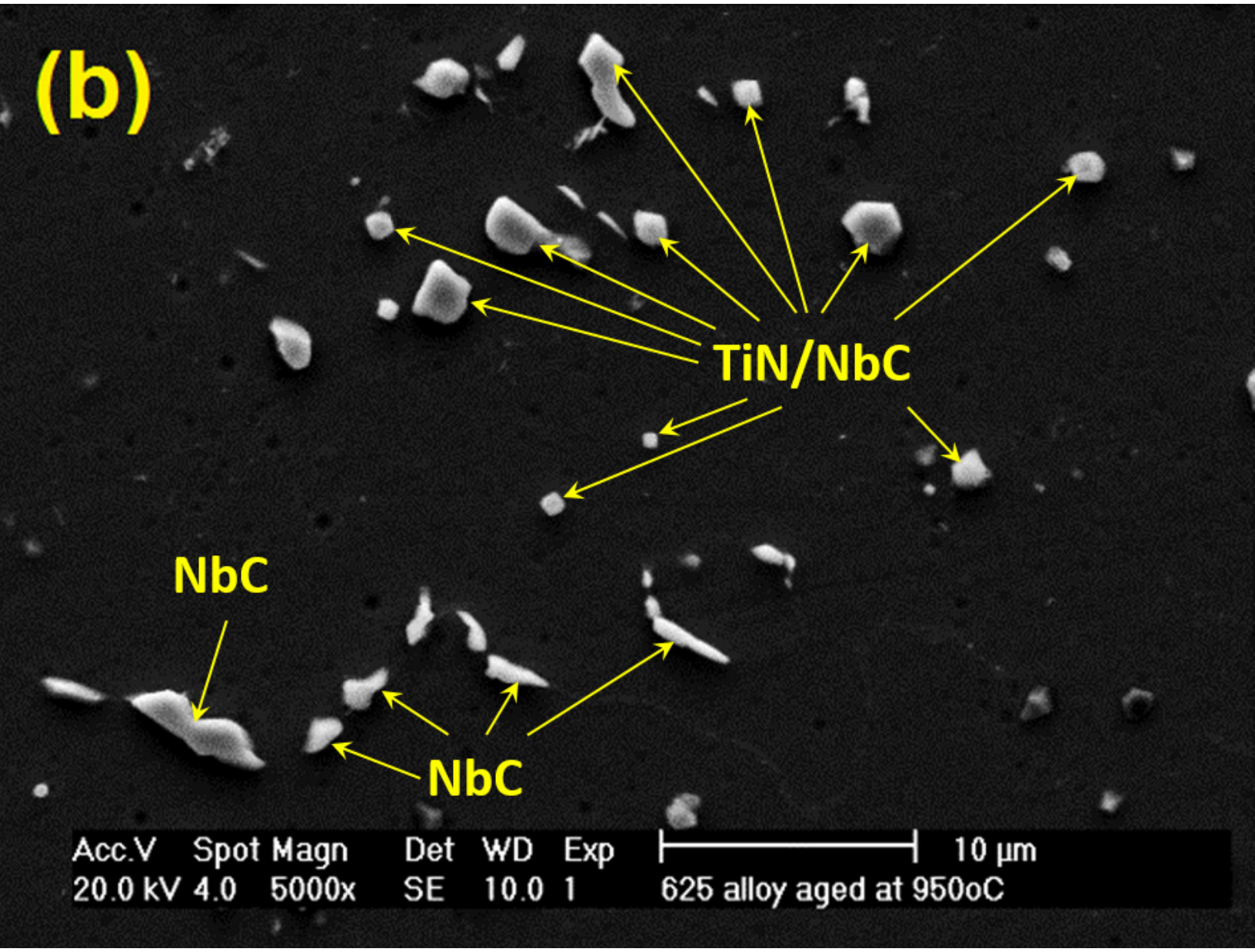
(b)
TiN/NbC
NbC
NbC
Acc.V Spot Magn Det WD Exp
20.0 kV 4.0 5000x SE 10.0 1
10 µm
625 alloy aged at 950oC

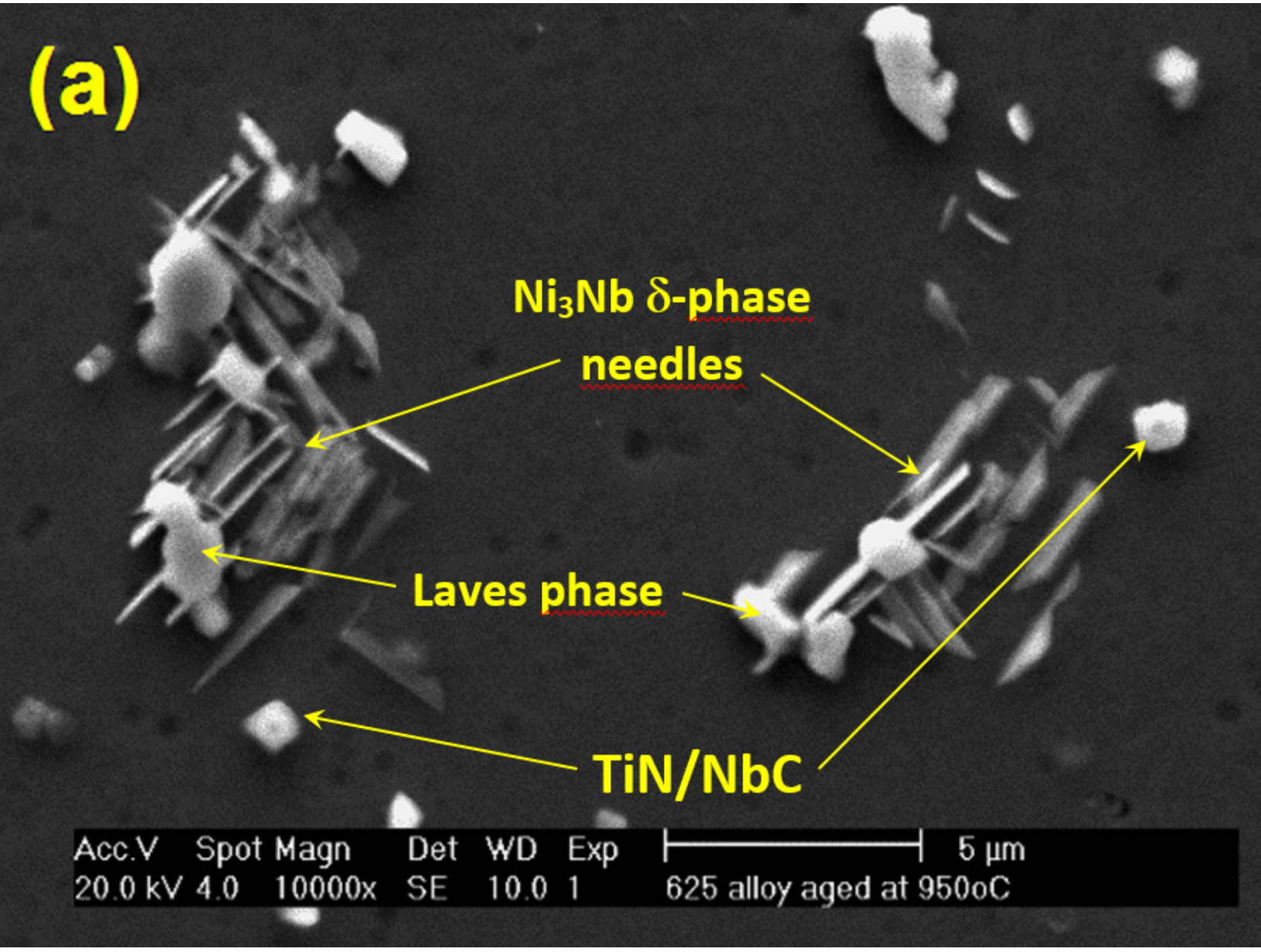
(a)
Ni3Nb δ-phase
needles
Laves phase
TiN/NbC
Acc.V Spot Magn Det WD Exp
20.0 kV 4.0 10000x SE 10.0 1
5 µm
625 alloy aged at 950oC

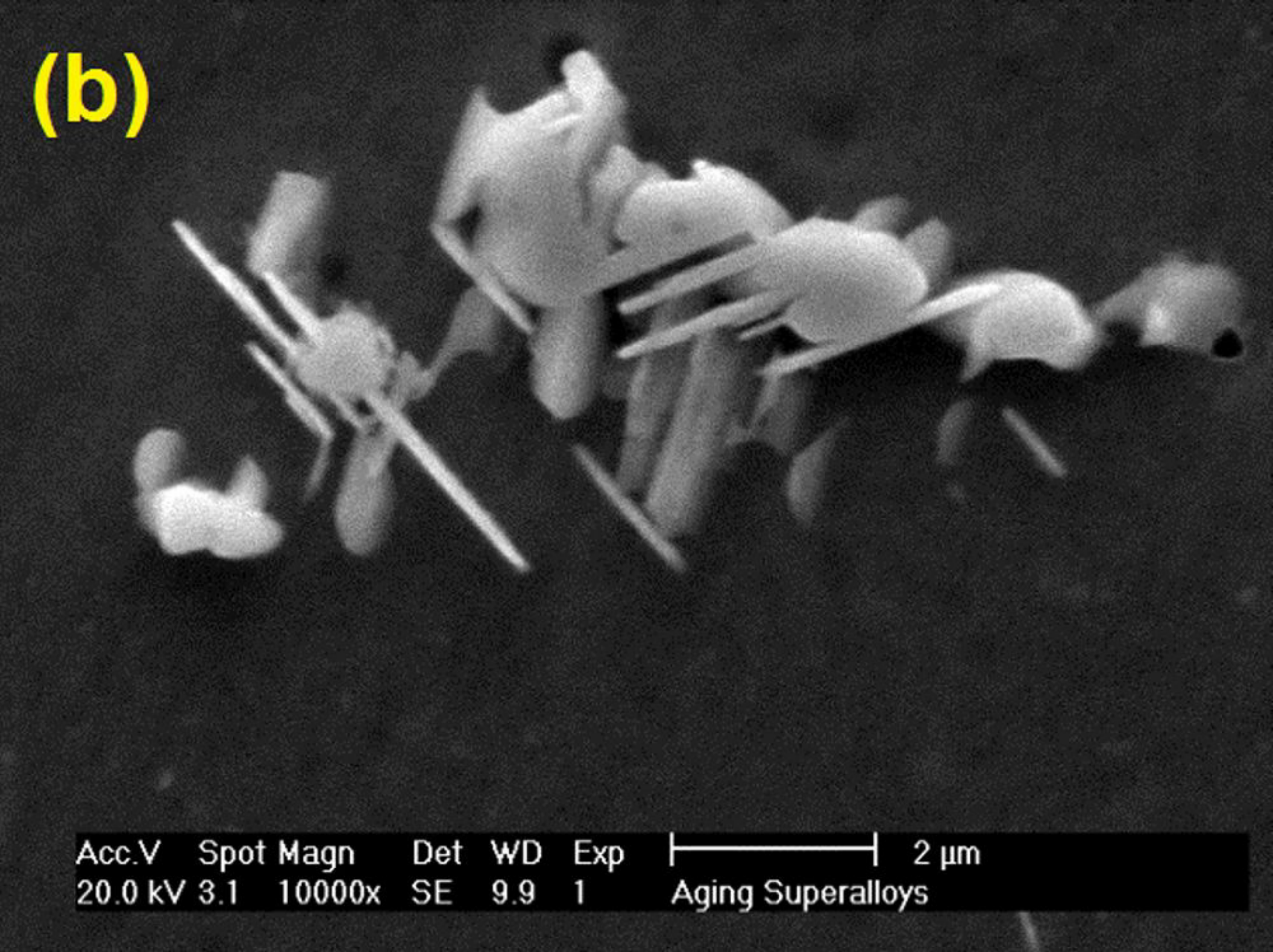
(b)
Acc.V Spot Magn Det WD Exp 2 µm
20.0 kV 3.1 10000x SE 9.9 1 Aging Superalloys

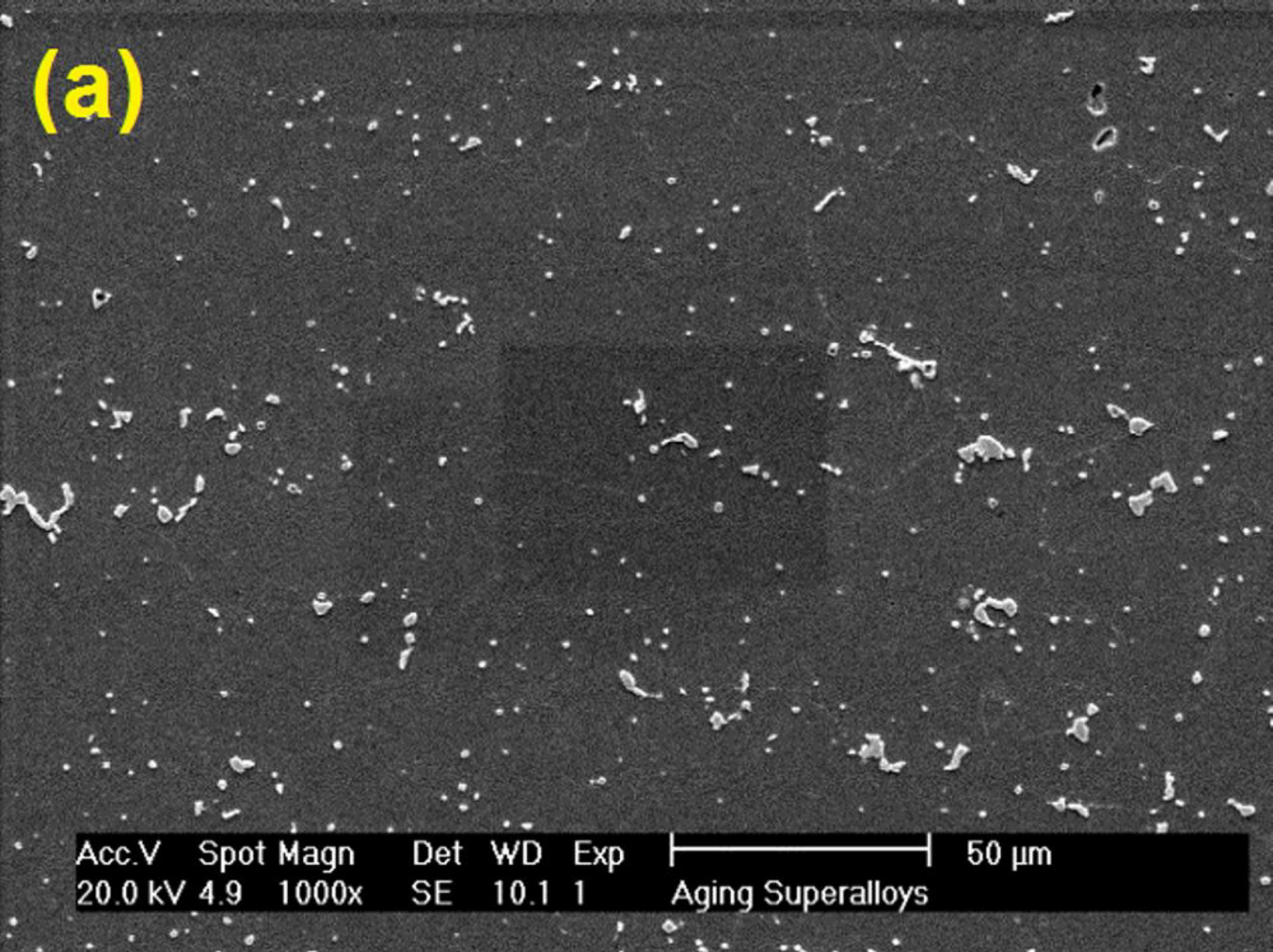
(a)
Acc.V Spot Magn Det WD Exp
50 µm
20.0 kV 4.9 1000x SE 10.1 1
Aging Superalloys

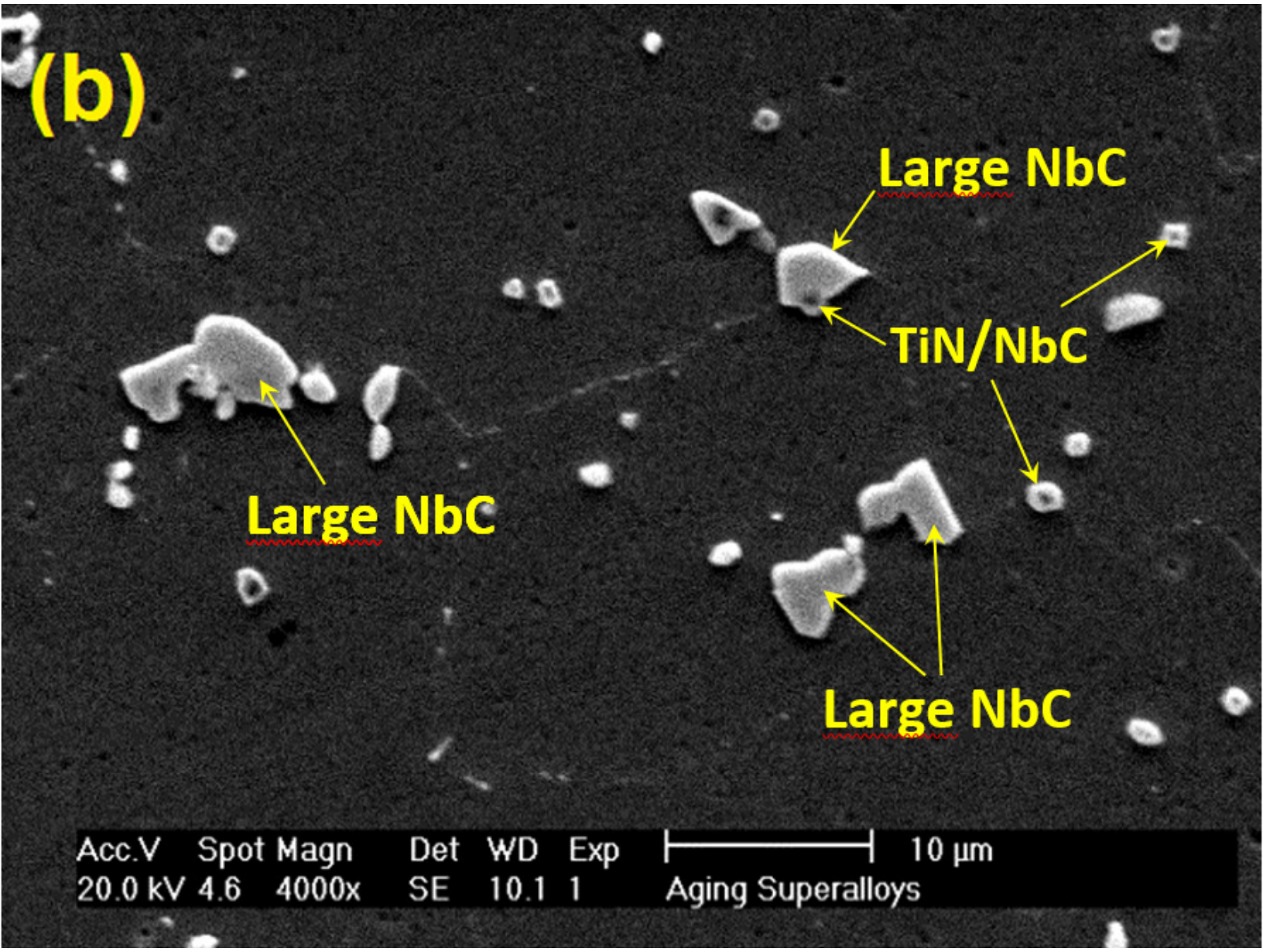
(b)
Large NbC
TiN/NbC
Large NbC
Large NbC
Acc.V Spot Magn Det WD Exp
10 µm
20.0 kV 4.6 4000x SE 10.1 1
Aging Superalloys

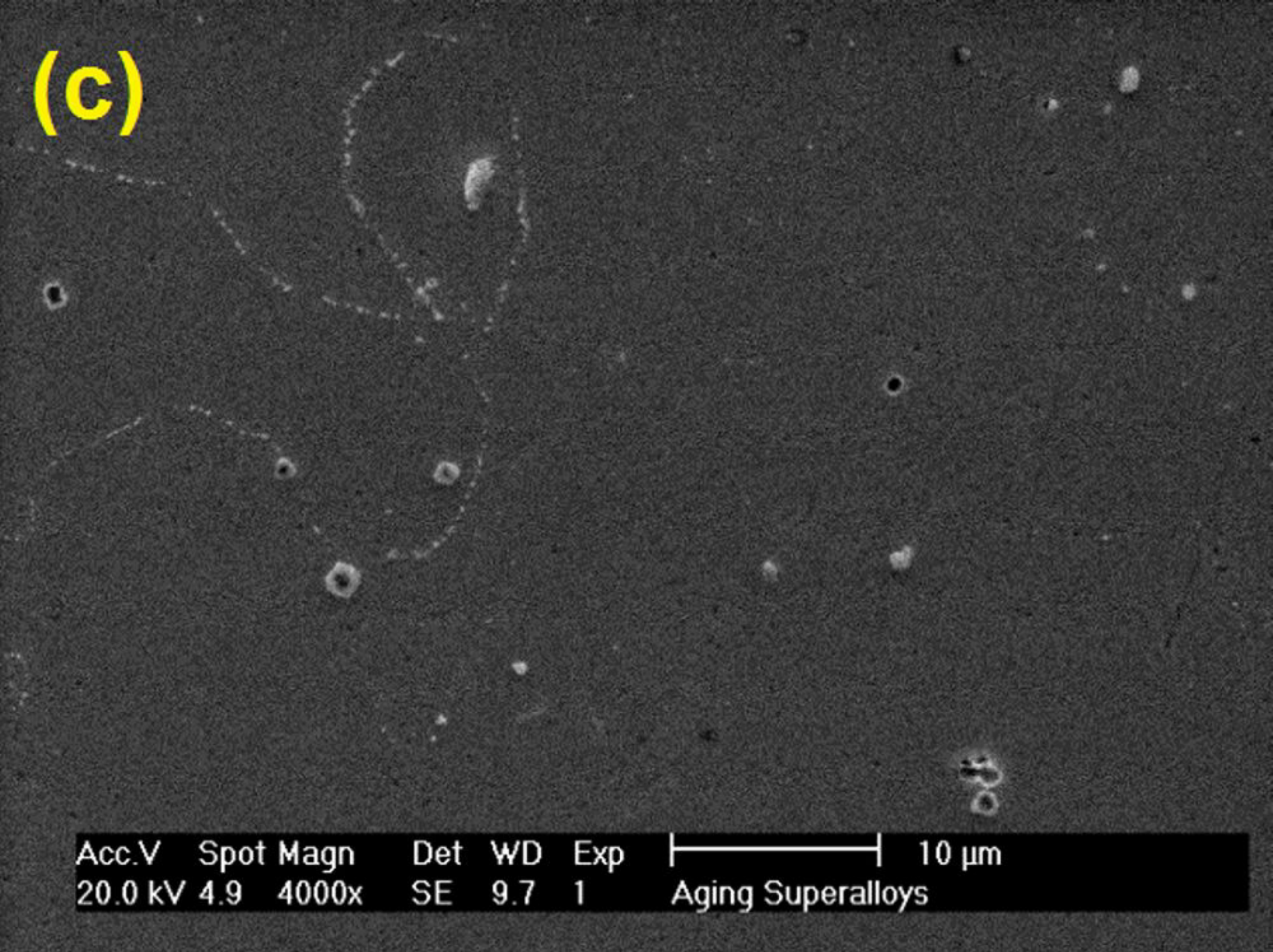
(c)
Acc.V Spot Magn Det WD Exp 10 µm
20.0 kV 4.9 4000x SE 9.7 1 Aging Superalloys

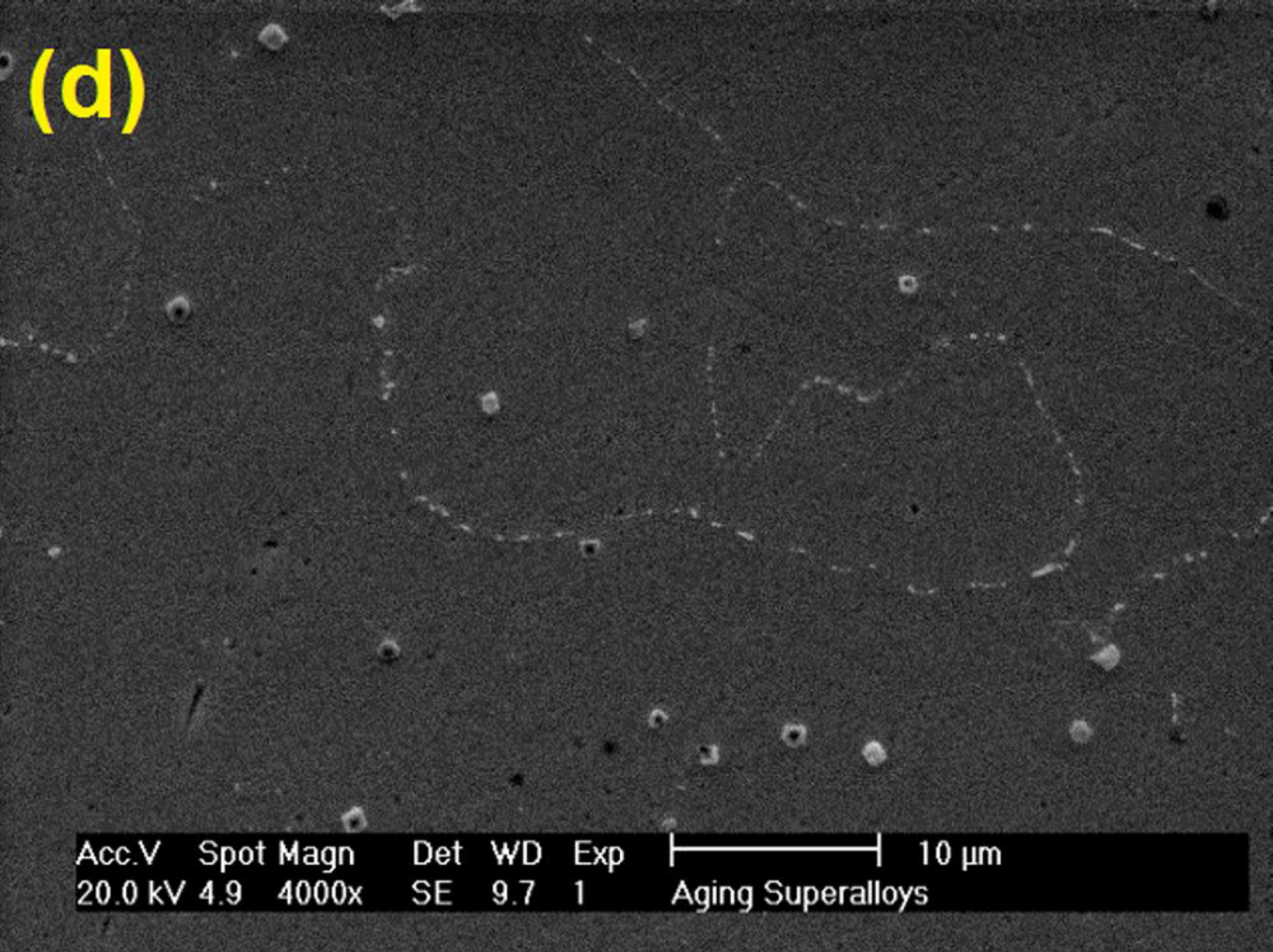
(d)
Acc.V Spot Magn Det WD Exp 10 µm
20.0 kV 4.9 4000x SE 9.7 1 Aging Superalloys

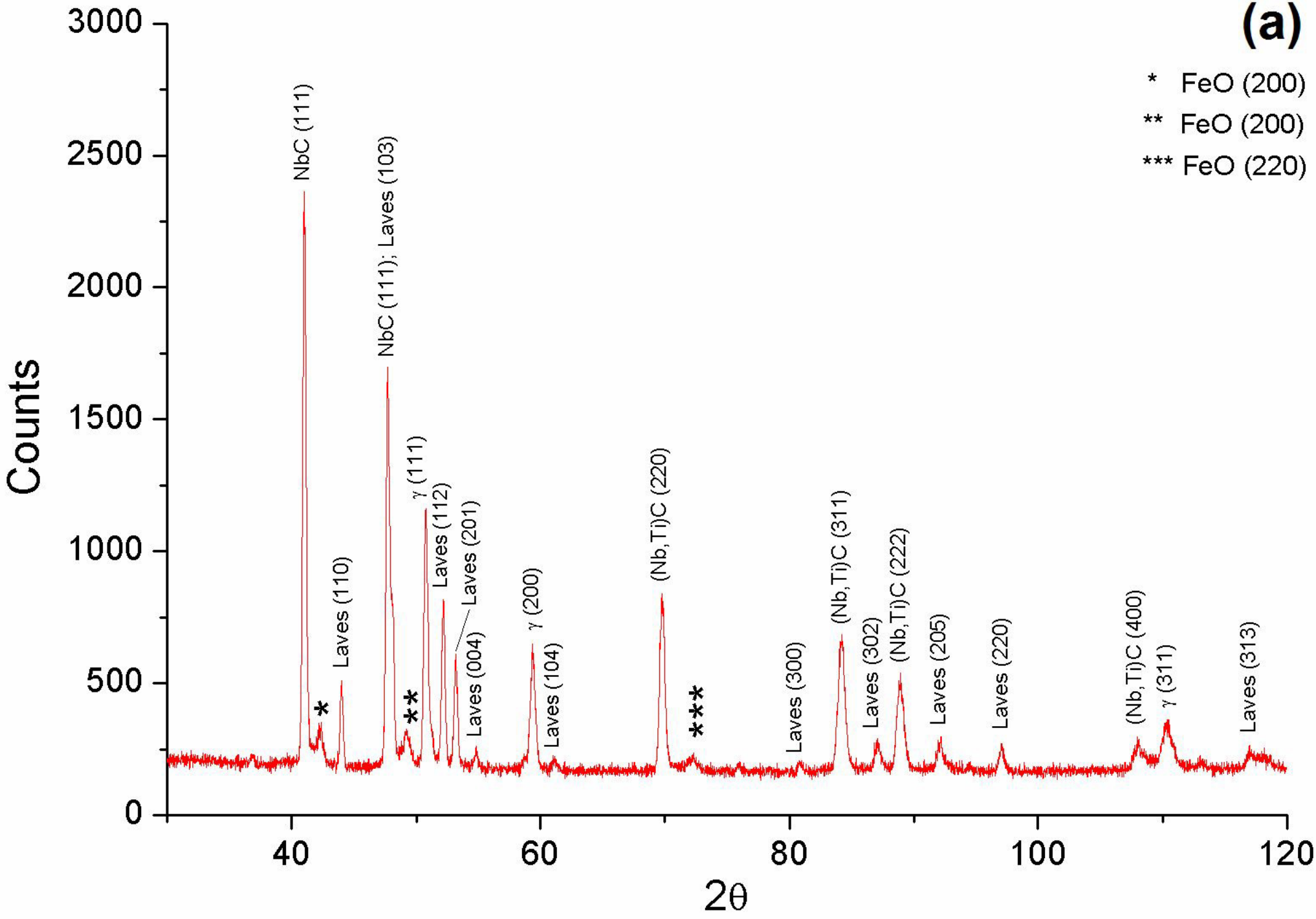
(a)
* FeO (200)
** FeO (200)
*** FeO (220)
Counts
2θ
0
500
1000
1500
2000
2500
3000
40
60
80
100
120
NbC (111)
Laves (110)
NbC (111); Laves (103)
γ (111)
Laves (112)
Laves (201)
Laves (004)
γ (200)
Laves (104)
(Nb,Ti)C (220)
Laves (300)
(Nb,Ti)C (311)
Laves (302)
(Nb,Ti)C (222)
Laves (205)
Laves (220)
(Nb,Ti)C (400)
γ (311)
Laves (313)
*
**
***

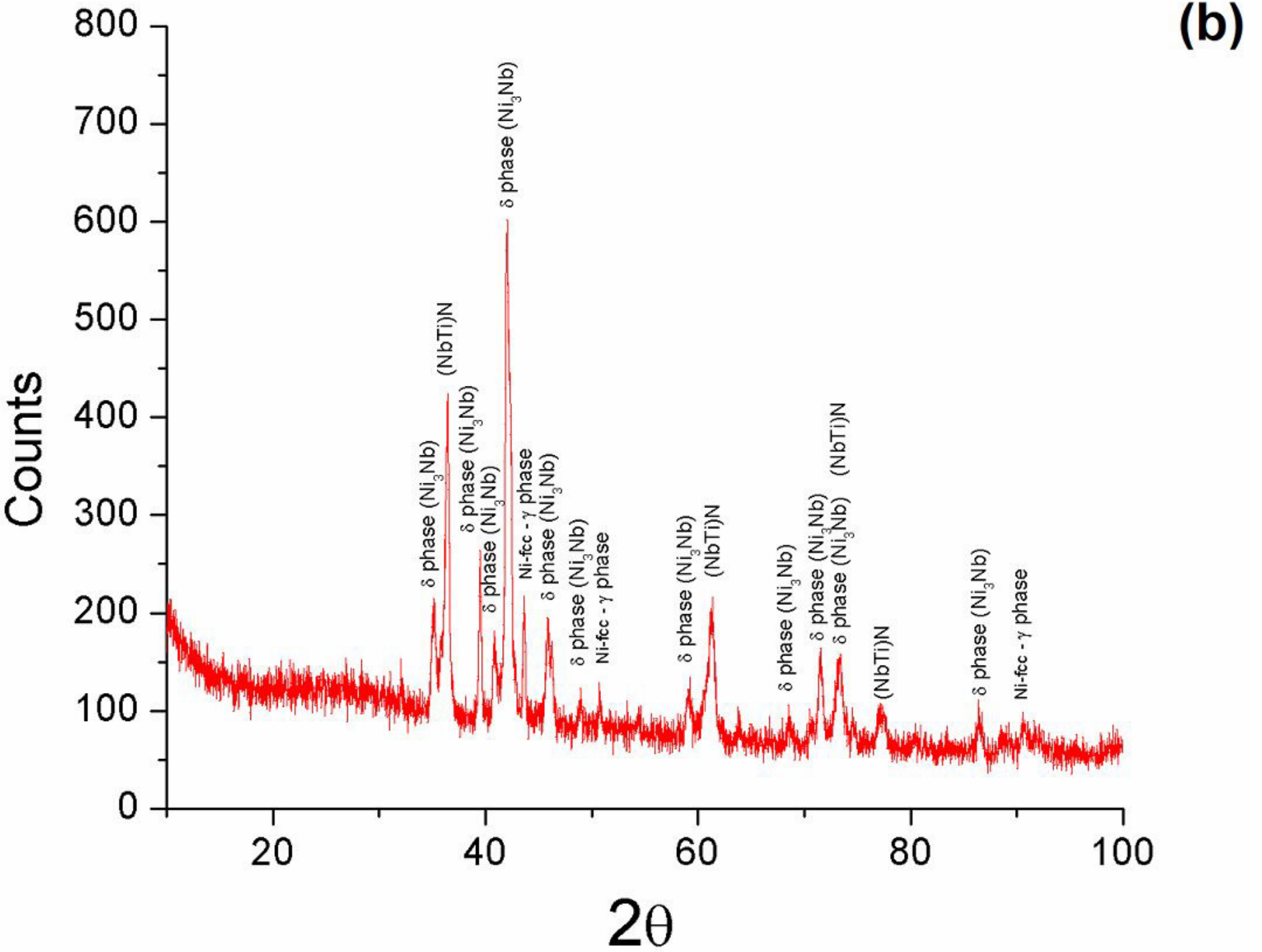
(b)
Counts
2θ
0
100
200
300
400
500
600
700
800
20
40
60
80
100
δ phase (Ni3Nb)
(NbTi)N
δ phase (Ni3Nb)
δ phase (Ni3Nb)
δ phase (Ni3Nb)
Ni-fcc - γ phase
δ phase (Ni3Nb)
δ phase (Ni3Nb)
Ni-fcc - γ phase
δ phase (Ni3Nb)
(NbTi)N
δ phase (Ni3Nb)
δ phase (Ni3Nb)
δ phase (Ni3Nb)
(NbTi)N
(NbTi)N
δ phase (Ni3Nb)
Ni-fcc - γ phase

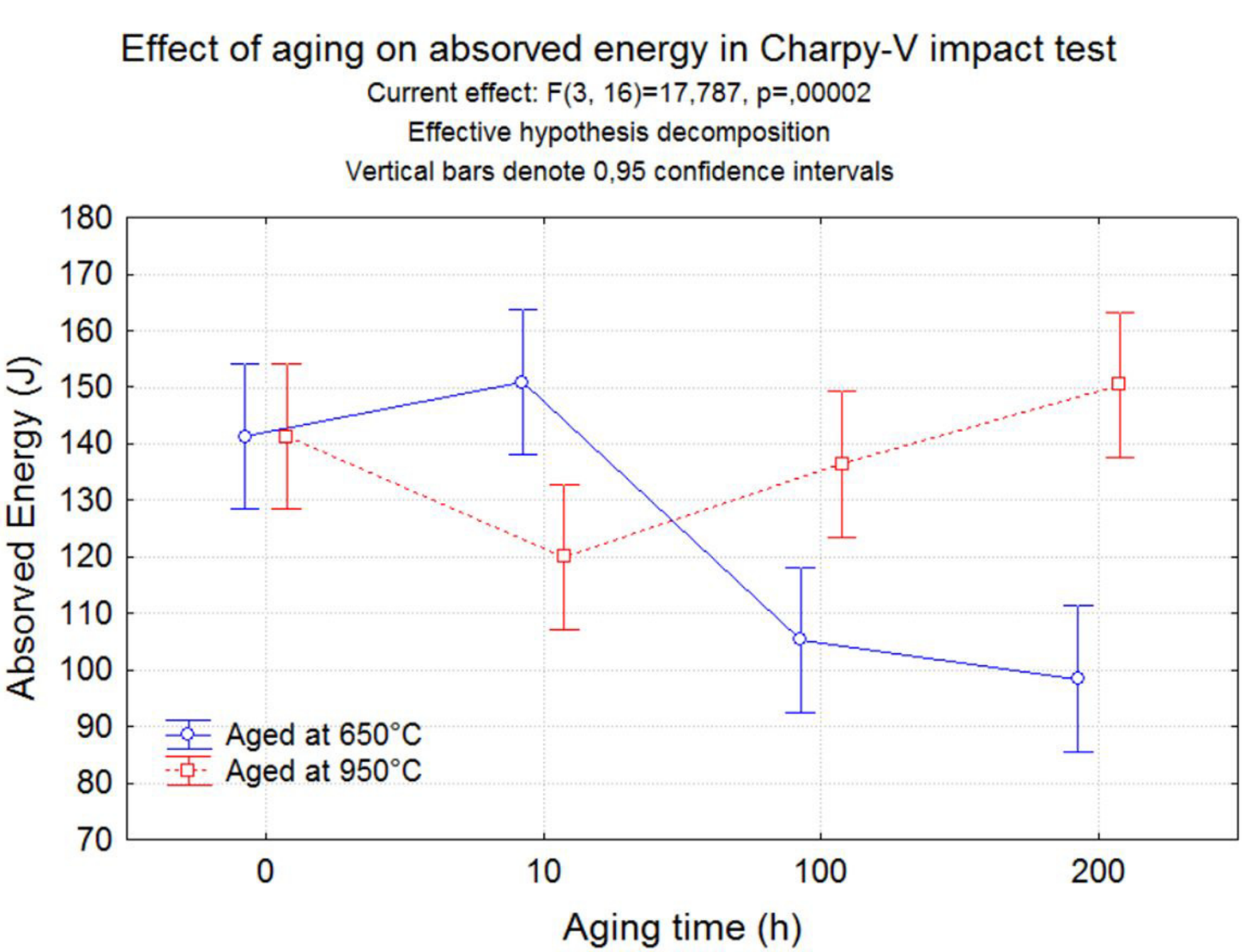
Effect of aging on absorved energy in Charpy-V impact test
Current effect: F(3, 16)=17,787, p=,00002
Effective hypothesis decomposition
Vertical bars denote 0,95 confidence intervals
Absorved Energy (J)
180
170
160
150
140
130
120
110
100
90
80
70
0
10
100
200
Aging time (h)
Aged at 650°C
Aged at 950°C

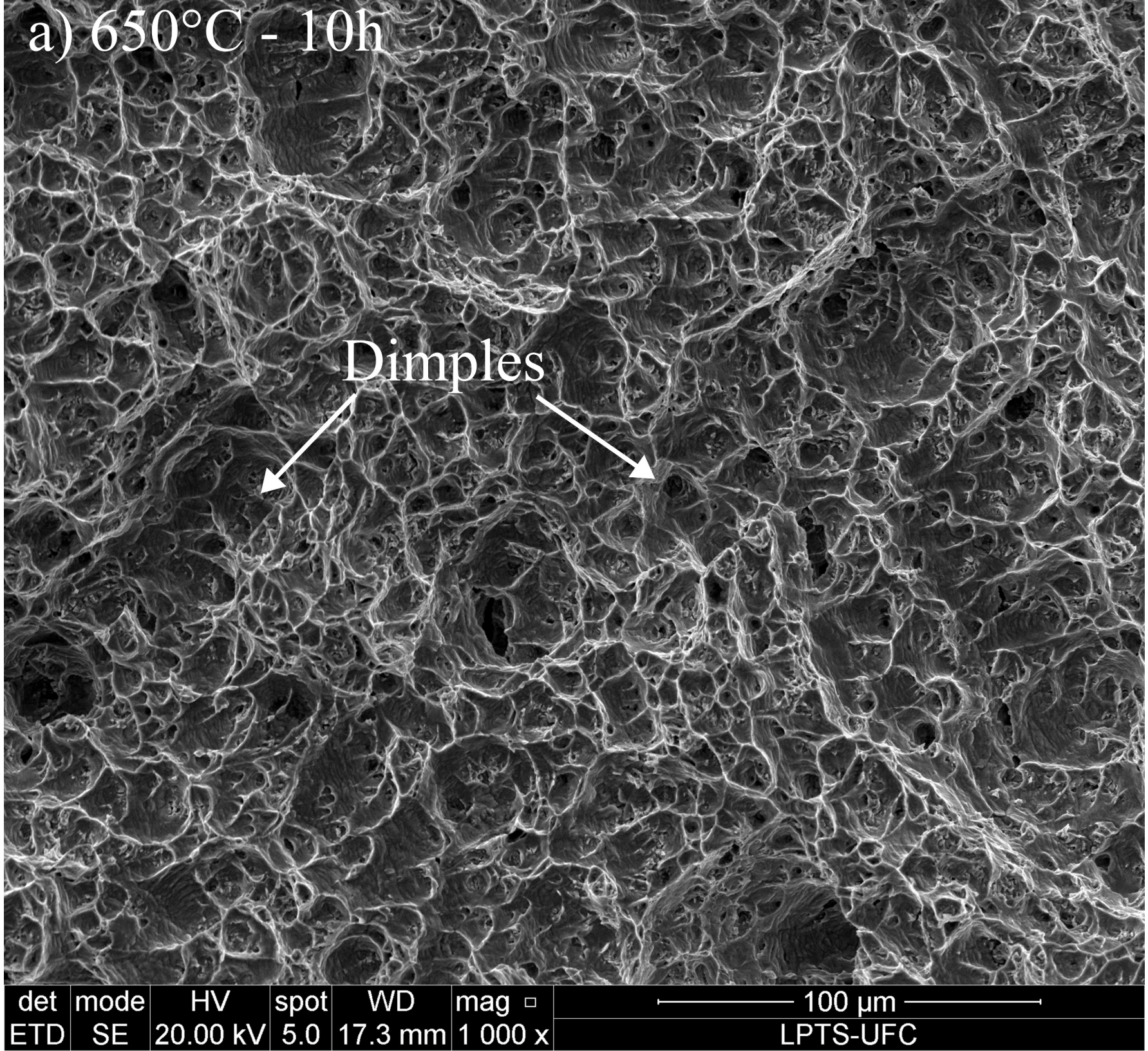
a) 650°C - 10h
Dimples
det ETD
mode SE
HV 20.00 kV
spot 5.0
WD 17.3 mm
mag ▫ 1 000 x
100 µm
LPTS-UFC

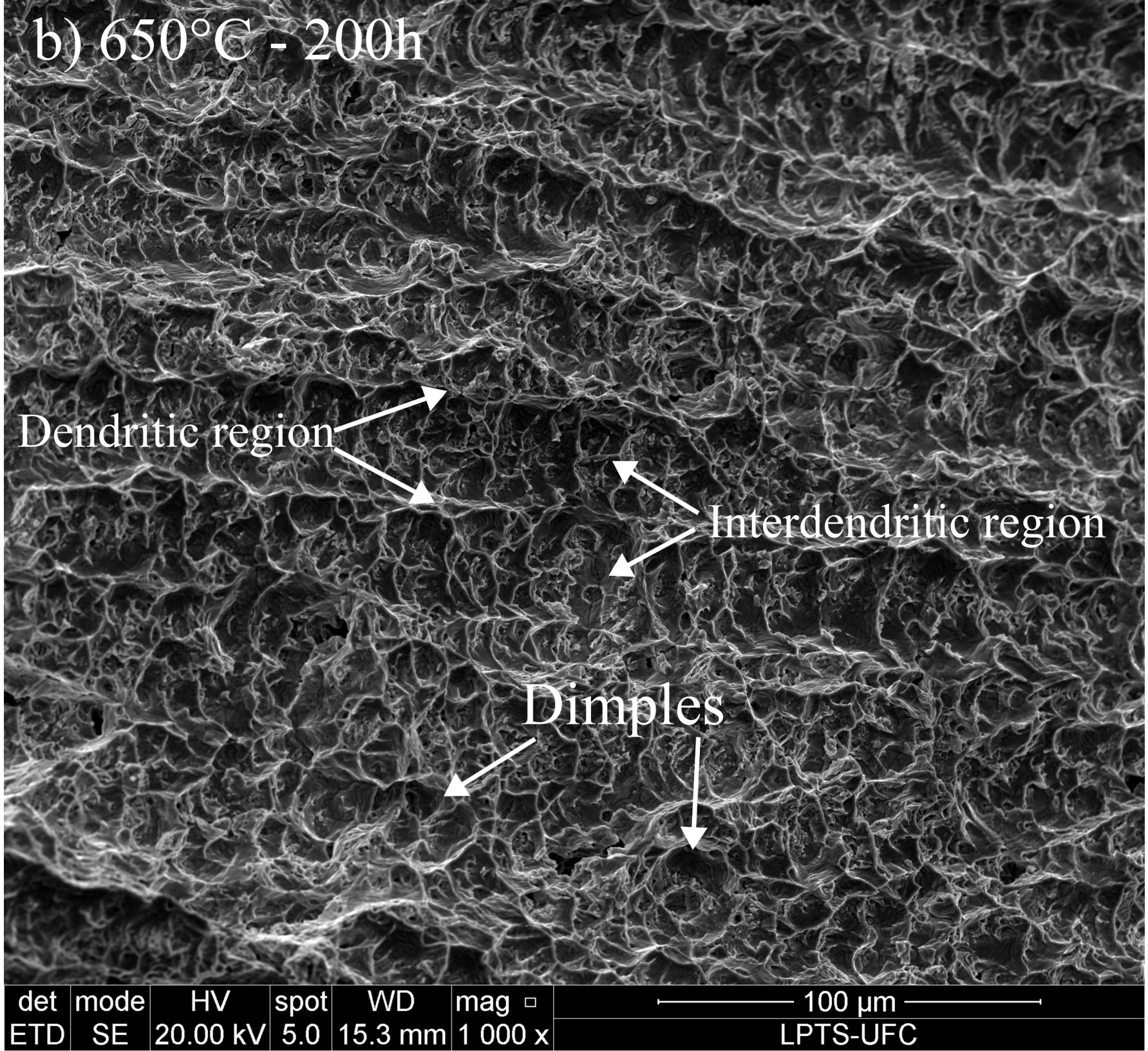
b) 650°C - 200h
Dendritic region
Interdendritic region
Dimples
det ETD
mode SE
HV 20.00 kV
spot 5.0
WD 15.3 mm
mag 1 000 x
100 µm
LPTS-UFC

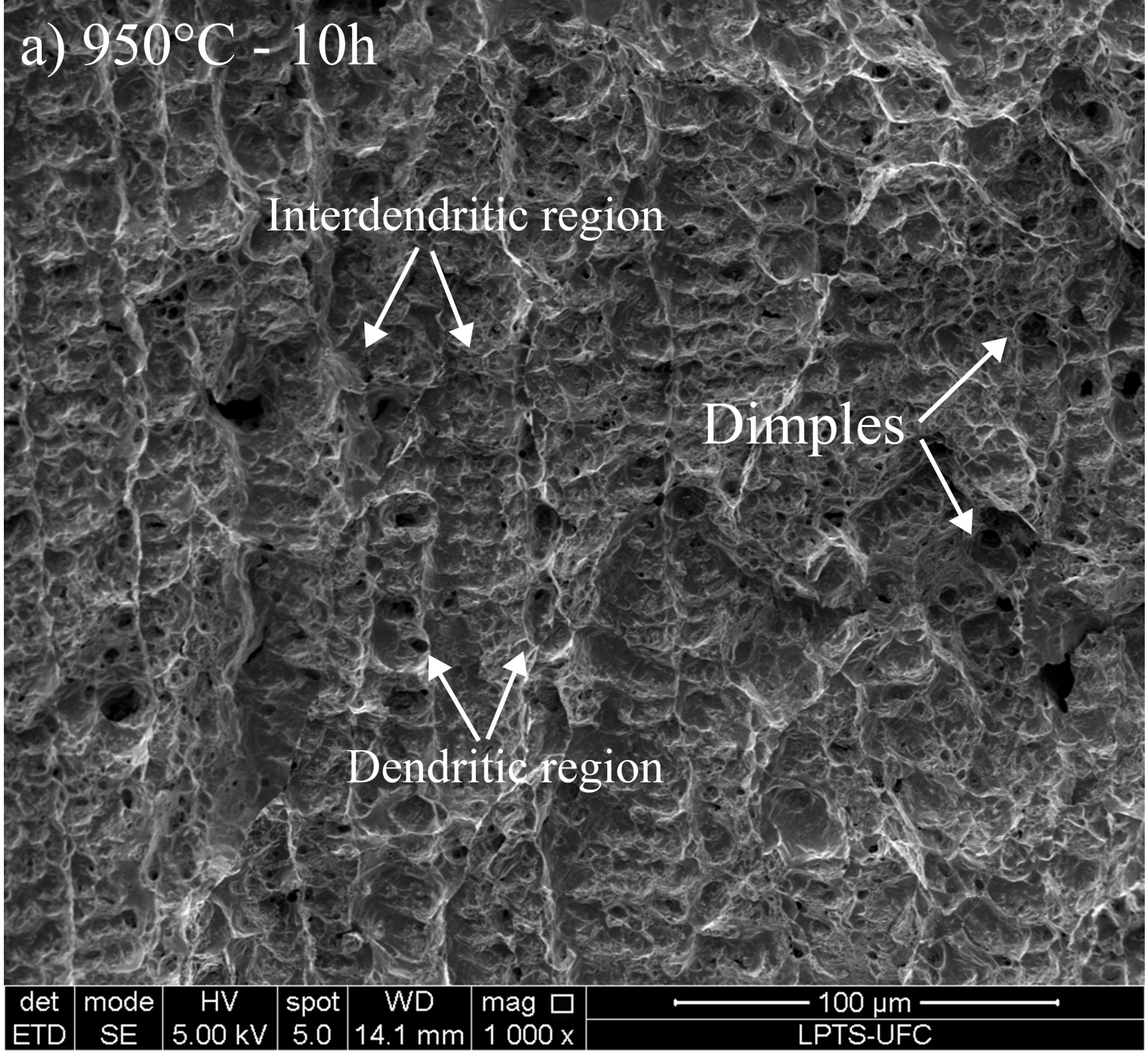
a) 950°C - 10h
Interdendritic region
Dimples
Dendritic region
det ETD
mode SE
HV 5.00 kV
spot 5.0
WD 14.1 mm
mag 1 000 x
100 µm
LPTS-UFC

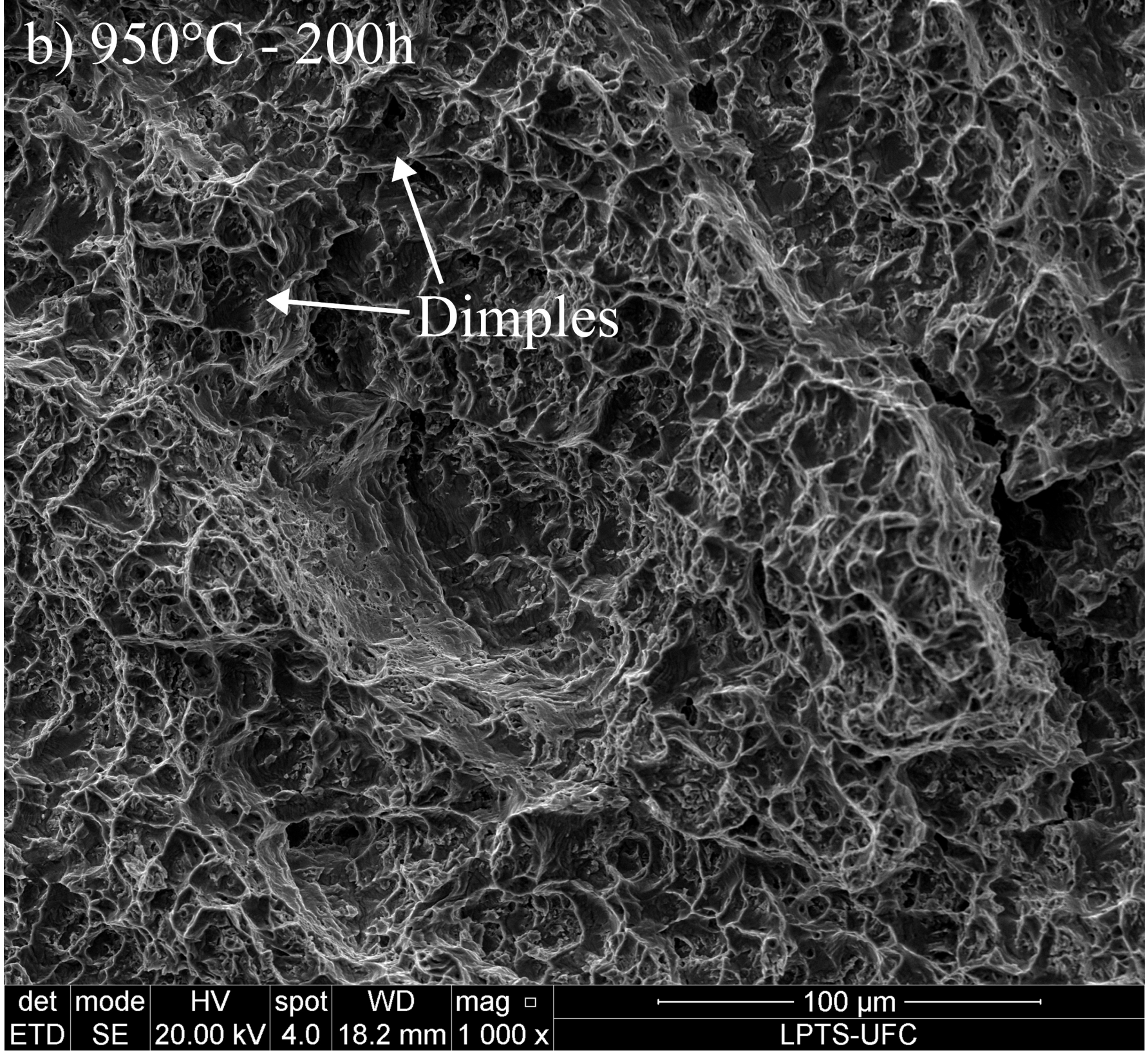
b) 950°C - 200h
Dimples
det ETD
mode SE
HV 20.00 kV
spot 4.0
WD 18.2 mm
mag 1 000 x
100 µm
LPTS-UFC

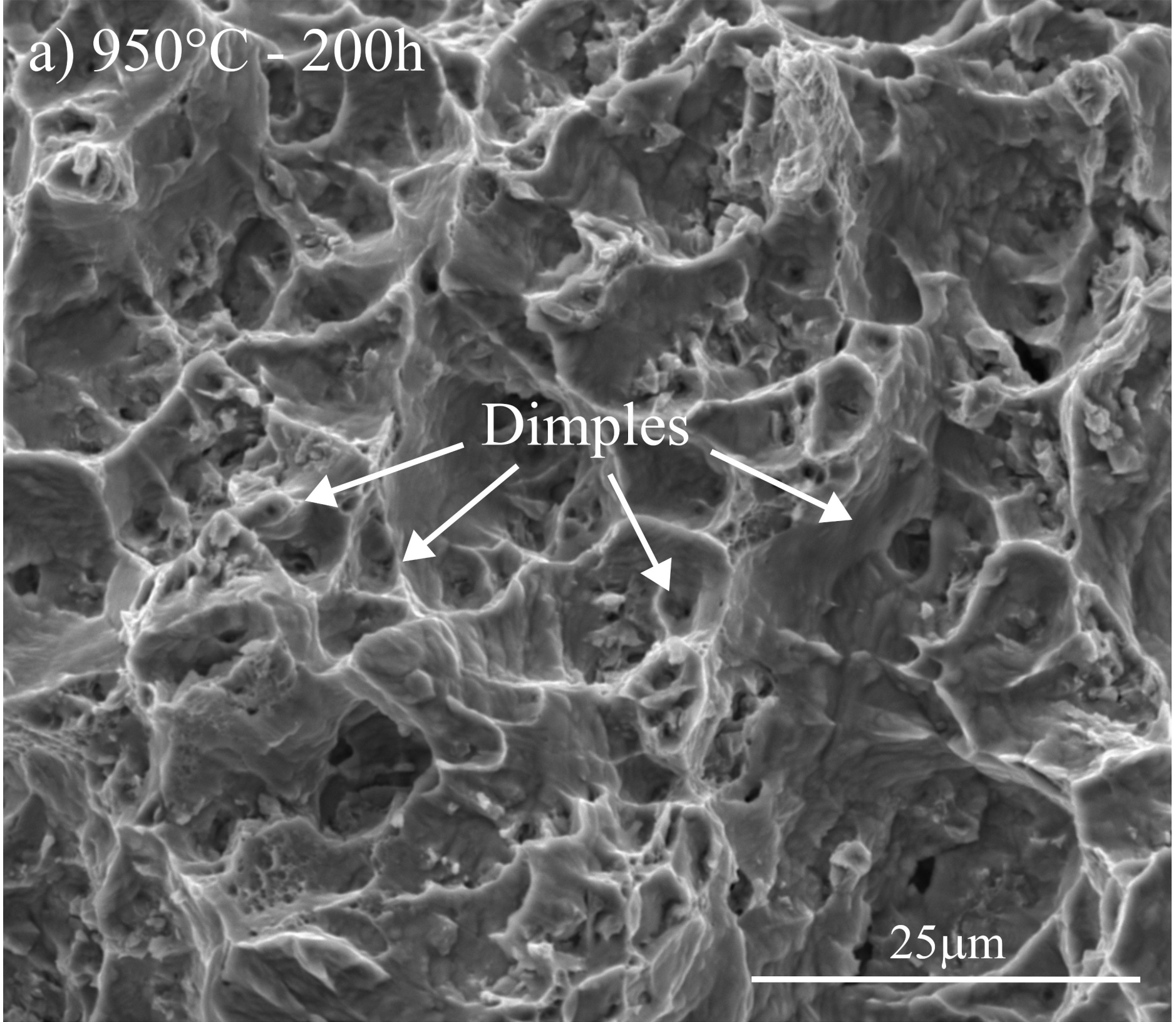
a) 950°C - 200h
Dimples
25µm

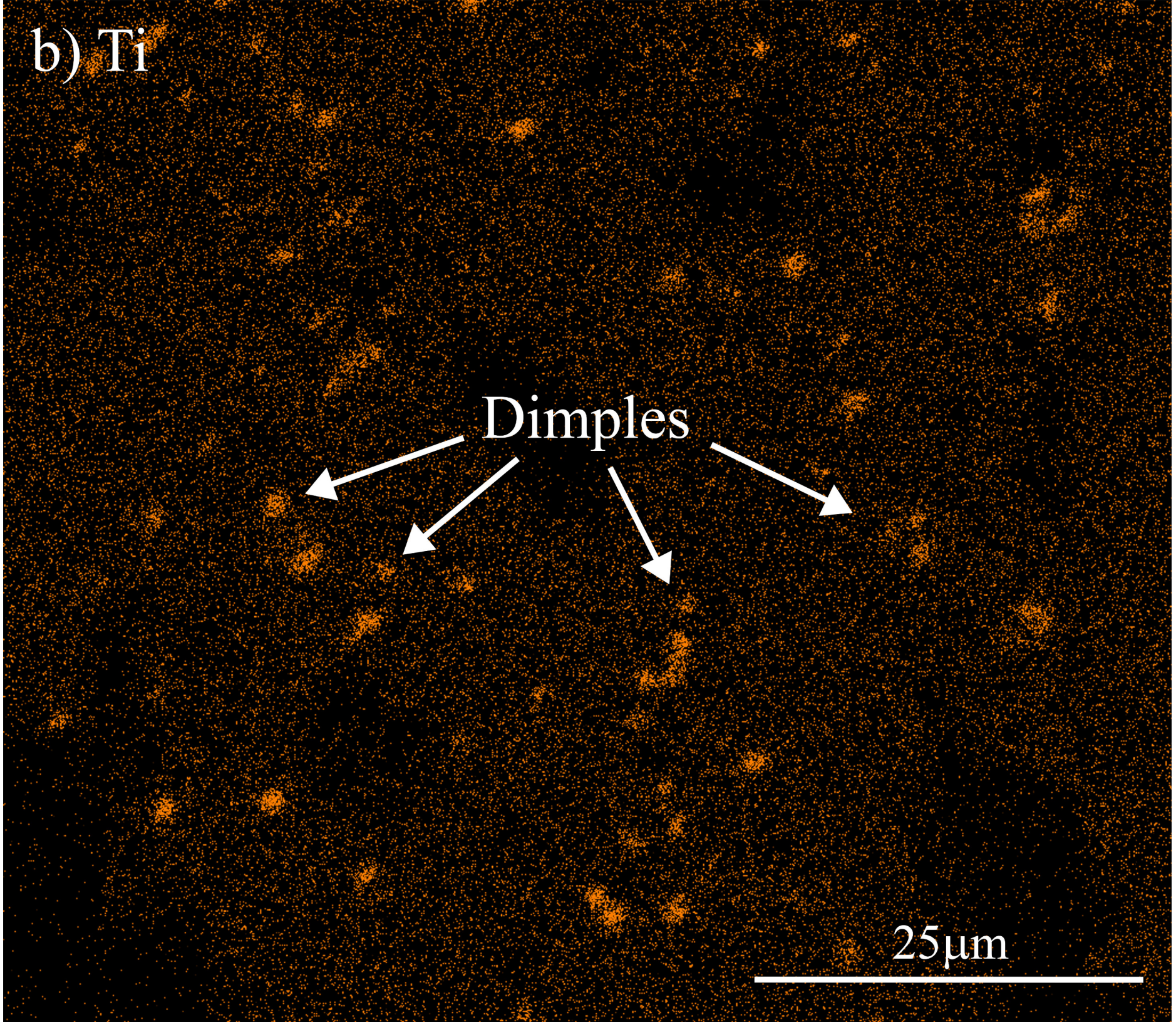
b) Ti
Dimples
25μm

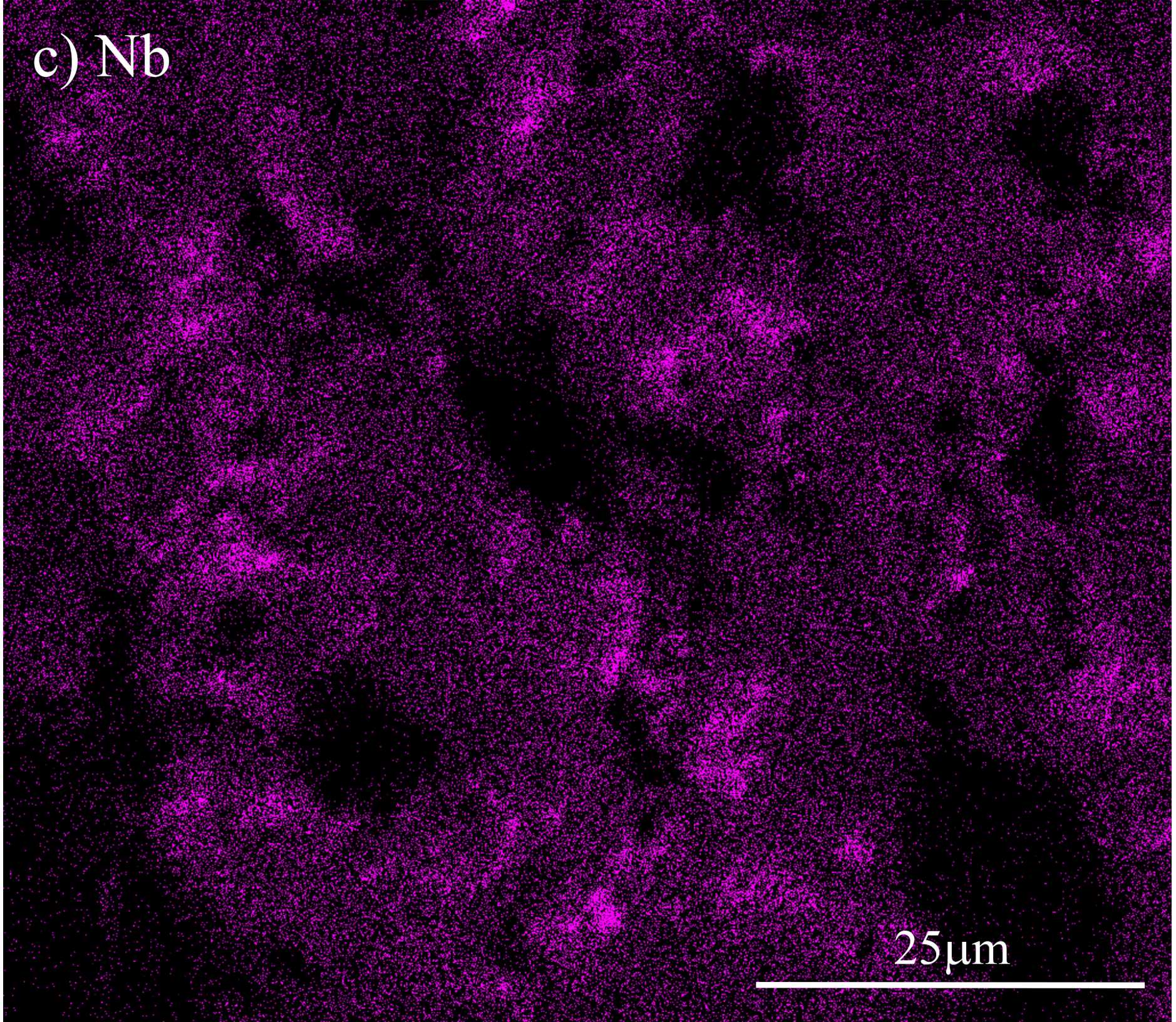
c) Nb
25μm

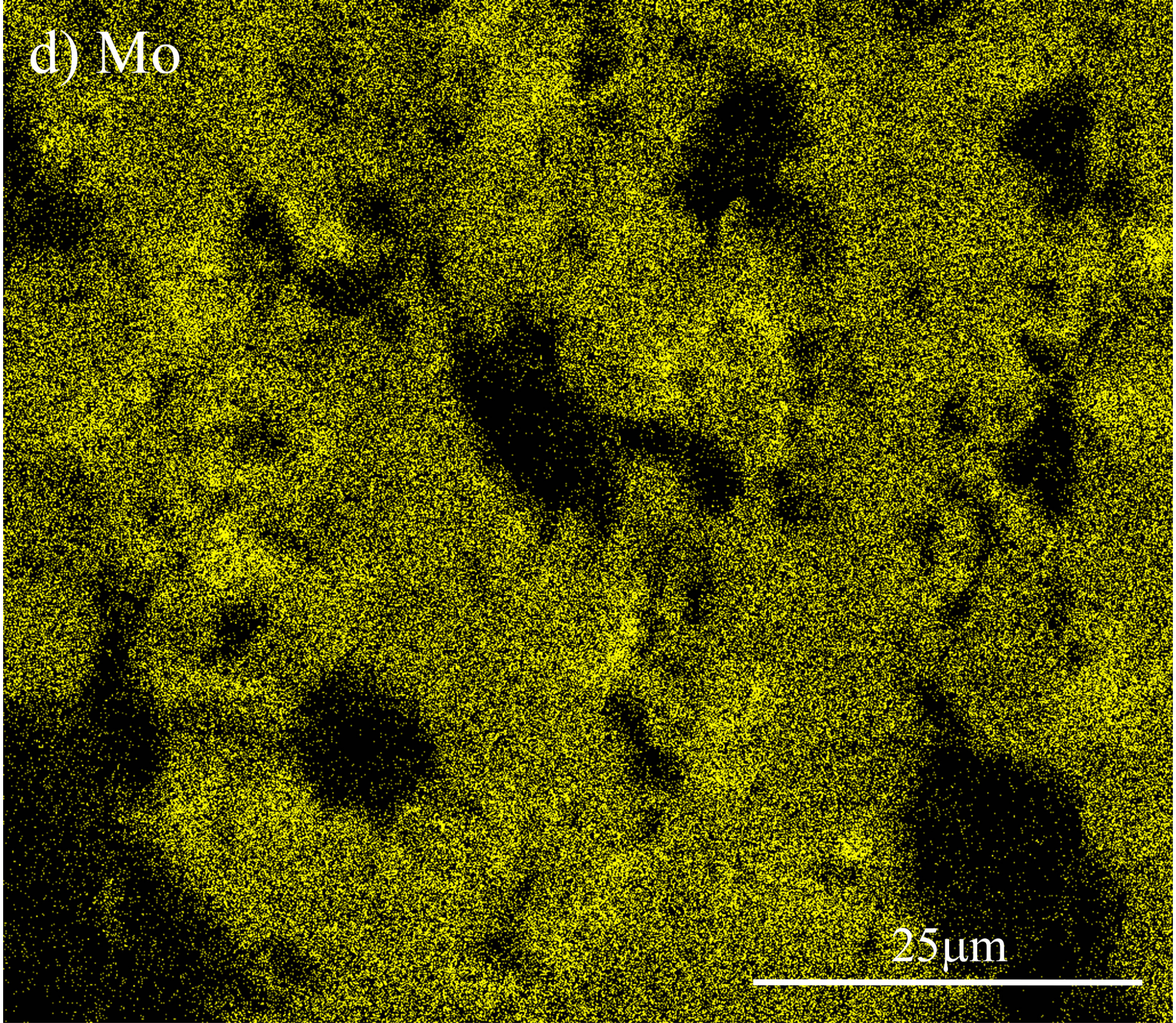
d) Mo
25μm

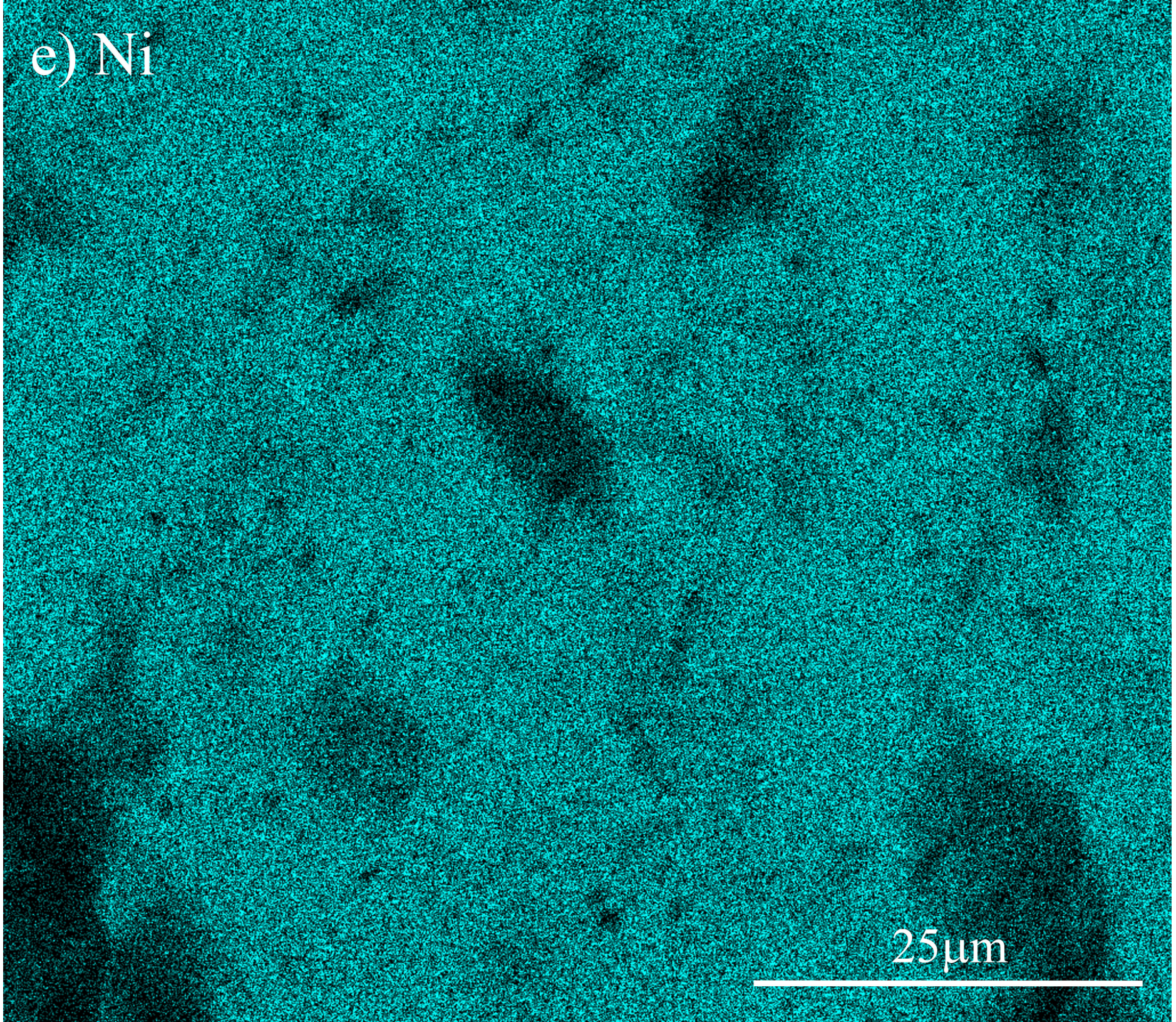
e) Ni
25µm

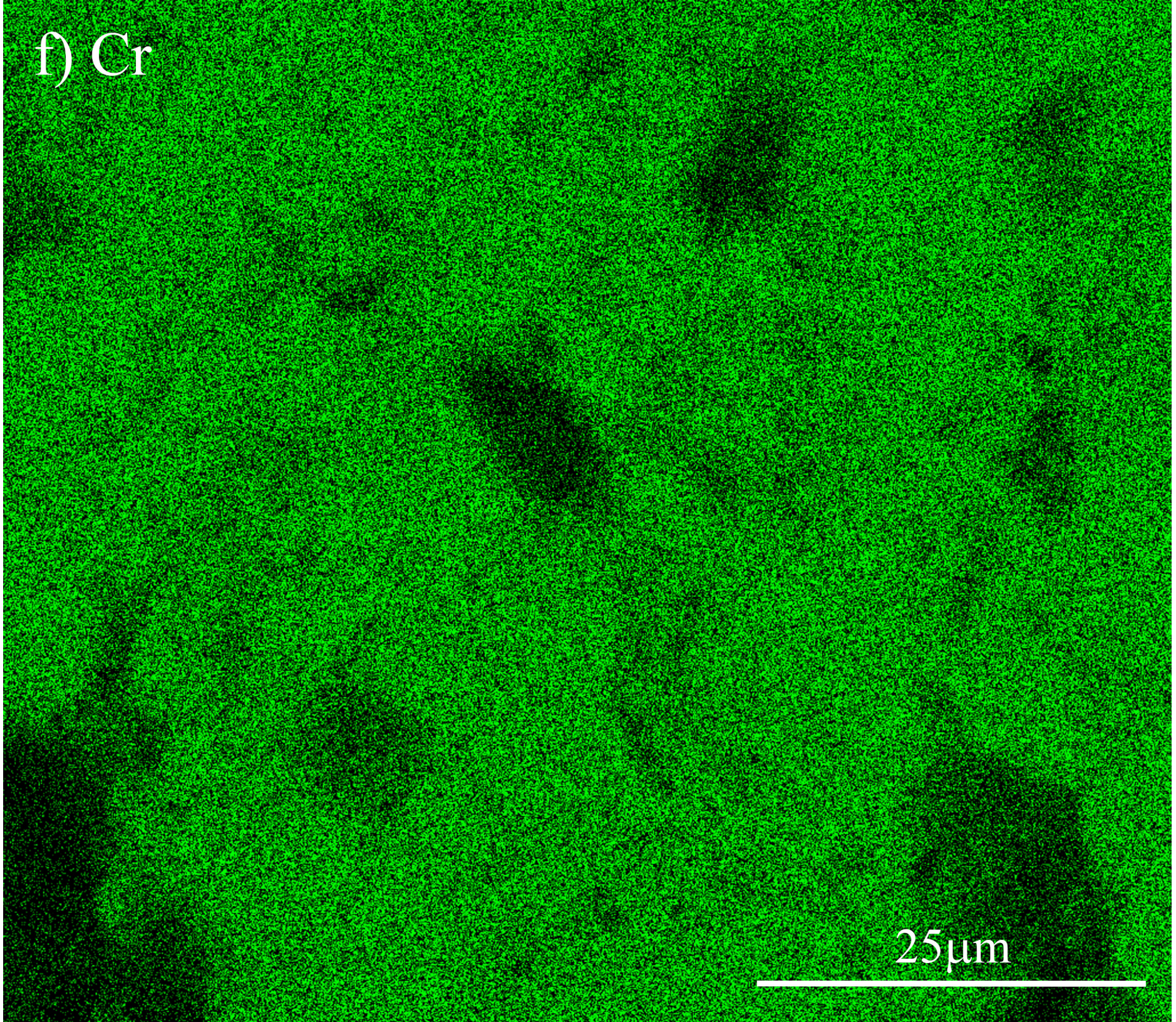
f) Cr
25µm

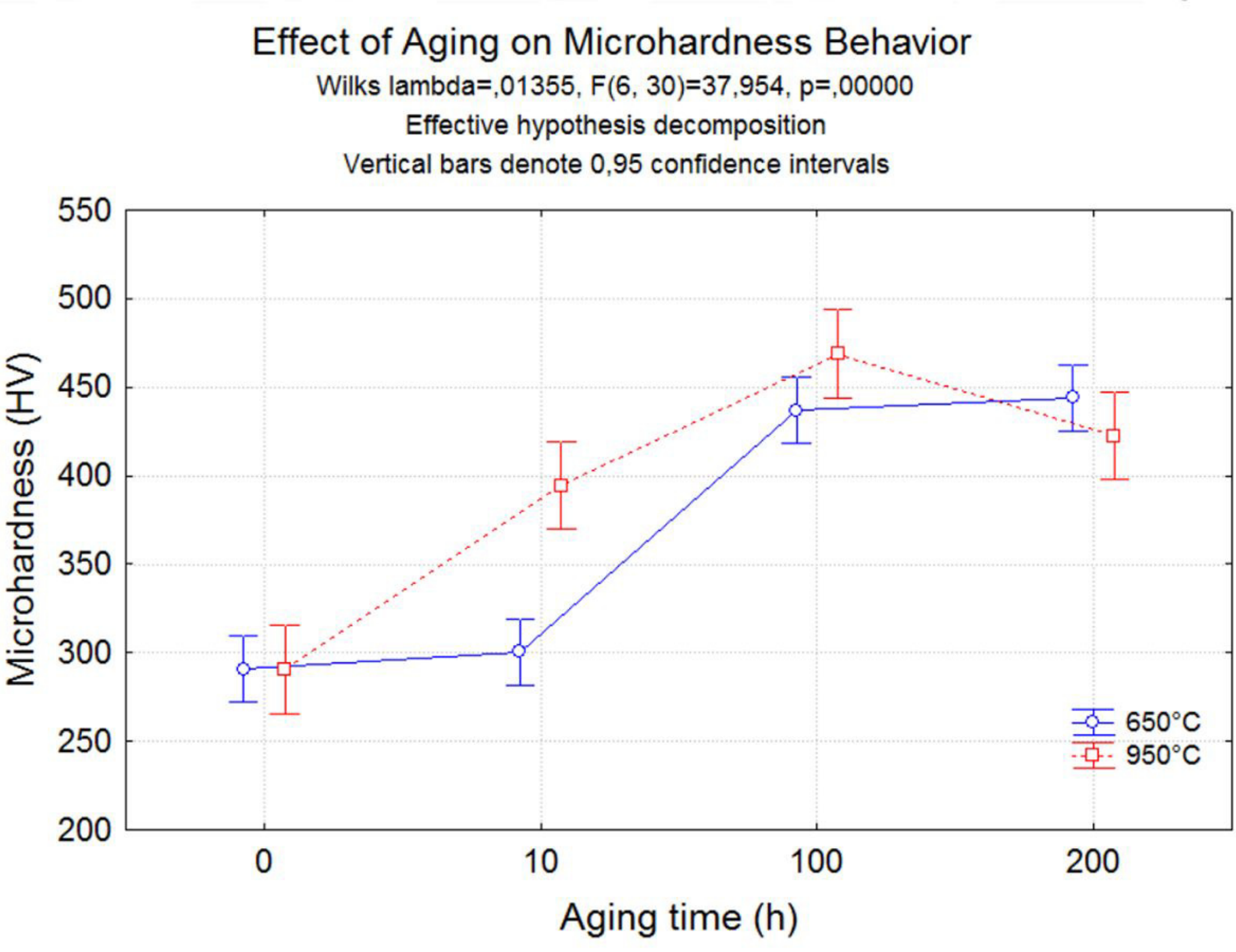
Effect of Aging on Microhardness Behavior
Wilks lambda=,01355, F(6, 30)=37,954, p=,00000
Effective hypothesis decomposition
Vertical bars denote 0,95 confidence intervals
Microhardness (HV)
550
500
450
400
350
300
250
200
0
10
100
200
Aging time (h)
650°C
950°C

(a)

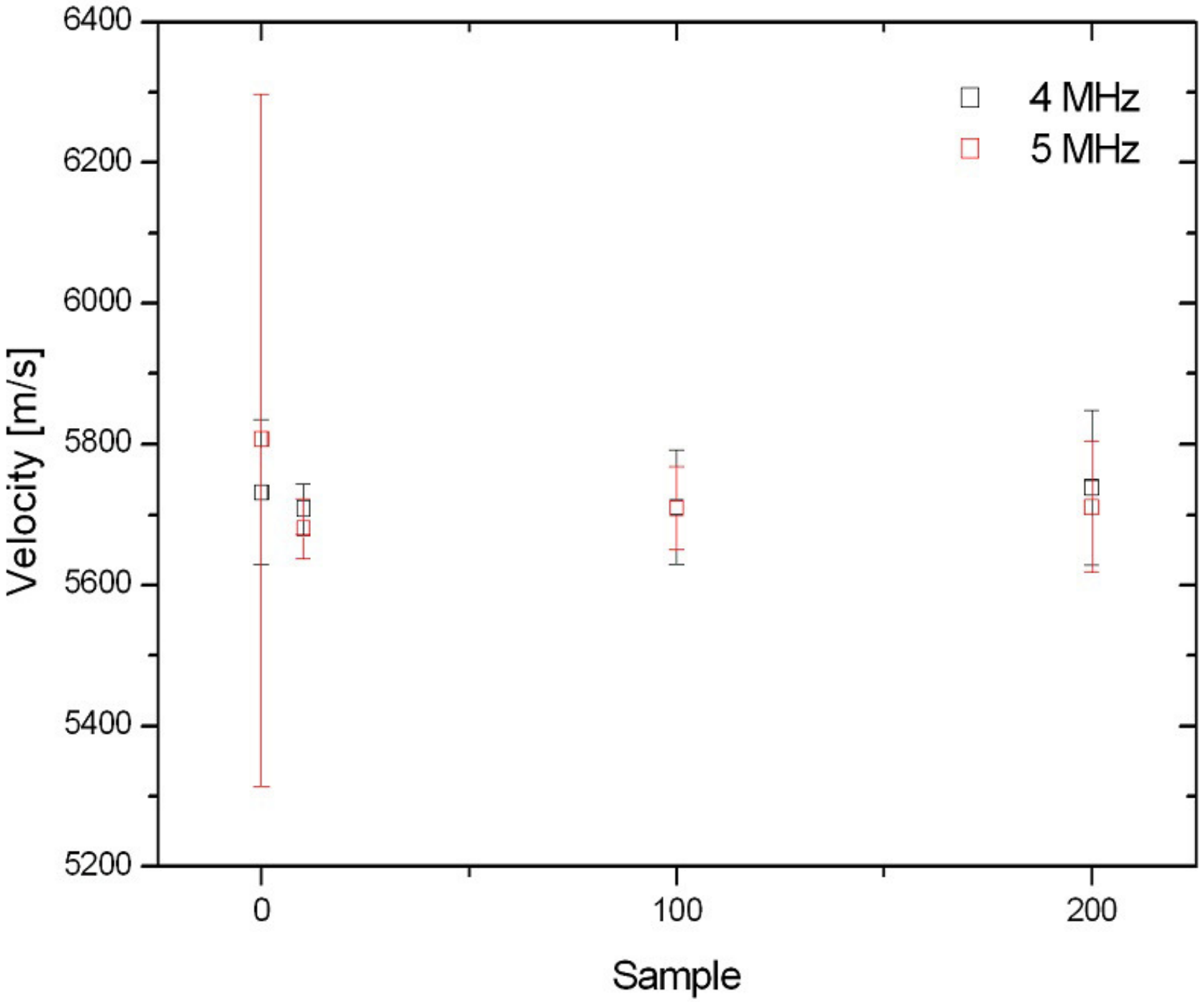
6400
6200
6000
5800
5600
5400
5200
Velocity [m/s]
0
100
200
Sample
4 MHz
5 MHz

(b)

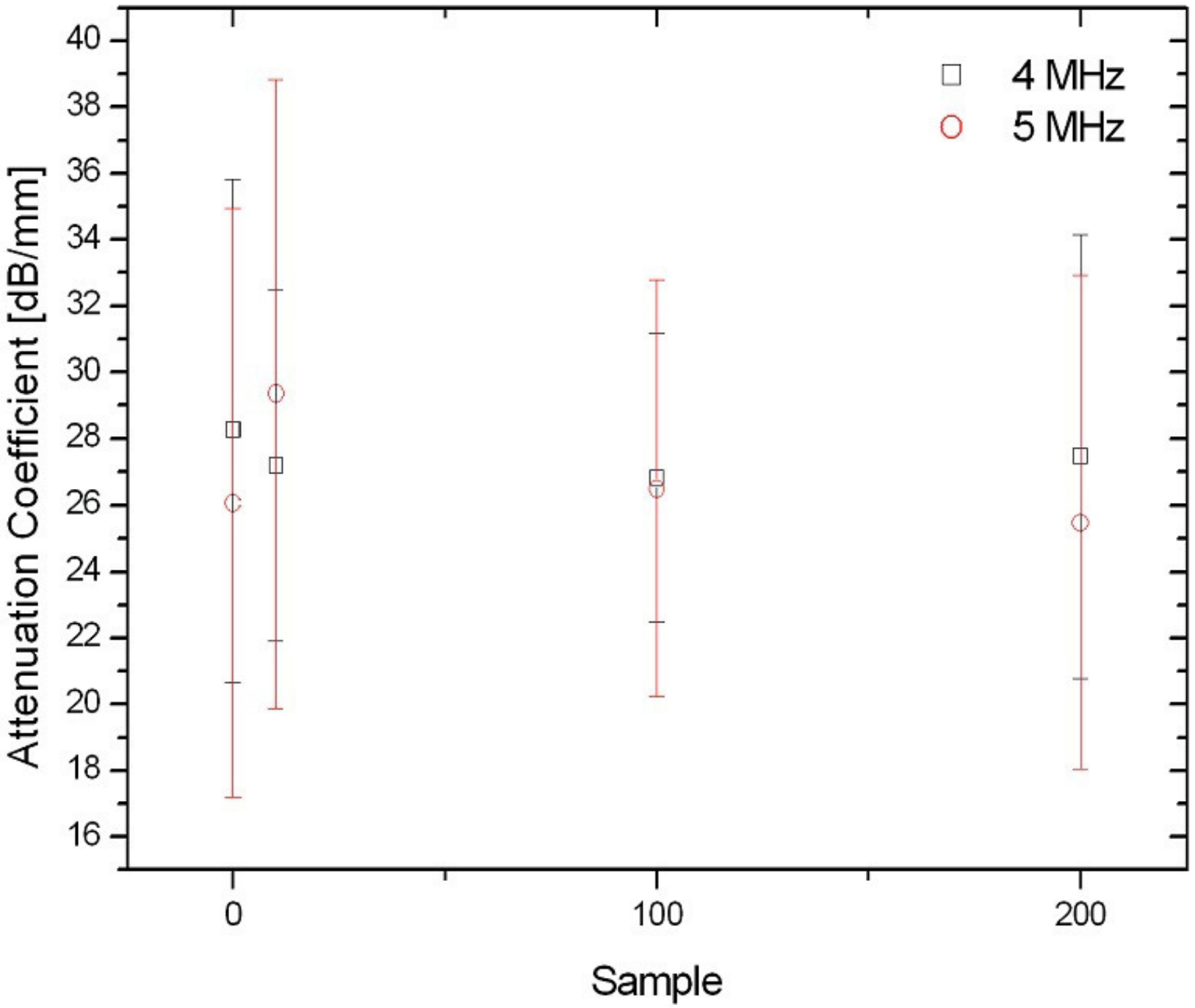
Attenuation Coefficient [dB/mm]
40
38
36
34
32
30
28
26
24
22
20
18
16
0
100
200
Sample
4 MHz
5 MHz

Table 1. Chemical composition in percent weight of the weld metal/coating and base metal.

AWS ERNiCrMo-3 (INCONEL 625 alloy – Weld metal)	Ni	C	Cr	Mo	W	Fe	Al	Ti
	64.43	0.011	22.2	9.13	-	0.19	0.09	0.23
	Nb	Mn	Si	Cu	Co	V	P	S
	3.53	0.01	0.05	0.01	0.03	-	0.002	0.002
ASTM A36 steel (Base metal)	Ni	C	Cr	Mo	Fe	Al	Mn	Si
	0.01	0.15	0.02	0.01	Balance	0.02	0.95	0.2

Table 2. Results of the chemical composition analysis performed by SEM/EDS on: (a) Laves phase and (b) Complex NbTi carbide/nitride.

a) Laves phase		b) NbTi carbide/nitride	
Element	wt. %	Element	wt. %
NbK	18.29	NK	6.37
MoL	21.18	NbL	25.23
CrK	17.27	MoL	8.39
NiK	43.26	TiK	15.60
-	-	CrK	13.88
-	-	NiK	30.52

Table 3. Mean weld metal chemical composition in % wt.

C	Cr	Mo	Nb	Fe	Ti	Si	Ni
0.1	21.51	7.455	3.285	2.31	0.665	0.145	Balance

Table 4. Impact strength of as-welded and aged condition obtained by the Charpy-V impact test.

Sample	Impact strength (J)
As-welded (0h)	141.3 ± 14.3
650°C/10h	150.9 ± 6.8
650°C/100h	105.3 ± 3.3
650°C/200h	98.4 ± 1.2
950°C/10h	120.0 ± 3.7
950°C/100h	136.4 ± 6.9
950°C/200h	150.4 ± 5.5